INFILTRATION STUDY USING TDR TECHNIQUES

by

SAURAV SINHA

Presented to the Faculty of the Graduate School of

The University of Texas at Arlington in Partial Fulfillment

of the Requirements

for the Degree of

MASTER OF SCIENCE IN CIVIL ENGINEERING

THE UNIVERSITY OF TEXAS AT ARLINGTON

August 2016

Copyright © by Saurav Sinha 2016

All Rights Reserved

Acknowledgements

I would like to express my sincere gratitude and appreciation to my thesis advisor, Dr. Xinbao Yu for being continually available and supporting me throughout this entire time. His expertise in working with sensor instruments improved my research skills and prepared me for the future challenges involved with the research. The valuable inputs and the skills that I have developed under his guidance, both academically and professionally would help in my future endeavors. I am highly obliged to Dr. Xinbao Yu for considering me for the position of Graduate Research Assistant and providing me scholarship throughout my Master's degree program. The valuable inputs and the skills that I have developed under his guidance, both academically and professionally would help in my future endeavors.

I would also like to thank my other committee members, Professors Dong-Jun Seo and Anand Puppala for their helpful suggestions and comments during my study. I offer my sincere gratitude for kindly taking out time from their busy schedule to administer suggestions and advice. I would like to thank all my research mates who were directly or indirectly associated with the research particularly Asheesh Pradhan, Nan Zhang, Xuelin Wang, Karthik Bolla, Amir Norouzi and Mohammad Rakib Hasan for helping me throughout my research work and encouraging me to go the extra mile.

Above all, I would like to express my special thanks to my father and mother for being a source of constant support and inspiration.

August 8, 2016

Abstract

INFILTRATION STUDY USING TDR TECHNIQUES

Saurav Sinha, MS

The University of Texas at Arlington, 2016

Supervising Professor: Xinbao Yu

The study of water flow or infiltration in an unsaturated soil is a highly non-linear and complex problem, simultaneous verification of field and laboratory results is a convenient and practical approach to test the results. In this study, Time domain reflectometry (TDR) sensors are installed at three different locations close to a water body (Creek) in Arlington, Texas which is a part of the National Science Foundation Project titled "Cyper SEES: Type 2: Integrative Sensing and Prediction of Urban Water for Sustainable Cities (iSPUW)". Time Domain Reflectometry (TDR) and Time Domain Transmissometry (TDT) sensors were deployed at five different depths i.e. 5 cm, 10 cm, 25 cm, 50 cm and 100 cm from the ground level. The infiltration process or the water movement through the soil was studied taking into consideration the soil moisture characteristics (moisture content, field capacity and permanent wilting point). Other soil parameters such as porosity, liquid limit and in-situ density were taken into account for having a better judgement of the soil. A turf-tech Infiltrometer was also employed at the three site locations for the measurement of the infiltration rate and saturated hydraulic conductivity of the soil.

To understand the concepts of the infiltration in the soil through laboratory experiments, a single 3 probe TDR sensor soil model was developed and tested with ASTM Graded Sand. Further improvement was made to design a 1 meter long soil column model.

In this laboratory study, the details of the soil column apparatus, the procedures adopted for constructing the soil column, and the performance of the apparatus are presented. The major instruments for the soil column apparatus consisted of time domain reflectometry (Strip and Probe), Data acquisition system, and Electronic Weighing Balance. By using these instruments, the vertical infiltration in the soil was studied w.r.t the ASTM Graded Sand.

From the field results, it was found that light rainfall increased moisture content in the top layer, whereas, heavy rainfall affected all the layers of the soil. Continuous rainfall had the effect of soil reaching nearly saturated or fully saturated state resulting in Steady State infiltration. Preferential flow was initially reported as the soil consisted of organic matter at different depths of soil profile. The deeper soil layer along all the three locations showed a much higher moisture content being close to the ground water table. From the laboratory tests, more or less the same conclusion was derived based on the wetting front and the moisture content variation curves.

Table of Contents

List of Illustrations

List of Tables

Chapter 1

INTRODUCTION

1.1 Background

Infiltration is the movement of water into the soil from the ground surface. The water is driven into the soil from the surface. The water is driven into the porous soil by force of gravity and capillary attraction. First, the water wets soil grains and then the extra water moves down due to resulting gravitational force. The rate at which a given soil can absorb water at a given time is called infiltration rate and it depends on soil characteristics such as soil texture, hydraulic conductivity, soil structure, vegetation cover, etc.

In the infiltration process, water enters the soil surface due to the combined influence of gravity and capillary forces. Both forces act in the vertical direction to cause percolation downward. Capillary forces also act to divert water laterally from larger pores to capillary pores spaces which are much smaller in dimension, but may be very numerous. As the process continues, the capillary pore spaces become filled, and with percolation to greater depths, the gravitational water normally encounters increased resistance to flow due to reduced extent or dimension of flow channels, increased length of channels, or an impermeable barrier such as rock or clay. At the same time, there may be an increased resistance to inflow of water at the soil surface due to the surface sealing effect as a result of the mechanical action of raindrops in breaking down the soil aggregates and subsequent in wash of the finer soil particles. The result is a rapid reduction of infiltration rate in the first few hours of a storm, after which the rate remains nearly constant for the remainder period of storm rainfall excess.

From this qualitative description of the infiltration process it can be recognized that the process involves both transmission and storage of water by the soil and the rate of infiltration may be governed by separate processes of:

(a) Entry of water through the surface layer

(b) Downward movement or percolation of water through the soil profile

The importance of the infiltration process in the hydrologic cycle as a phenomenon deserves special attention and study. In these regards, it would be expected that a complete understanding of the process and factors affecting would assist in quantitatively evaluating infiltration amounts and hence, increase his confidence in water balance, hydrologic design and other studies.

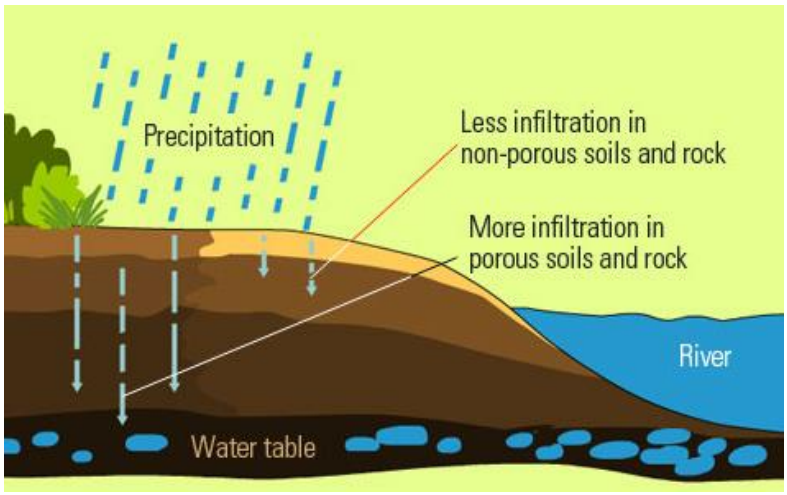

Figure 1-1 Infiltration Process in the Soil (eschooltoday.com Website)

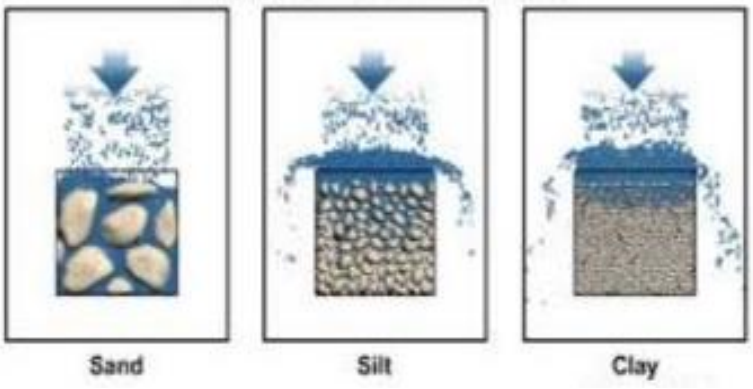

Figure 1-2 Infiltration variation by Soil Texture (MetEd Website)

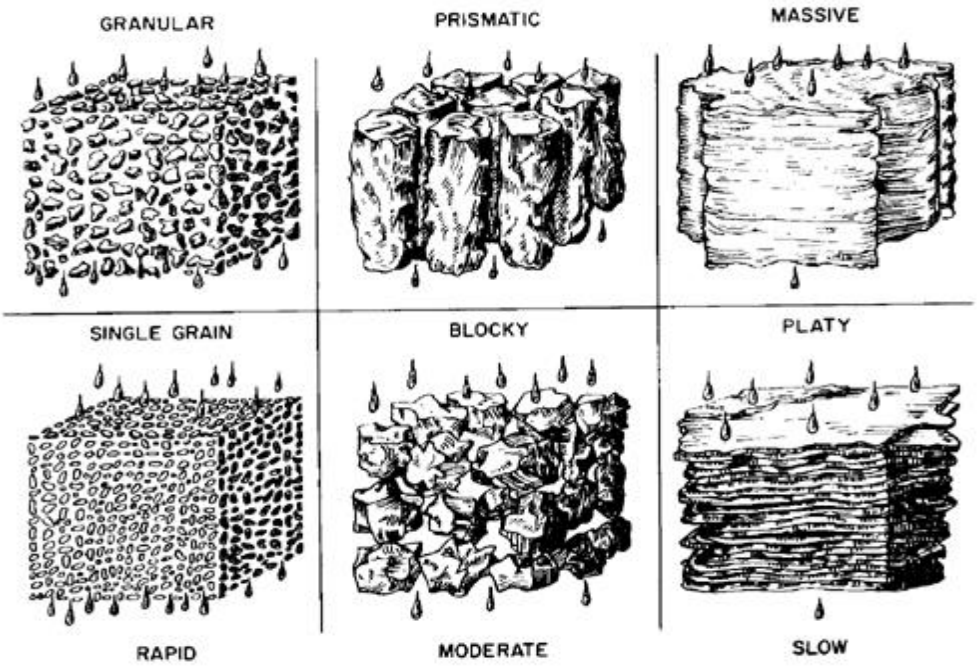

Figure 1-3 Infiltration variation by Soil Structure (Colorado State Extension Service)

1.2 Research Objectives and Tasks

The objective of the study was to determine the infiltration based on the effect of rainfall intensity and duration through the soil associated with the moisture content variation through the different layers of soil. Also, a comprehensive infiltration study of water through the soil was achieved by constructing a soil column apparatus. The specific tasks that were accomplished in the current study are presented below:

i. Conducted Atterberg Limit Test for the three site locations
ii. Performed Sieve Analysis, Specific Gravity and Hydrometer Test for the three site locations
iii. Determined the moisture content of the soil for the TDR location using Topp's Equation, comparison of the water content variation w.r.t the depth of the soil layers.
iv. Determined the Infiltration capacity curve using Philip's Equation

v. Determined the wetting front for the ASTM Graded Sand through the Soil Column Experiment

1.3 Organization of the Study

A summary of the current study is abridged as mentioned below

Chapter 1 presents the background of infiltration in soils, the process considered, and objective of the study and thesis organization.

Chapter 2 provides a detailed literature review for the works previously performed to study the infiltration through the soil, various models and innovative approach adopted for the Field and the laboratory experiments.

Chapter 3 describes the installation of the TDR and TDT sensors at different site locations, methodology for analyzing the data.

Chapter 4 describes the soil column experiment performed in the laboratory and the specific conditions that were maintained while performing the test.

Chapter 5 provides the summary, final conclusion and future recommendations of the current study.

Chapter 2

LITERATURE REVIEW

2.1 Introduction

Infiltration of water in unsaturated soils has long been an interest of study in many branches of science and engineering such as soil science, hydrology, and geotechnical engineering.

Infiltration in soil science refers to the soil's own ability to allow water movement into and through the soil profile. Various definitions for infiltration appear in the literature and several but, there are many factors governing the soil infiltration. It has been an active topic of research because of its fundamental role in land-surface and sub-surface hydrology, and agricultural irrigation (Milla and Kish, 2006).

2.2 Background

Infiltration is most often associated with precipitation and evapotranspiration, as together they form an important part of the hydrologic cycle. A subcommittee of the soil science society of America on terminology, chaired by Richards (1952), defined infiltration as the downward entry of water into the soil. Again, Hutchinson and Stoesz (1970) defined infiltration as the flow of a liquid into a substance through pores or other openings, connoting flow into a soil in contradistinction to the word percolation which connotes flow through a porous substance. Lately, J.H., Gregory et al. (2005) expressed that infiltration is the methodology by which water moves descending at the soil surface pass in the soil. This system influences surface runoff, soil erosion, and groundwater recharge. Infiltration rate is the maximum rate at which water can enter the soil which is altogether determined by the soil characteristics under specific conditions including excess of water present within the soil. The rate of infiltration is defined in terms of inches or centimeters per hour. Infiltration capacity is termed as the ability to infiltrate rainfall, it usually determines how much of the rainfall enters the soil and indirectly the amount of surface runoff. The study of water flow or infiltration in an unsaturated soil can be conducted using several methods. The methods include field test,

laboratory experiment, and numerical modelling. Since, no restrictions are placed on the divergence of flow in to the soil, it is necessary to describe the method employed for individual research project.

2.3 Factors affecting infiltration and contributing to infiltration rate

Basically, the soil characteristics are the principal factors affecting infiltration. Pore-size and pore-size distribution are directly related to soil texture and soil structure which are the inherent factors affecting soil infiltration. Some of the other factors, that contribute to the infiltration ability of the soil are colloidal swelling, aggregate stability, compaction of soil surface, organic matter content, biological activity, entrapped air, root penetration, freezing and previous land use (Stephen J. Stephen). Present temperature and interception by vegetation affect the amount of water available for infiltration as well as the duration and intensity of the rainfall, size of raindrop and rainfall impact. These latter characteristics of the precipitation may account for the turbidity of the surface water (if any) and the depth of water over the soil surface or its head. Subsurface factors such as thickness of the different soil horizons, permeability of underlying strata and antecedent moisture also influence water intake.

Because of involvement of many variables, there are diverse opinions on the ones pertaining to greatest influence on infiltration. Horton (1940) suggested the following factors which affect the infiltration of water into the soil. He grouped them as

i. Soil type and soil profile
ii. Biologic and Macro-structure within the soil
iii. Vegetal cover.

Lewis and Power (1938) divided all the factors into two major headings as

i. Factors influencing the infiltration rate at a given time, and point such as texture, structure and organic matter.
ii. Factors influencing the average infiltration rate over a considerable area and period of time such as slope, vegetation and surface roughness.

As it is generally agreed that a large number of variables are involved, only a limited number of factors are studied at a time. Some researchers think that soil mass is the single important factor that control the infiltration rate and therefore it is largely independent of the surface conditions or macro-structures near the surface of the soil.

Porosity is another important factor that influences infiltration. The flow of water into the soil depends on the sizes, continuity and distribution of pores. The porosity of a given soil varies with its texture and structure. Soil texture is the size distribution of the individual soil particles, whereas soil structure is the arrangement of the soil particles into specific groupings. The texture varies from sandy to loamy to clayey, depending on the percentage of particles of sand, silt and clay in each type. The structure, which is basically a field description, can vary from platy to crumb (Lyon, Buckman and Brady, 1952). Hillel, 1982 classified the soil type and the steady infiltration rate for a very deeply wetted condition as abridged below

Table 2-1 Steady infiltration rates for general soil texture groups

Soil Type	Steady infiltration rate (inches per hour)
Sands	> 0.8
Sandy and silty soils	0.4 - 0.8
Loams	0.2 - 0.4
Clayey soils	0.04 – 0.2
Sodic clayey soils	< 0.04

Baver (1938) classified pores as capillary and non-capillary. The diameter of the capillary pores are less than 0.05 mm and those of the non-capillary pores are greater than 0.05 mm. In order that the water may continue to infiltrate, it must be able to move relatively freely down through the soil. However, a point to be considered is that there is a major difference between saturated and unsaturated flow. Millar and Turk (1943) explained that gravity causes water to move when the soil is saturated, hence, the larger the pore the faster the flow provided that the pores are connected.

When the soil is not completely wetted then forces of adhesion (mutual attraction between soil and water) and cohesion (attraction of water molecules to each other) act. Because of unequal tensions developed on the curvature of the surface water film, the direction of the flow is determined by the direction of this force. Water can move upward or outward in a drier soil as easily as it can move downward. This is called capillary movement. Gumbs and Warkentin (1972) noted that the swelling of soils increases the porosity and conductivity of the surface layers which have a large influence on the infiltration rate.

Browning (1939) found that the moisture content of the soil was a determining factor in its volume. As the soil swells or increases in volume it decreases the volume of the soil pores. Non-capillary pores become capillary in size and smaller capillary pores may be sealed to the movement of water within the soil. Surface soil had a greater volume change than the subsoil because of the latter's higher bulk density values indicating that the subsoil was compacted, therefore it had less space for expansion.

Zimmerman (1936), Free and Palmer (1940), and Christiansen (1944) conducted studies in the laboratory on soil columns to observe the effect of entrapped air on infiltration and permeability. Complex interrelationships between pore size, air and water movement were noted which pointed to the importance of pore space in the infiltration process.

Factors that control infiltration rate include soil properties that are strongly affected by these three forces, such as hydraulic conductivity, diffusivity and water holding capacity. These soil properties are related to the characteristics of soil texture, structure, composition, and degree of compaction, which influence soil matric forces and pore space. Additionally, antecedent water content, type of vegetative or other ground cover, slope, rainfall intensity and movement and entrapment of soil air are important factors that also affect infiltration rates. The hydraulic conductivity is of critical importance to infiltration rate since it expresses how easily water flows through soil and is a measure of 9 the soil's resistance to flow. The unsaturated hydraulic conductivity is a function of pressure head (Serrano, 1997) and distribution of water in the soil matrix.

The saturated hydraulic conductivity, the hydraulic conductivity at full saturation, is used as a parameter in many of the infiltration equations, since it is easier to determine than either the unsaturated hydraulic conductivity or the diffusivity.

Diffusivity is equal to the hydraulic conductivity divided by the differential water capacity (the rate of change of water content with soil water pressure), or the flux of water per unit gradient of water content in the absence of other force fields (SSSA, 1975). Since diffusivity is directly proportional to hydraulic conductivity, usually only the saturated hydraulic conductivity is used in the approximate infiltration equations. Water holding capacity is the amount of water a soil can hold due to pore size distribution, texture, structure, percentage of organic matter, chemical composition, and current water content. For saturated conditions, the water holding capacity is zero and the hydraulic head is positive (Skaggs and Khaleel, 1982). While the water holding capacity can be found in the h based Richards's equation (2.7), it is not directly used as a parameter in the approximate equations. However, the water holding capacity influences the values of the average suction at the wetting front and sorptivity, as well as some of the empirical parameters. The soil texture which refers to the proportion of sand, silt, and clay that a soil comprises directly affects the hydraulic conductivity, diffusivity and water holding capacity. Soils with higher sand percentages have larger size particles, larger pores, lower water holding capacity and higher hydraulic conductivity, diffusivity and infiltration rates than clay soils which have smaller micro pores and bind water molecules more tightly.

Soil structure describes the adhesion and aggregation of soil particles and formation of plates, blocks, columns, lumps, and cracks and is affected by chemical composition of soil particles, amount of organic matter present, soil texture, water content, and activity of organisms such as earthworms, insects, fungi, plant roots and microbes. Soil structure affects the path by which water moves through the soil (Brady and Weil, 1999). Micro pores are generally less than a micrometer in width, and occur typically in clayey soils (Hillel, 1998). Water in these pores is referred to as adsorbed, bound or residual water because it is discontinuous and is affected by such phenomena

as cation adsorption, hydration, anion exclusion and salt sieving, and therefore does not participate in normal flow behavior (Hillel, 1998). Water in these pores obey the laws of capillarity and Darcian flow (Hillel, 1998). A deep homogeneous soil (containing only capillary pores), as is assumed in many infiltration equations, is subject to uniform flow in which the infiltration rate decreases as the moisture gradient declines. Macropores are diverse structural pores that are relatively large compared to those in the surrounding soil (Beven and Germann, 1982). They are channels formed by biological activity such as that of plant roots and earthworms, and cracks and fissures caused by physical and chemical weathering processes (Beven and Germann, 1982).When water is pushed out, macropores constitute barriers to capillary flow, permitting only slow film-creep along their walls. When filled with water, however, macropores permit very rapid, often turbulent, downward movement of water to lower layers of the soil profile (Hillel, 1998). This rapid channel drainage that often bypasses much of the soil matrix and can drastically alter infiltration rates is called preferential flow (Simunek et al. 2003). Even for relatively small earthworm channels, the flow rate in macropores seems to be always higher than the rainfall intensity (Bouma et al., 1982). However, because of the inherent modeling difficulties, most infiltration equations assume uniform flow, ignoring the existence of preferential flow. Correct assessment of the internal hydrological behavior of the soil profile is especially important for the simulation of pollutant transport processes or for assessment of land-use (Weiler, 2005).

Soil compaction results from applying pressure on the soil surface, which reduces pore space, damages soil structure, reduces the air available to plant roots and other soil organisms and reduces infiltration rates. Rainfall on bare soil can cause soil compaction. Often where soils have been plowed repeatedly with heavy equipment there is a hardened and compacted layer below the topsoil called a plowpan, which may impede redistribution. Stienbrenner (1955) found that under wet conditions one pass of a tractor wheel can reduce the non-capillary pore space by 50 percent and the Infiltration rate by as much as 80 percent. Doneen (1953) found two passes of a tractor wheel reduced the infiltration rate from 1.4 to 0.6 inches per hour or a net reduction of 0.8 inches

per hour. Heavily grazed pastures, because of the increased compaction of the soil surface are susceptible to a higher volume of runoff and reduced infiltration. Compaction of the soil decreases its total porosity, especially under wet conditions. A naturally hardened layer called a fragipan may also obstruct the vertical movement of water (Brady and Weil, 1999).

Antecedent moisture was investigated by Tisdall (1951) using 12 inch ring infiltrometers to determine its relationship to the infiltration rates. Observation indicated the lower the soil moisture, the higher the infiltration rate. Also, the longer the period of water application, the less the effects of the antecedent moisture had on the infiltration rates. Antecedent or initial water content affects the moisture gradient of the soil at the wetting front, the available pore space to store water and the hydraulic conductivity of the soil. Initial water content is therefore a critical factor in determining the rate of infiltration and the rate at which the wetting front proceeds through the soil profile. The drier the soil is initially, the steeper the hydraulic gradient and the greater the available storage capacity; both factors that increase infiltration rate (Skaggs and Khaleel, 1982). The wetting front proceeds more slowly in drier soils, because of the greater storage capacity, which fills as the wetting front proceeds (Philip, 1957c).

Vegetation and other ground covers such as mulches and plant residues reduce soil temperature and evaporation from the soil surface, but vegetation also loses moisture through transpiration. Vegetation increases infiltration rates by loosening soil through root growth and along with natural mulches and plant residues, intercept rain drops, which compact and damage the structure of bare soil and cause surface sealing and crusting. Living and dead plant material also add organic matter to the soil which improves soil structure and water holding capacity and provide habitat for earthworms which further enhance the soil constitution and increase infiltration rates. Organic matter influences the water intake of a soil in various ways. Soil that is low in organic matter content is easily eroded. Besides the litter and humus providing a spongy protection for the mineral portion of the soil particles, it also aids as a binding agent in the formation of aggregates. Most research has been done on forest soils where the detection of the various stages of organic matter

decomposition is more easily performed. Auten (1933), Arend (1941), and Johnson (1940) all agreed from their respective investigations that the removal of the 'forest floor' reduces infiltration. Johnson (1957) found that the decomposition of organic residues clogged pores, resulting in a decreased infiltration rate. However, he concluded that this effect was offset by the high initial infiltration rate. Additional tests showed that percolation rates increased due to soil structure Improvement. Wischmeier and Mannering (1965) found that wide textural ranges of soils had only minor Influences on runoff. The entry of water into the soil was influenced much more by the organic matter and management than by texture and topography. Soil water content is also affected by seasonal changes in water use by plants, stage of plant growth, spacing of plants, type of vegetation, depth of roots, and extent of canopy coverage.

Soil micro-organisms have important direct and indirect effects on infiltration. Previous investigators have observed that soils subjected to an extended period of water submergence exhibit a typical S-shaped infiltration rate curve. According to Parr and Bertrand (i960) the initial rapid decline seems to be due to the slaking of aggregates and the swelling of soil colloids whereas the final decline in infiltration rate has been associated with microbial activity which is dependent upon the amount of organic matter in the surface soil. McCalla's (1942) work seemed to indicate that microbial slimes, gums etc. increased infiltration rate.

Slope also affects infiltration rate. A decrease in water infiltration rate was observed with increase in the slope steepness for grass covered slopes (Haggard et al., 2005; Huat et al., 2006). According to Haggard et al. (2005), the slope may have the greatest effect on surface runoff production and infiltration rate when the soil is close to saturation. On the other hand, there is evidence that on bare sloping land infiltration rates are higher than on bare flat land (Poesen, 1984). This effect is most likely due to reduced seal development on sloping land, as greater runoff velocities maintain a larger proportion of sediment particles in a suspended state resulting in more open pore structure (Römkens et al., 1985).

Rainfall intensity is the instantaneous rainfall rate, and for a uniform storm rainfall simulation may be obtained by dividing the depth of rainfall by the duration of rainfall. For non-ponded conditions, the maximal rate of infiltration called the infiltration capacity by Horton (1940) or infiltrability by Hillel (1971), equals or exceeds the rainfall intensity. The rainfall intensity provides the upper limit for the infiltration rate. The infiltration rate, therefore equals the rainfall rate until the time of ponding. If the rate of rainfall is less than the saturated hydraulic conductivity for the soil, infiltration may continue indefinitely at the rainfall rate without the occurrence of ponding. In this case the water content of the soil does not reach saturation, but approaches a limiting value, which depends on the rainfall intensity. For a given rainfall intensity, R, the soil profile approaches a uniform water content θ_L, where θ_L is the water content for which the hydraulic conductivity, K, is equal to the rainfall rate, R; $K(\theta_L) = R$. Since unsaturated hydraulic conductivity increases with increasing water content, the higher the rainfall intensity, the higher the value of θ_L (Skaggs and Khaleel, 1982).

When the rainfall intensity exceeds the ability of the soil to absorb water, infiltration proceeds at the infiltration capacity. At the time of ponding, the infiltration capacity can no longer keep pace with the rainfall intensity and depression storage fills up and then overflows as runoff. If the rainfall has a higher intensity, depression storage will fill faster and time of runoff will occur sooner, after the time of ponding. The rate of infiltration (f) after time of ponding, however, will not depend on rainfall intensity (R) for f less than R except to the degree that more intense rainfall may cause greater raindrop splash and greater surface sealing. Raindrop splash is the splashing of soil particles (and water) into the air when bombarded by raindrops. This damages the surface soil structure and causes soil detachment and surface sealing which occurs when enough soil particles that splash into the air, land in pore openings, and block them from infiltrating water. Much of the decrease in infiltration rate seen in unprotected soils is attributed to surface sealing (Shirmohammadi, 1984). Vegetation protects the soil from raindrop splash by intercepting and absorbing the energy of the raindrops. Crusting is the drying out and hardening of the surface sealed layer. Crusting may cause

immediate ponding with very low infiltration rate. A long soaking rain will tend to soften the crust so that after a time, infiltration rate may increase.

Water moving into a soil profile displaces air, which is forced out ahead of the wetting front. If there is a barrier to the free movement of air, such as a shallow water table, or when a permeable soil is underlain by a relatively impermeable soil, the air becomes confined and the pressure becomes greater than atmospheric. Compressed air ahead of the wetting front and the counter flow of escaping air may drastically reduce infiltration rates (Shirmohammadi, 1985). Wangemann et al. (2000) found that for dry soils and for interrupted flow, the main retardant to infiltration was entrapped air, while for wet soils, reduced aggregate stability and surface sealing were the main causes for reduced infiltration rates. Le Van Phuc and Morel-Seytoux (1972) showed that for a two phase flow treatment of infiltration, infiltration rate after a certain time was well below the saturated hydraulic conductivity, which was considered to be a lower limit by all the previous authors. Infiltration tends to be increased for deeper water tables, since the impedance of the compressed air on infiltration is reduced and the soil profile tends to be drier compared to shallow water table conditions (Shirmohammadi, 1984).

Free et al (1940) investigated 68 soils to determine relative infiltration and the related soil characteristics. The experiments were conducted in situ using a tube type infiltrometer over a wide range of soil types representing most great soil groups, parent materials and climatic provinces. In the laboratory, mechanical analyses of the samples were performed and the porosity of the soils measured. A definite association was indicated between Infiltration and all indices of large pores or those factors affecting pore size. Non-capillary porosity, degree of aggregation, organic matter and amount of clay in the subsoil were variables that were tested statistically. When the factors were combined in multiple regression, the correlation coefficient of 0.71 was obtained. From this study, the most important single factor influencing infiltration is non-capillary porosity. Organic matter and clay content affect it to a lesser degree.

Verma and Toogood (1969) measured infiltration rates for the major soil types of the Edmonton area. High initial infiltration rates were noticed in all soils. The concentric ring method was used in which a one cm head was maintained. A comparison of rainfall intensity with infiltration rates showed that there was little erosion hazard for the area.

It has been shown that many variables affect the infiltration process. A difficulty arises as to the relative value of each one of the individual variables that influence infiltration. It must be emphasized that the results from each investigation are relevant only to the specific environment and that particular technique employed. Research results tend to show considerable variance quantitatively but this should neither deter one from further research nor lead one to think that his own results are erroneous. Musgrave and Free (1937) concluded that it was unreasonable to attach a specific infiltration rate to a particular soil type and the measured rates are essentially comparative values.

2.4 Measurement of infiltration

2.4.1 Field Measurement of Infiltration

Methods of testing and measuring infiltration are widely varied. In many instances the method used has been developed to meet a specific requirement and as such are not easily adapted to other situations. Parr and Bertrand (I960) classified the instruments into three groups

i. Instruments in which infiltration is determined as the difference between water applied and runoff,
ii. Instruments which Impound water in a confined area thus maintaining a head of water,
iii. Instruments which allow the determinations of infiltration from rainfall data.

Three sub-groups add refinement to the above classification of infiltration instruments. They are

i. Installations that encase the soil in various sized enclosures, such as tubes, cylinders etc. which do not allow lateral movement of the water,

ii. those which allow unrestricted lateral movement,

iii. those which provide buffer compartments to compensate for lateral subterranean flow of water from the plot.

Musgrave and Holtan (1964) classified the methods used for infiltration work under two headings (a) the analysis of hydrographs of runoff from natural rainfall on plots and watersheds, (b) the use of infiltrometers with artificial application of water to enclosed areas.

2.4.1.1 Field Measurement of Infiltration using Infiltrometers

An infiltrometer is a device for measuring the rate of entry of a fluid into a porous body, for example water into soil. Infiltrometers may be classified into two general types, (1) rainfall simulators, (2) cylinders. They are usually used for experimental plots or very small watersheds. Repetitive runs for each plot are taken in order to obtain hopefully more reliable data. Much of the work that has been done using rainfall simulators was for erosion calculations but some has been done for Infiltration rates. Many types of rainfall simulators have been devised. Most of them are rather elaborate and once they have been installed are difficult to move although several portable devices have also been built. They employ a series of nozzles that spray water into the air allowing it to drop on the surface as artificial rain. Then arose the difficulty of rain drop size and Intensity. Diebold (1941) tested F and FA type I Infiltrometers on forest soils. Both of these infiltrometers used the type F nozzle which produced drops varying in size from 3.2 to 5.0 mm. in diameter. A tent was used to protect the spray pattern from the wind. Type F has a pressure of 35 p.s.i. and type FA operates at 15 p.s.i. The type F has 13 nozzles that disperse the artificial rainfall onto a 6.6 by 12 foot plot in an arch-like pattern. The rainfall is measured by two 12-foot trough gauges. Modification of these infiltrometers have led to such instruments as the Rocky Mountain infiltrometer or the North Fork infiltrometer. Some experimenters also studied the effect of buffer areas on infiltration rates using the sprinkling infiltrometers.

Many varied types of cylinder infiltrometers have been used for collecting Infiltration data. They are usually metal rings but sometimes square compartments that are driven into the soil to

depths ranging from a few Inches to one or two feet. Water is added in known amounts to include such principles as falling heads, constant heads or even a sprinkling application. Single ring, double ring or multi-ring devices have been used. The latter two which attempt to control the lateral water movement in the soil by creating a buffer zone have been used in later studies. Supposedly, the high variability of infiltration with the single type was due to lateral movement of water but since results are to be considered relatively then this data can be useful. Caution and uniformity must be exercised when the rings are pressed into the soil surface. It is important to disturb the soil structure as little as possible so that replicated infiltration runs show a minimum of variation. Also, water may seep down the sides of the infiltrometer which results in unnatural flow. With columns that are driven deeply into the ground entrapped air inside the soil column will impede the downward movement of the applied water. Auten (1933) used rings 2 inches deep and 12 inches in diameter and pressed 3 centimeters into the soil surface to study infiltration characteristics. In further experiments he used a 12-inch square metal compartment and he obtained similar results. Musgrave (1935) used a 6-inch diameter cylinder Jacked into the soil to reach the B horizon to obtain his infiltration data. Smith et al (1937) followed Musgrave's procedure to study the effect organic matter had on infiltration. The 6-inch diameter steel cylinder was forced into the soil to a depth of 12 Inches by a Jack screw set against a tractor. Although variability was obvious after repeated runs, it was evident that organic matter in the form of barnyard manure significantly influenced the rate of infiltration.

Tests were conducted by Burgy and Luthin (1956) using single and double ring infiltrometers. They found no significant difference between the two types under the conditions of their experiments. Single ring cylinders 4.5 inches in diameter and 4.5 inches long were placed half their depth into the soil by Slater (1957). The infiltration rates were then compared with those results from an FA type infiltrometer. It was found necessary to conduct 15 replications for a 20 percent accuracy of the single ring type. The median was comparable to one run with the FA type or three runs on hand sprinkled plots.

2.4.1.2 Field Measurement of Infiltration using Time domain Reflectometry

Time Domain Reflectometry (TDR) is now well accepted as a method for measurement of soil water content. Time domain reflectometry (TDR) technology has been shown (Benson and Bosscher 1999; Noborio 2001) to be reliable, fast, and safe technology for field monitoring soil moisture in the form of volumetric water content, θ, i.e., volume of water compared to the total volume of soil. Promotion of TDR technology for soil moisture monitoring is largely attributed to Topp et al. (1980), who established a relation between soil volumetric water content and soil apparent dielectric constant. Later research (Dalton et al. 1984) showed that, in additional to apparent dielectric constant, it is also possible to obtain bulk electrical conductivity from TDR waveforms.

Siddiqui and Drnevich (1995) made an improvement in which they developed a calibration equation relating apparent dielectric constant to soil gravimetric water content and dry density. The first step involves laboratory calibration to obtain soil dependent constants for subsequent field measurements. In the second step, the field installation of two TDR probes

i. One TDR test is taken with probe consisting of four coaxially configured spikes driven into the soil.
ii. Second TDR test conducted in a compacted mold on the same soil that was rapidly excavated within the four spikes and hand compacted into the mold.

Assuming the gravimetric constant is the same for both the tests, the apparent dielectric constants from the two TDR readings along with the measured total density of the soil in the mold are used to calculate soil water content and dry density. The laboratory and field results were close enough indicating sufficient accuracy.

Yu et al. (2004) used a Campbell scientific TDR 100 tester as shown in Figure 2-1 connected to a specially designed multiple rod probe (MRP) head by a 1.8 m long, 50 Ω coaxial cable. The MRP head was kept on the heads of four common spikes driven into the soil. As shown in Figure 2-2, one reflection occurs as the electromagnetic wave pulse reaches the soil surface (denoted by the downward pointing triangle) and another one occurs as it reaches the end of the probe (upward

pointing triangle). Soil dielectric constant, K_a, or apparent dielectric constant as proposed by Topp's was determined from the TDR waveforms using the equation

$$k = \left(\frac{L_a}{L_p}\right)^2 \quad (1)$$

Where L_p = length of the probe in the soil; and L_a = scaled horizontal distance between reflection from the soil surface and the reflection from the end of the probe (called apparent length).

Different methods are followed for the picking up of the two reflection points namely:

i. Methods of Tangents

ii. Method of Peaks

In this particular study, Yu et al. (2004) adopted an algorithm developed by Drnevich et al. (2004).

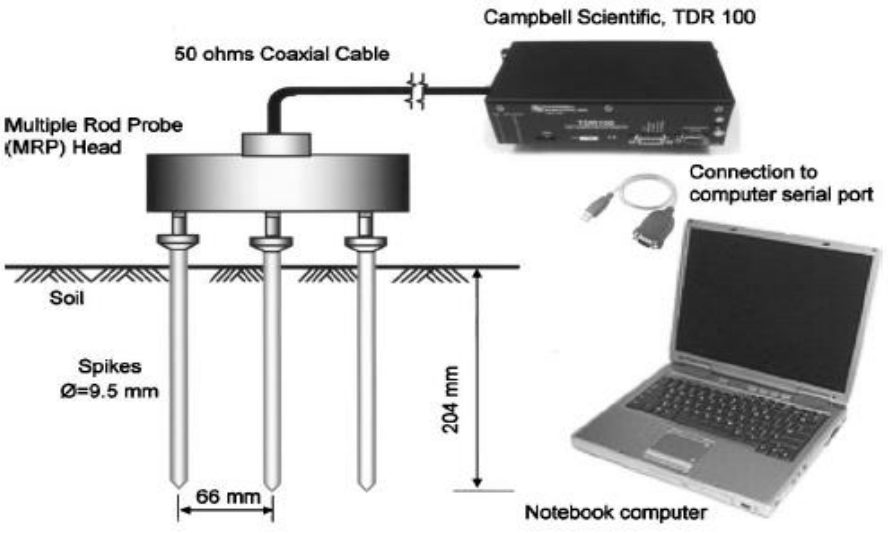

Figure 2-1 Schematic of components of the TDR system

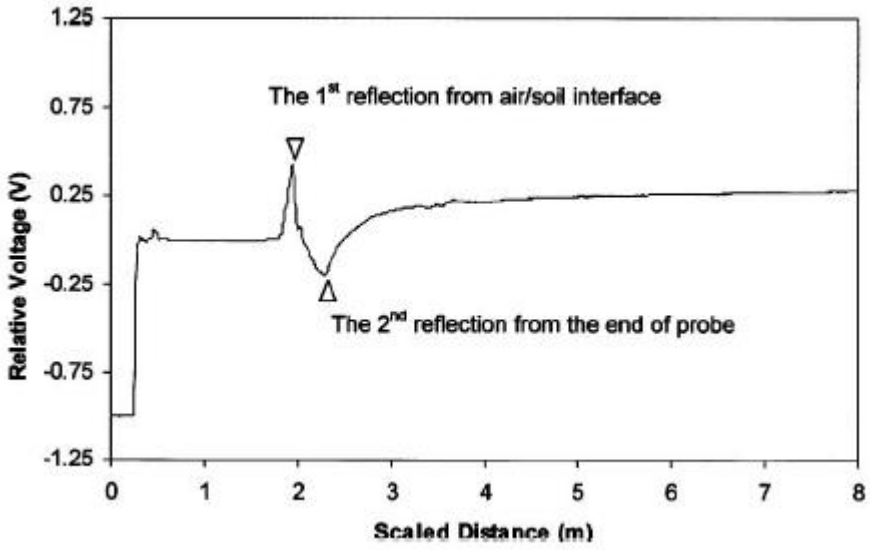

Figure 2-2 Resulting TDR waveform from the TDR system

Topp et al. (1980) showed that for soils with a wide range of mineral content, a single equation was adequate and was practically independent of soil bulk density, ambient temperature, and salt content. The relation is widely used and referred as Topp's Equation

$$\theta = 4.3 \text{ x } 10^{-6}\ K_a^3 - 5.5 \text{ x } 10^{-4} K_a^2 + 2.92 \text{ x } 10^{-6} K_a - 5.3 \text{ x } 10^{-2} \quad (2)$$

However, it is observed that for organic soils, fine textured soils, and clays, the dependency of K_a on θ differs from Topp's Equation (Dobson et al. 1985; Dasberg and Hopmans 1992; Roth et al. 1992; Dirksen and Dasberg 1993).

The study by Siddiqui and Drnevich (1995) and Siddiqui et al (2000) utilized gravimetric water content along with soil dry densities as given by the equation

$$\sqrt{K_a}\frac{\rho_w}{\rho_d} = a + bw \quad (3)$$

Where a and b = soil specific calibration constants; ρ_d= dry density of soil; ρ_w = density of water; and w = gravimetric water content.

Electrical Conductivity is another parameter that can be obtained from TDR waveforms. Measurement of electrical conductivity using TDR is based on attenuation of the applied signal

voltage as it transverse electromagnetic waves propagate along TDR probes buried in the soil, the signal energy is attenuated in proportion to the electrical conductivity along the travel path. Comparisons between the electrical conductivity measured in solutions using both TDR and standard methods have repeatedly demonstrated the potential accuracy and precision of TDR measurements (e.g. Spaans and Baker, 1993; Heimovaara et al., 1995; Mallants et al., 1996; Reece, 1998).

Originally proposed by Giese and Tiemann (1975), the thin-section approach has been shown to be a particularly effective means of quantifying EC_a using TDR. The Giese and Tiemann equation may be written as:

$$EC\ (Sm^{-1}) = \frac{\varepsilon_o c}{L}\frac{Z_o}{Z_c}\left(\frac{2V_o}{V_f} - 1\right) \quad (4)$$

Where ε_o is the dielectric permittivity of free space (8.9 x 10^{-12} F m^{-1}), c is the speed of light in vacuum (3 x 10^8 ms^{-1}), L (m) is probe length, Z_0 (Ω) is the characteristic probe impedance, Z_c is the TDR cable tester output impedance (typically 50Ω), V_0 is the incident pulse voltage after multiple reflections have died out as shown in Figure 2-3

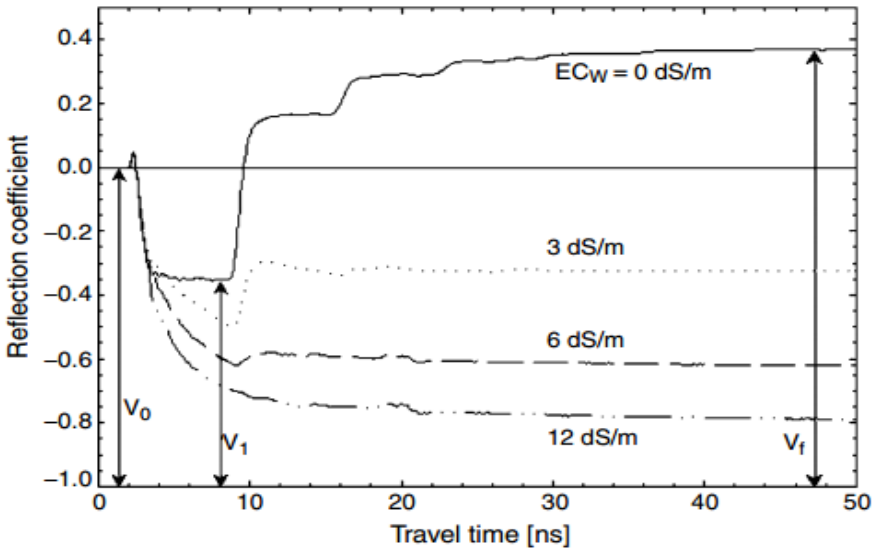

Figure 2-3 Attenuation of TDR signal due to increasing soil solution electrical conductivity

Dalton et al. (1984) showed soil water content is obtained from the measurement of velocity of propagation of high-frequency electromagnetic pulse signals which can be determined from the time axis of the TDR trace. The determination of electrical conductivity is possible by measuring the attenuation of the reflected signal, making use of the reflection coefficient or amplitude axis of the TDR trace.

At the end of each TDR wave guide, the launched electromagnetic pulse is reflected back to its source (see Figure 2-4). Therefore, the path length is twice the length of the wave guide, / (in meters), and the measured transit time, t (in seconds), gives the propagation velocity of the pulse (in meters per seconds):

$$v = \left(\frac{2l}{t}\right) \tag{5}$$

if dispersion is negligible, then v can be given simply in terms of relative dielectric constant of the medium, E, and the velocity of light in free space, c (meters per seconds)

$$v = \left(\frac{c}{\varepsilon}\right)^{\frac{1}{2}} \tag{6}$$

Therefore, the relative dielectric constant is given by:

$$\varepsilon = \left(\frac{ct}{2l}\right)^{\frac{1}{2}} \tag{7}$$

Since, the dielectric constant of water is much greater than that of the air and the soil grains, the presence of water should be easily detected.

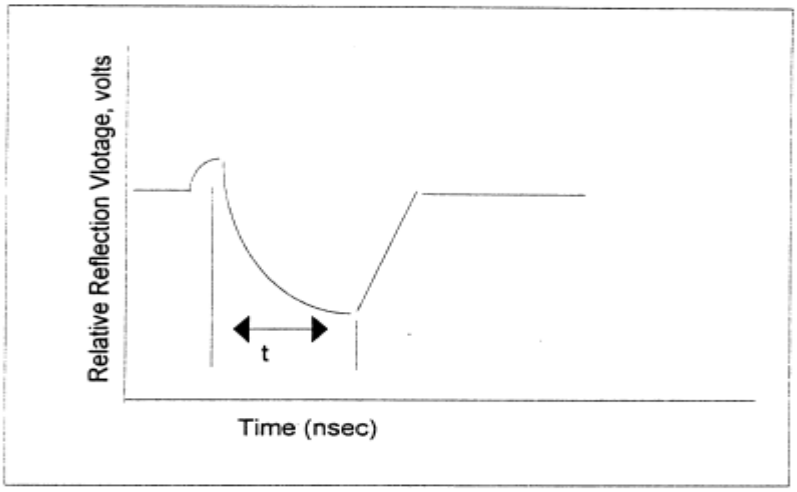

Figure 2-4 Schematic Diagram of a typical signal of the TDR showing the travel time (Dalton et al. 1984)

The electrical conductivity from pore fluid is generally the dominating term in bulk electrical conductivity of soils. This is similar to the contributions of dielectric constant by different components of soils (Sihvola 1999). By this analogy, it is assumed that a calibration relationship for bulk electrical conductivity similar to that for soil apparent dielectric constant can be expressed as

$$\sqrt{EC_b}\frac{\rho_w}{\rho_d} = c + dw \tag{8}$$

Given the calibration equations relating apparent dielectric constant and bulk electrical conductivity to soil water content and dry density, it is natural to assume that we can obtain soil water content and dry density by simultaneously solving equations (3) and (8) which gives

$$\rho_d = \frac{d\sqrt{K_a} - b\sqrt{EC_b}}{ad - cb}\,\rho_w \tag{9}$$

$$w = \frac{c\sqrt{K_a} - a\sqrt{EC_b}}{b\sqrt{EC_b} - d\sqrt{K_a}} \tag{10}$$

Time domain transmissometry (TDT) is an analogous technique that measures the transmitted (rather than reflected) impulse. Together, they provide a powerful means of analyzing

electrical or optical transmission media such as coaxial cable and optical fiber. The TDT method of permittivity determination is similar to TDR in that signal travel time is measured , which is directly related to the apparent permittivity(K_a) of the sample in which the probe is embedded, as described by:

$$K_a = \left(\frac{c.t}{L}\right)^2 \quad (11)$$

Where $K_a \sim \varepsilon$ under lossless conditions, c the speed of light in vacuum (3×10^8 ms^{-1}), t the travel time (s) of an EM signal propagating along the embedded probe and L is the probe length (m). For most applications, θ_{sensor} (water content estimated with the sensor) can be estimated from K_a measurements using either empirical equations (Topp et al., 1980; Malicki et al., 1996) or dielectric mixing models (Dirksen and Dasberg, 1993; Friedman, 1998; Robinson et al., 2005).

Most popular Acclima TDT sensor is a transmission line sensor employing Equation 11 to measure K_a. From the measured K_a value, the TDT system estimates θ (θ_{sensor}) using a simple dielectric mixing model (Roth et al., 1990) applicable to many soil types, as given by the equation

$$\theta_{sensor} = \left[\left(\frac{K_a^{\alpha} - (1-\emptyset)\epsilon_s^{\alpha} - \emptyset\epsilon_a^{\alpha}}{\epsilon_w^{\alpha} - \epsilon_a^{\alpha}}\right)\right]$$

Where $\varepsilon_s = 4$, $\varepsilon_w = 80$, $\varepsilon_a = 1$, $\alpha = 0.5$ and ϕ = soil porosity and is 0.5.

2.4.2 Laboratory Measurement of Infiltration

A large number of mathematical models have been developed to evaluate the computation of infiltration. In general, One-dimensional vertical infiltration can be described by employing the infiltration models which can be classified into physically based models, semi-empirical and empirical models (Mishra et al., 1999). The semi-empirical and empirical models such as Kostiakov and Horton models are usually derived from either field or laboratory experimental data, and they are always in the form of simple equations (Lie et al., 1988; Mishra et al., 2003). However semi-empirical models cannot provide the detailed information of infiltration process and their physical meaning is not robust. Compared to the semi-empirical and empirical models, the physically based models can

substantially describe the detailed infiltration process. Among the physically based models, the most commonly used ones are Richard's equation and Green-Ampt model. Also, these models in general do not describe the soil water redistribution process and the hysteretic behavior within the unsaturated zone (Espinoza 1999). Owing to these limitations, it is useful to perform laboratory investigation as an alternative approach of study. Laboratory study also offers the advantage that all related conditions and soil properties can be carefully controlled when compared with the field tests.

2.4.2.1 Laboratory Measurement of Infiltration using Soil Column Model

Soil Column apparatus is a well adopted approach for infiltration study. Several researchers have used soil column apparatus in infiltration studies. Freeze and Banner (1969) described a soil column apparatus to simulate unsaturated flow above a recharging or discharging groundwater flow system. In the apparatus, the tensiometer–transducer system was used to measure total head at different elevations. The tensiometers were connected to one transducer through a 24-port valve and further linked to an oscillator and a chart recorder. The inflow system of the apparatus could apply water to the top of the soil column, and the outflow system could produce two basal boundary conditions, which were constant outflow rate and constant atmospheric pressure. The size of the acrylic cylinder was 101 mm in outer diameter, 88 mm in internal diameter, and 1340 mm in height. However, there was no Time-domain reflectometry (TDR) sensors used for volumetric water content measurement.

Houston and Houston (1995) conducted various experiments using vertical and horizontal soil columns to study the effects of initial soil suction, direction of infiltration, and void ratio on the infiltration rates of various soils. Stormont and Anderson (1999) used a soil column apparatus to study the infiltration behavior of layered soils. The apparatus included an acrylic cylinder of 203 mm in diameter and 800 mm in height. A tensiometer-transducer system was used in the apparatus. Each tensiometer was connected to a transducer, and all the tensiometer-transducers were linked to a personal computer and data acquisition system. A water content reflectometer using two waveguides was used in the study to measure water content indirectly. Only a partial of the

waveguides could be inserted into the soil, since they are greater than the diameter of the soil column.

Choo and Yanful (2000) also reported a soil column apparatus that was comprised of an acrylic cylinder of 1022 mm in height and 108 mm in internal diameter, and a number of tensiometers and TDR waveguides. Waveguides were inserted into the soil through the wall of the acrylic column, so that part of the waveguide was attached to the acrylic wall of the soil column.

Though the soil column apparatus has been widely used in infiltration studies, there are not many details associated with the construction of the apparatus. Stauffer and Kinzelbach (2001) have used a column device consisting of a 927 mm long vertical plexiglass tube of diameter 53.5 mm for obtaining drying and wetting SWCC of sand. Four tensiometers and two gamma ray absorption probes were used to measure suction and water content variations during wetting and drying test performed in the column apparatus. The water content profile was allowed to establish within seven days, controlled by a constant head at the lower inlet of the column.

Yang et al. (2004) have presented a column testing device for infiltration study where tensiometer-transducer system and time-domain reflectometry (TDR) were placed at different depths to measure suction and water content respectively. The size of the soil column used in the study was 1 m high and 190 mm diameter. It can also be extended to 2 m or 3 m high if necessary. The TDR was placed fully into the soil column horizontally to measure the water content more accurately. The SWRs during the rain (wetting) and after rain (drying) were obtained using the column testing device.

Lins et al. (2009) have obtained drying and wetting SWCC of sandy soils from steady state and transient state experiments under various flow rates performed in a column testing device. A column of 780 mm high and 305 mm in diameter was used to place a sandy soil specimen of 540 mm high. Five tensiometers and five 3-rod TDR sensors were installed horizontally along the soil specimen for measuring suction and water content respectively. A tensiometer and a TDR sensor were installed at different depth.

Zaradava et al. (2009) have developed a column testing device for performing drainage experiment to establish suction-water content relationship for defining the unsaturated soil hydraulic conductivity. The column consists of a persplex cylinder with an inner diameter of 260 mm and 1 m in height. Four manometers were installed along the column length for measuring soil suction drainage experiment. For water content determination, vertical sand cores were removed using a copper tube (Clayton and Siddique, 1999).

All the studies showed that the transient process of infiltration is complex due to the high non-linearity of soil water characteristics and soil permeability and various boundary and initial conditions. The complexity is further increased by the hysteretic behavior of soil water interaction (e.g., Dane and Wierenga 1975; Serrano 1990).

2.5 Models for prediction of infiltration

Infiltration of water into the soil, like many other flow processes in porous media, is governed by the Richards soil moisture diffusion equation,

$$\frac{\partial \theta}{\partial t} = \nabla . k \nabla \emptyset \tag{11}$$

in which θ = the volumetric moisture content, k = the capillary conductivity, and ϕ = the total potential.

Equation 11, is the continuity equation for flow which has the flux, V, at any point defined by the Darcy equation,

$$V = -k \nabla \emptyset \tag{12}$$

It is evident from equation 12 that the flux at any point in a soil system, including the soil surface, is proportional to the hydraulic or capillary conductivity, k, and the total potential gradient, $\nabla\phi$. Therefore, the infiltration process will be affected by any factor which affects either of these two quantities.

The moisture content of a soil affects the magnitude of both k and$\nabla\phi$. It has been well recognized that infiltration to a given soil decreases with an increase in the soil moisture content. Even though earlier studies such as those conducted by Schiff and Dreibelbis (1949) and Tisdall (1951) were undertaken in specific attempt to establish this relationship, it has only been in recent years, through theoretical consideration of the mechanics of the infiltration process that general solutions of the equations of flow have been proposed which may be used to quantitatively evaluate the effect of soil moisture on infiltration.

Many equations have been developed or suggested to define the mass or depth of water infiltrated, M_f, after given time, t, into a uniform soil at constant moisture content. Some of the most common of these expressions are the following:

Kostiakov (1932) and Lewis (1937)

$$M_f = at^n \tag{13}$$

Gardner and Widtsoe (1921) and Horton (1940)

$$M_f = f_c t + de^{-kt} \tag{14}$$

Kirkham and Feng (1949)

$$M_f = S\, t^{\frac{1}{2}} + g \tag{15}$$

Philip (1954)

$$M_f = S\, t^{\frac{1}{2}} + At \tag{16}$$

As indicated, most of the equations take the form of an exponential or power function of time in which the constants (e.g. a and n of equation 13) characterize the ability of soil in its given condition to absorb water.

One of the most significant contributions to understanding the infiltration process was given by Philip (1957a) in which he presented the solution to the diffusion equation (Equation 11) for one-dimensional vertical infiltration into a uniform, semi-infinite medium, initially at a constant moisture

content. The resulting equation gives the distance from the soil surface to a point in the profile, at which the moisture content is θ as,

$$x(\theta) = \lambda(\theta)t^{\frac{1}{2}} + x(\theta)t + \psi(\theta)t^{\frac{3}{2}} \quad (17)$$

Equation 17 is particularly pertinent to the discussion in as much as it provides an insight of the importance of the soil moisture content to the infiltration process because the quantities $\lambda(\theta)$, $x(\theta)$ and $\psi(\theta)$ are functions of θ which can be evaluated from capillary conductivity and capillary diffusivity curves, and therefore reflect the quantitative influence of soil moisture on infiltration rates and amounts. It should be noted however that as time approaches infinity, Equation 17 diverges and is no longer valid.

The mass infiltration occurring in time, t, can be expressed by

$$M_f = \int_{\theta_i}^{\theta_n} x(\theta)\, d\theta + k_i t \quad (18)$$

in which θ_i = initial moisture content, θ_n = moisture content maintained at the soil surface (usually saturation), and K_i = capillary conductivity at θ_i.

Thus, according to Equation 8, the mass infiltration is equal to the sum of the water stored in the profile (represented by the integral) plus the depth of water which has flowed through the profile due to the unit gradient under dry conditions. This latter quantity, $K_i t$, can usually be neglected when the initial soil conditions are quite dry since in these cases, k_i, will be small.

2.6 Summary

From this brief review of the many papers written on diverse Infiltration aspects it should be re-emphasized that the conclusions drawn should be considered relative to the other variables in each experiment. The results of studies completed at different times in different places may or may not be comparable. The individual focus of each study may also make it difficult to relate several studies in a general manner.

Chapter 3

INFILTRATION STUDY IN FIELD

3.1 Introduction

The main objective of the study was to monitor the infiltration of rainfall water into the soil layers. As a part of the study, the site location were chosen close to the Creek where the water table is high. The three site locations are denoted as Station 1, Station 2, and Station 3. Campbell Scientific Time domain Reflectometry (TDR) Sensors and Acclima Digital Time domain Transmissometry (TDT) soil moisture sensors were installed at three different site locations as shown in Figure 3-1, 3-2, 3-3 and 3-4.

Station 1 comprised of five numbers of Acclima Digital Time domain Transmissometry (TDT) soil moisture sensors installed at different depths at a site location close to the Creek flowing near the Civil Engineering Laboratory Building area of The University of Texas at Arlington. Station 2 comprised of five numbers of Acclima Digital Time domain Transmissometry (TDT) Soil moisture sensors installed at different depths at a site location close to the Johnson Creek flowing near the Cemetery area. Station 3 comprised of five numbers of Campbell Scientific Time domain reflectometry (TDR) sensors installed at different depths at a site location close to the Creek. All these sensors are installed at a depth of 5 cm, 10 cm, 25 cm, 50 cm and 100 cm from the ground level.

The analysis and interpretation of the data obtained from different stations throws light into the variation of water content or moisture content in the soil.

Figure 3-1 Aerial View of the Three Site Locations for the installations of Sensors

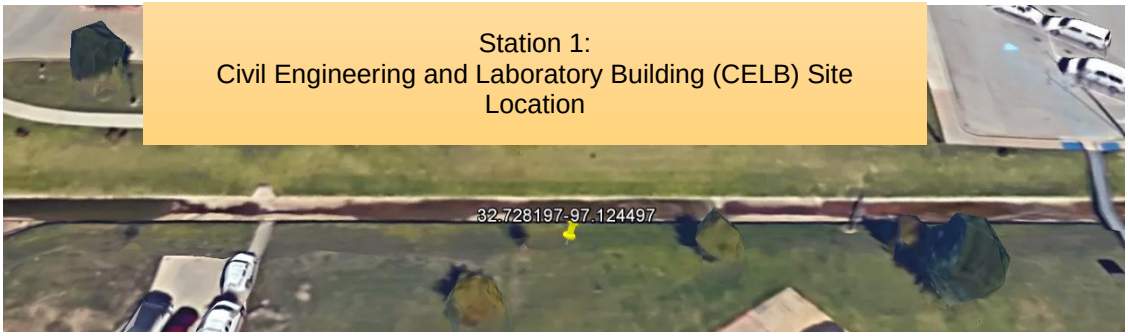

Figure 3-2 Aerial View of Civil Engg. and Lab. Building (CELB) Site Location of Station 1

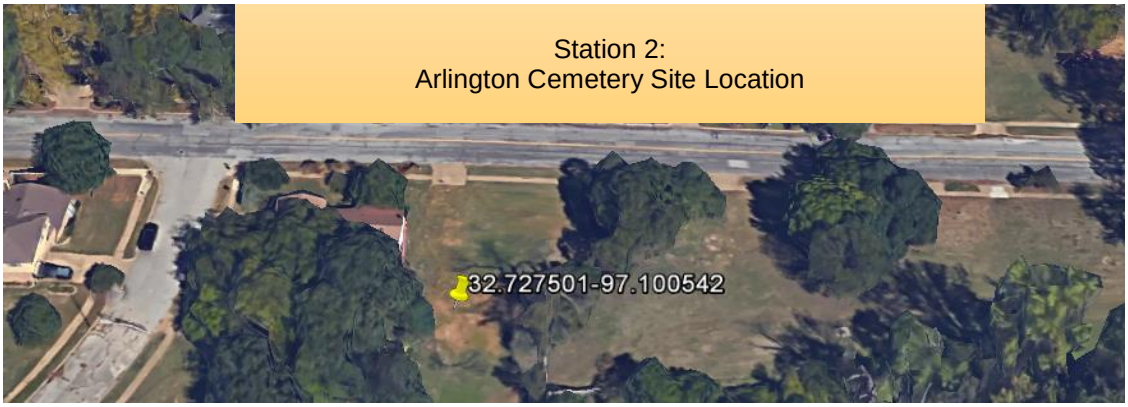

Figure 3-3 Aerial View of Arlington Cemetery Site Location of Station 2

Figure 3-4 Aerial View of W. Mitchelle St. (Bridge) Site Location of Station 3

3.2 Soil Characterization and Classification at Site Locations

3.2.1 Sieve Analysis, Specific Gravity and Hydrometer Test

Sieve Analysis (or gradation test) is a practice or procedure used (commonly used in civil engineering) to assess the particle size distribution (also called gradation) of a granular material.

The size distribution is often of critical importance to the way the material performs in use. A sieve analysis can be performed on any type of non-organic or organic granular materials including sands, crushed rock, clays, granite, feldspars, coal, and soil, a wide range of manufactured powders, grain and seeds, down to a minimum size depending on the exact method.

The sieve analysis is performed in the laboratory for the soil samples of the 3 site locations according to the ASTM Standard C 136 and the sieve data is presented in Table 3-1, 3-2, and 3-3 and the corresponding gradation graph is shown in Figure 3-5, 3-6 and 3-7.

Table 3-1 Sieve Analysis data for Station 1 Site Location

Sieve No	Diameter (mm)	Mass of Empty Sieve (g)	Mass of Sieve + Soil Retained (g)	Soil Retained (g)	Percent Retained	Cumulative Percent Retained	Percent Finer
4	4.750	775.000	775.000	0.000	0.000	0.000	100.000
10	2.000	494.000	495.000	1.000	0.230	0.230	99.770
20	0.840	630.000	680.000	50.000	11.494	11.724	88.276
40	0.425	588.000	675.000	87.000	20.000	31.724	68.276
60	0.250	551.000	613.000	62.000	14.253	45.977	54.023
200	0.075	515.000	688.000	173.000	39.770	85.747	14.253
Pan	-	500.000	562.000	62.000	14.253	100.000	0.000
			Total Weight =	435.000			

From Grain Size Distribution Curve:

% Gravel =0, D10 = 0.068 mm

%Sand =85.747, D30 = 0.125 mm

%Fines = 14.253, D60 = 0.305 mm

C_u = 4.485, C_c = 0.753

Unified Classification of Soil: SC-SM

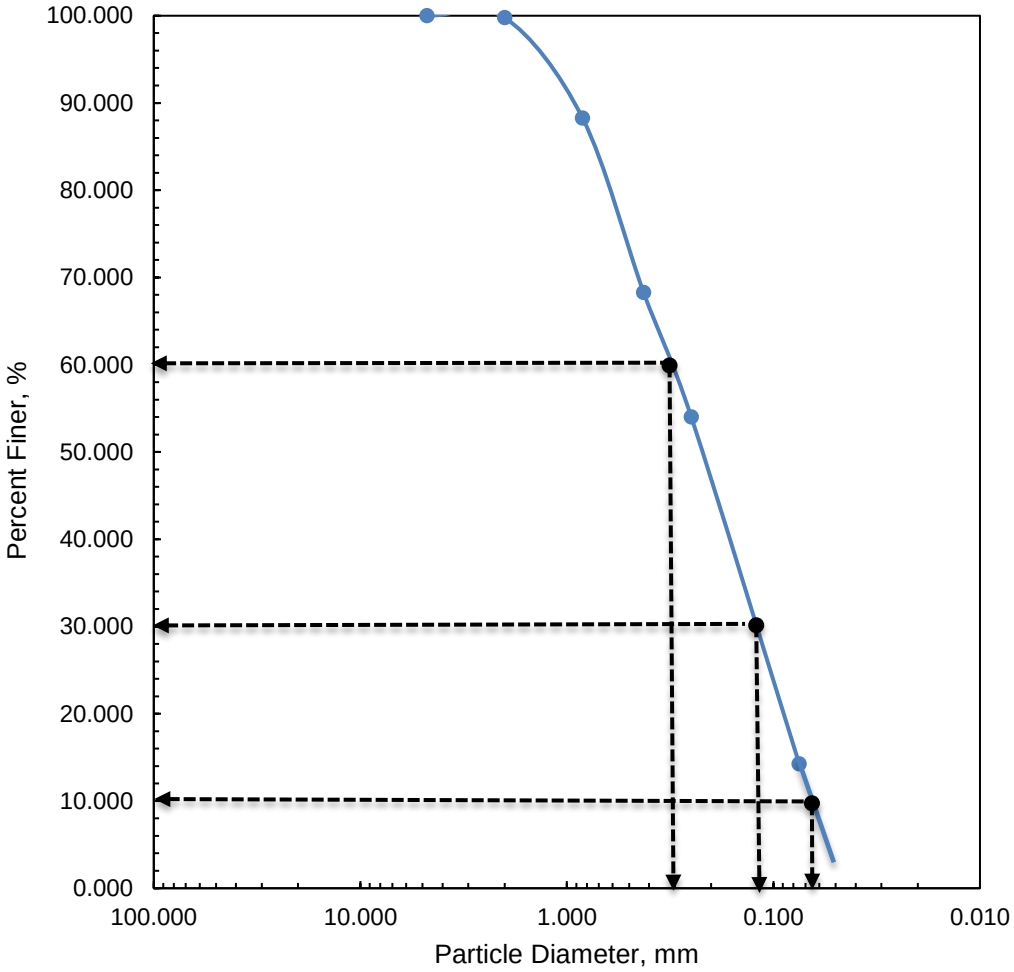

Figure 3-5 Sieve Analysis for the Station 1 Site Location

Weight of the container = 88.600 gms

Weight of the container + Dry Soil = 542.100 gms

Weight of the dry sample = 435.500 gms

Table 3-2 Sieve Analysis data for Station 2 Site Location

Sieve No	Diameter (mm)	Mass of Empty Sieve (g)	Mass of Sieve + Soil Retained (g)	Soil Retained (g)	Percent Retained	Cumulative Percent Retained	Percent Passing
4	4.750	775.000	776.000	1.000	0.231	0.231	99.769
10	2.000	494.000	501.000	7.000	1.617	1.848	98.152
20	0.840	630.000	674.000	44.000	10.162	12.009	87.991
40	0.425	588.000	663.000	75.000	17.321	29.330	70.670
60	0.250	551.000	625.000	74.000	17.090	46.420	53.580
200	0.075	515.000	685.000	170.000	39.261	85.681	14.319
Pan	0	500.000	562.000	62.000	14.319	100.000	0.000
			Total Weight =	433.000			

From Grain Size Distribution Curve:

% Gravel = 0.231, D10 = 0.065 mm

%Sand = 85.681, D30 = 0.120 mm

%Fines = 14.319, D60 = 0.265 mm

C_u = 4.077, C_c = 0.836

Unified Classification of Soil: SC

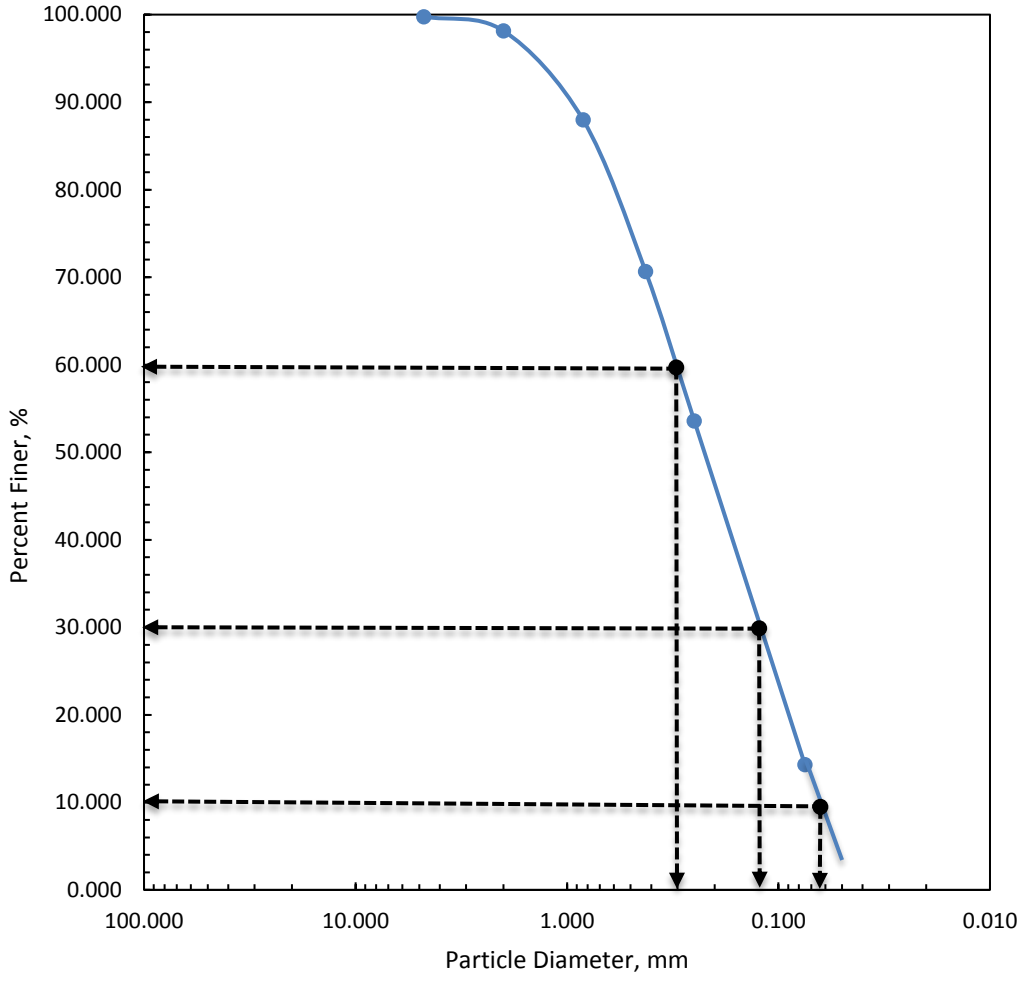

Figure 3-6 Sieve Analysis for the Station 2 Site Location

Weight of the container = 88.600 gms

Weight of the container + Dry Soil = 542.100 gms

Weight of the dry sample = 435.500 gms

Table 3-3 Sieve Analysis data for Station 3 Site Location

Sieve No	Diameter (mm)	Mass of Empty Sieve (g)	Mass of Sieve + Soil Retained (g)	Soil Retained (g)	Percent Retained	Cumulative Percent Retained	Percent Passing
4	4.750	775.000	775.000	0.000	0.000	0.000	100.000
10	2.000	494.000	495.000	1.000	0.253	0.253	99.747
20	0.840	630.000	694.000	64.000	16.203	16.456	83.544
40	0.425	588.000	679.000	91.000	23.038	39.494	60.506
60	0.250	551.000	612.000	61.000	15.443	54.937	45.063
200	0.075	515.000	632.000	117.000	29.620	84.557	15.443
Pan	-	500.000	561.000	61.000	15.443	100.000	0.000
			Total Weight =	395.000			

From Grain Size Distribution Curve:

% Gravel = 0.000, D10 = 0.061 mm

%Sand = 84.557, D30 = 0.140 mm

%Fines = 15.443, D60 =0.405 mm

C_u = 6.639, C_c =0.793

Unified Classification of Soil: SC

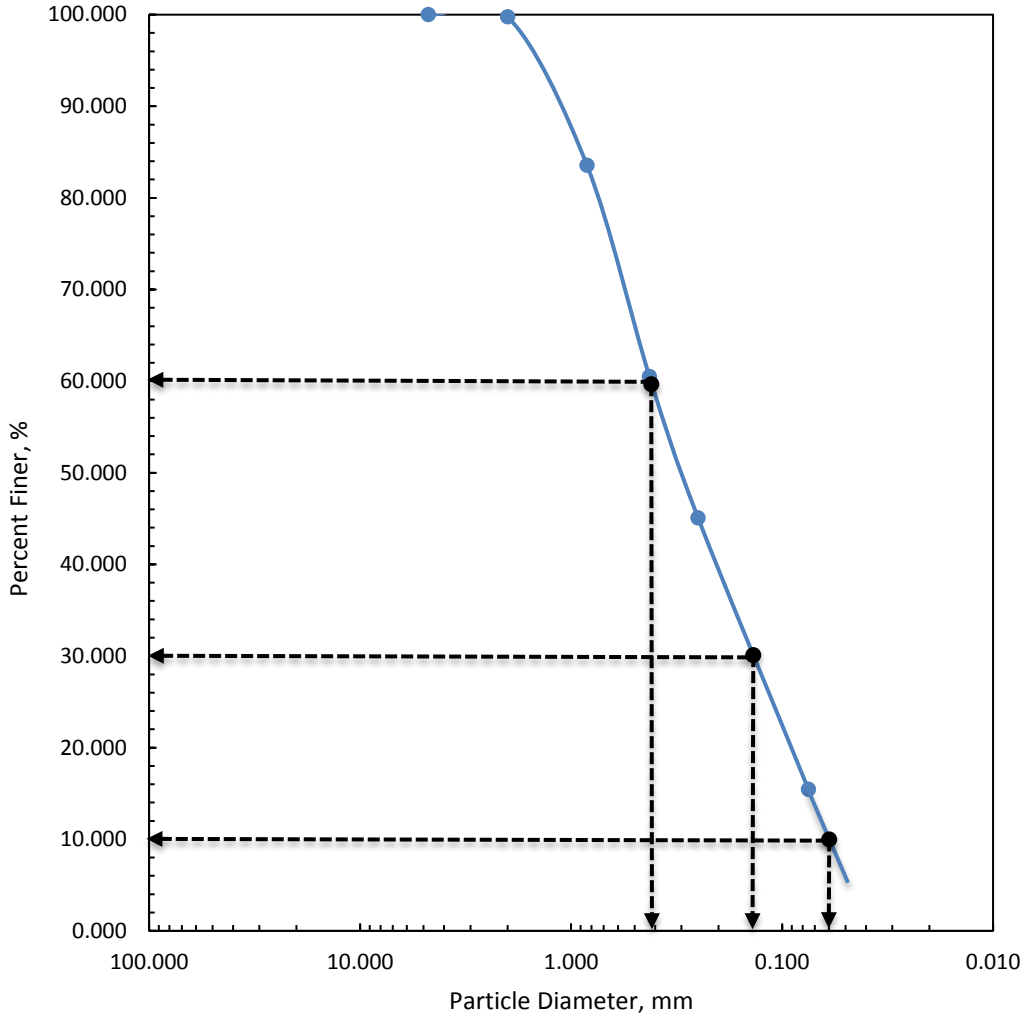

Figure 3-7 Sieve Analysis for the Station 3 Site Location

Weight of the container for Station 3 = 88.600 gms

Weight of the container + Dry for Soil Station 3= 542.100 gms

Weight of the dry sample for Station 3= 435.500 gms

Specific Gravity of soil solids is defined as the ratio of the unit weight (or density) of soil solids only to unit weight (or density) of water. Specific Gravity test is performed in the laboratory according to the ASTM D854 standards as shown in Figure 3-8. The specific gravity for the 3 site locations are calculated as shown in Table 3-4, 3-5 and 3-6.

Figure 3-8 Specific Gravity calculated according to ASTM D854

Table 3-4 Tabulation for Specific Gravity at Station 1 Site Location

Specimen No	**1**	**2**
Pycnometer Bottle Number	1	2
W_p = Mass of empty, clean pycnometer (grams)	161.23	161.25
W_{ps} = Mass of empty pycnometer + dry soils (grams)	224.43	225.11
W_B = Mass of pycnometer + dry soil + water (grams)	696.76	697.19
W_A = Mass of pycnometer + water (grams)	657.08	657.13
Specific Gravity (G_s)	2.69	2.68
Water Temperature	24	24
Correction Factor (K)	0.9991	0.9991
Specific Gravity of soil solids at 20° C (G_s)	2.68	2.68
Final Specific Gravity	2.68	

Table 3-5 Tabulation for Specific Gravity at Station 2 Site Location

Specimen No	**1**	**2**
Pycnometer Bottle Number	1	2
W_p = Mass of empty, clean pycnometer (grams)	161.25	161.25
W_{ps} = Mass of empty pycnometer + dry soils (grams)	213.47	215.63
W_B = Mass of pycnometer + dry soil + water (grams)	690.14	691.59
W_A = Mass of pycnometer + water (grams)	657.45	657.68
Specific Gravity (G_s)	2.67	2.66
Water Temperature	23	23
Correction Factor (K)	0.9993	0.9993
Specific Gravity of soil solids at 20° C (G_s)	2.67	2.65
Final Specific Gravity	2.66	

Table 3-6 Tabulation for Specific Gravity at Station 3 Site Location

Specimen No	**1**	**2**
Pycnometer Bottle Number	1	2
W_p = Mass of empty, clean pycnometer (grams)	161.23	161.25
W_{ps} = Mass of empty pycnometer + dry soils (grams)	226.48	225.33
W_B = Mass of pycnometer + dry soil + water (grams)	698.17	697.59
W_A = Mass of pycnometer + water (grams)	657.03	657.20
Specific Gravity (G_s)	2.71	2.70
Water Temperature	25	25
Correction Factor (K)	0.9988	0.9988
Specific Gravity of soil solids at 20° C (G_s)	2.70	2.70
Final Specific Gravity	2.70	

Hydrometer Analysis is done to measure the proportion of particles smaller than 0.075 mm. The hydrometer test is performed in the laboratory according to ASTM D 422 Standard. The hydrometer analysis data are shown in Table 3-7, 3-8, and 3-9 and the corresponding graphs are shown in Figure 3-9, 3-10 and 3-11.

Table 3-7 Hydrometer Analysis Data for Station 1 Site Location

Date	Time	Elapsed Time (min)	Temp	Actual Hydrometer Reading Ra	Hydrometer Correction for Meniscus	**L** from Table 1	**K** from Table 2	**D** (mm)	C_T from Table 3	**a** from Table 4	Corrected Hydrometer Reading R_c	% Finer (**P**)	% Adjusted Finer P_A
4/10/2016	21:17	0	25	57	58	6.8	0.01267	0.000	1.30	0.99	-	-	-
	21:19	2	25	45	46	8.8	0.01267	0.026	1.30	0.99	41.30	74.34	0.94
	21:22	5	25	41	42	9.4	0.01267	0.017	1.30	0.99	37.30	67.14	0.85
	21:25	8	25	38	39	9.9	0.01267	0.014	1.30	0.99	34.30	61.74	0.78
	21:32	15	25	31	32	11.1	0.01267	0.011	1.30	0.99	27.30	49.14	0.62
	21:47	30	24	26	27	11.9	0.01282	0.008	1.00	0.99	22.00	39.6	0.50
	22:17	60	24	21	22	12.7	0.01282	0.006	1.00	0.99	17.00	30.6	0.39
4/11/2016	21:17	1440	23	14	15	13.8	0.01297	0.001	0.70	0.99	9.70	17.46	0.22

Specific Gravity of Solids: 2.68, Dispersing Agent: Sodium Hexametaphosphate.

Weight of Soil Sample: 55 gms.

Zero Correction: 5, Meniscus Correction: 1.

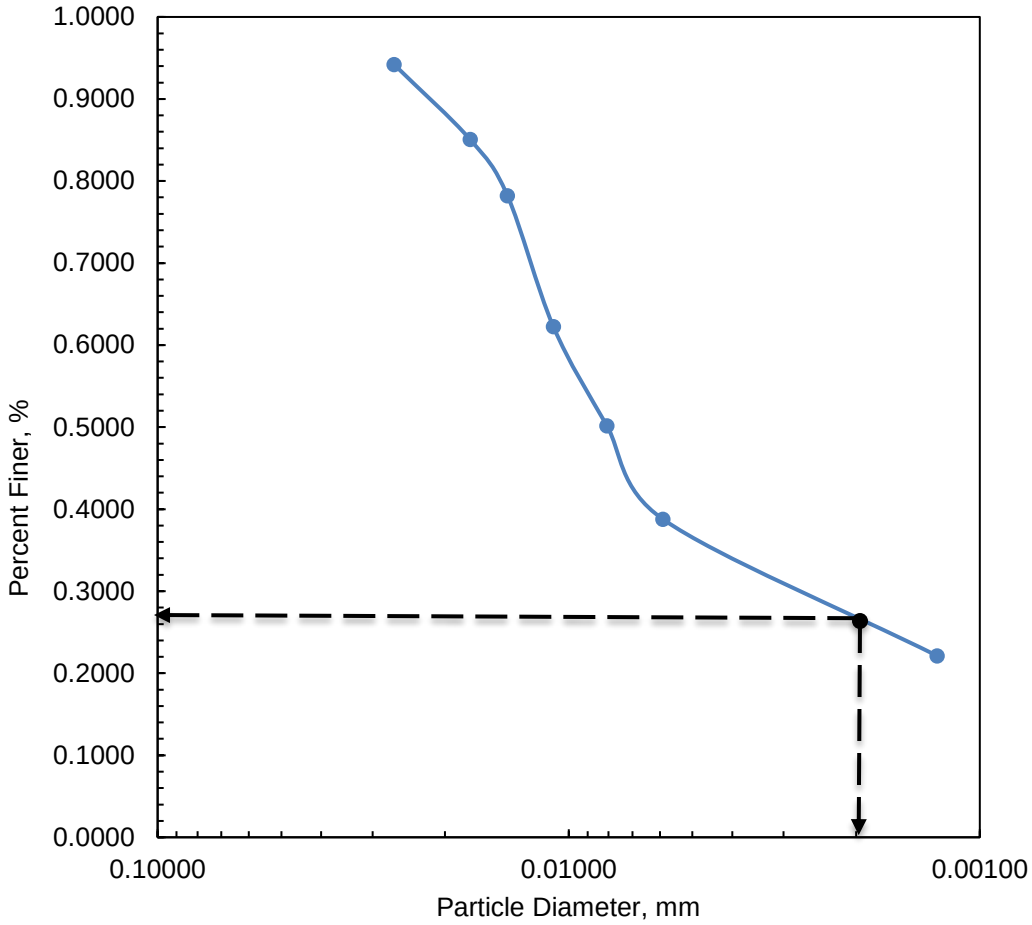

Figure 3-9 Hydrometer Analysis for the Station 1 Site Location

% Silt = 73 corresponding to 10.405 for the total sample.

% Clay = 27 corresponding to 3.848 for the total sample.

Specific Gravity of Solids: 2.66,

Dispersing Agent: Sodium Hexametaphosphate.

Weight of Soil Sample: 50 gms.

Zero Correction: 5,

Meniscus Correction: 1.

Table 3-8 Hydrometer Analysis Data for Station 2 Site Location

Date	Time	Elapsed Time (min)	Temp	Actual Hydrometer Reading Ra	Hydrometer Correction for Meniscus	**L** from Table 1	**K** from Table 2	**D** (mm)	$\mathbf{C_T}$ from Table 3	**a** from Table 4	Corrected Hydrometer Reading $\mathbf{R_c}$	% Finer (**P**)	% Adjusted Finer $\mathbf{P_A}$
4/12/2016	20:07	0	25	59	60	6.5	0.01286	0.000	1.30	1.00	-	-	-
	20:09	2	25	55	56	7.1	0.01286	0.024	1.30	1.00	51.30	102.6	1.32
	20:12	5	25	47	48	8.4	0.01286	0.017	1.30	1.00	43.30	86.6	1.11
	20:15	8	25	45	46	8.8	0.01286	0.013	1.30	1.00	41.30	82.6	1.06
	20:22	15	24	42	43	9.2	0.01301	0.010	1.00	1.00	38.00	76.0	0.98
	20:37	30	24	38	39	9.9	0.01301	0.007	1.00	1.00	34.00	68.0	0.87
	21:07	60	23	36	37	10.2	0.01317	0.005	0.70	1.00	31.70	63.4	0.81
4/13/2016	20:07	1440	22	32	33	10.9	0.01332	0.001	0.40	1.00	27.40	54.8	0.70

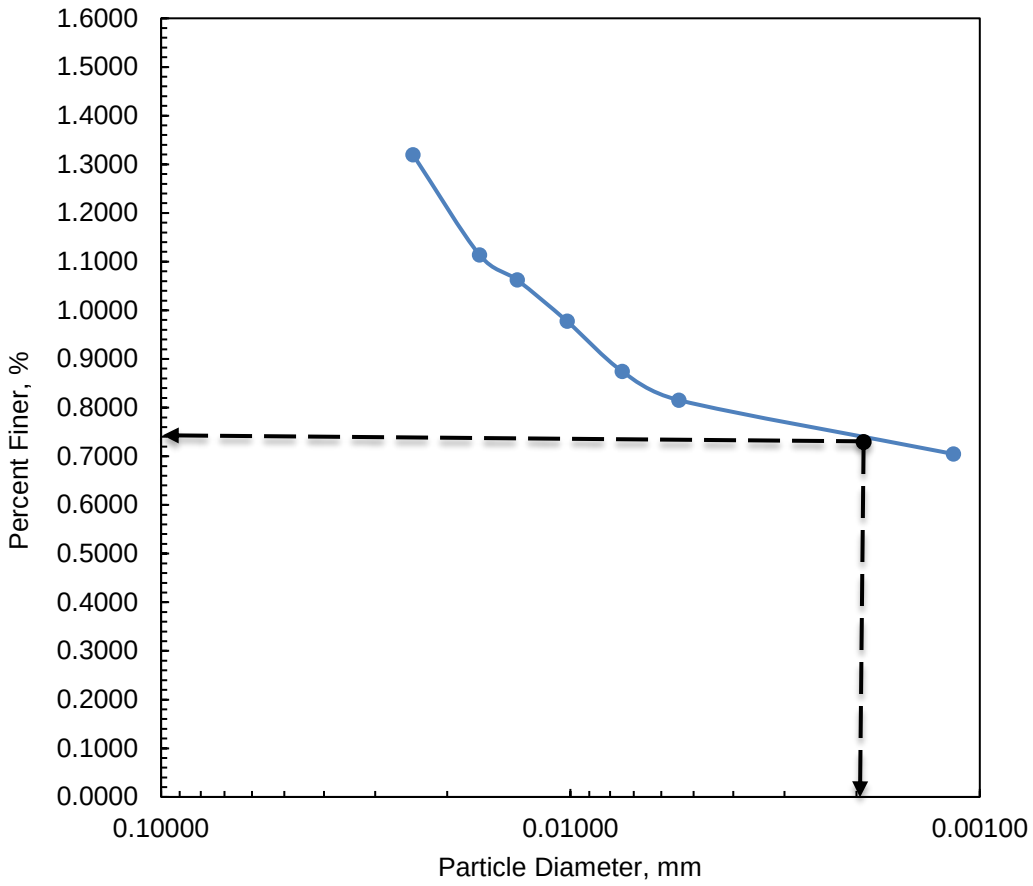

Figure 3-10 Hydrometer Analysis for the Station 2 Site Location

% Silt = 26 corresponding to 3.723 for the total sample.

% Clay = 74 corresponding to 10.596 for the total sample.

Specific Gravity of Solids: 2.7,

Dispersing Agent: Sodium Hexametaphosphate.

Weight of Soil Sample: 60 Gms.

Zero Correction: 4

Meniscus Correction: 1.

Table 3-9 Hydrometer Analysis Data for Station 2 Site Location

Date	Time	Elapsed Time (min)	Temp	Actual Hydrometer Reading Ra	Hydrometer Correction for Meniscus	**L** from Table 1	**K** from Table 2	**D** (mm)	C_T from Table 3	**a** from Table 4	Corrected Hydrometer Reading R_c	% Finer (**P**)	% Adjusted Finer P_A
4/14/2016	10:49	0	24	57	58	6.8	0.01282	0.000	1.00	0.99	-	-	-
	10:51	2	24	52	53	7.6	0.01282	0.025	1.00	0.99	49.00	80.85	1.03
	10:54	5	24	47	48	8.4	0.01282	0.017	1.00	0.99	44.00	72.60	0.93
	10:57	8	24	45	46	8.8	0.01282	0.013	1.00	0.99	42.00	69.30	0.89
	11:04	15	24	40	41	9.6	0.01282	0.010	1.00	0.99	37.00	61.05	0.78
	11:19	30	24	36	37	10.2	0.0128	0.007	1.00	0.99	33.00	54.45	0.70
	11:49	60	23	31	32	11.1	0.0129	0.005	0.70	0.99	27.70	45.70	0.58
4/15/2016	10:49	1440	23	29	30	11.4	0.0129	0.001	0.70	0.99	25.70	42.40	0.54

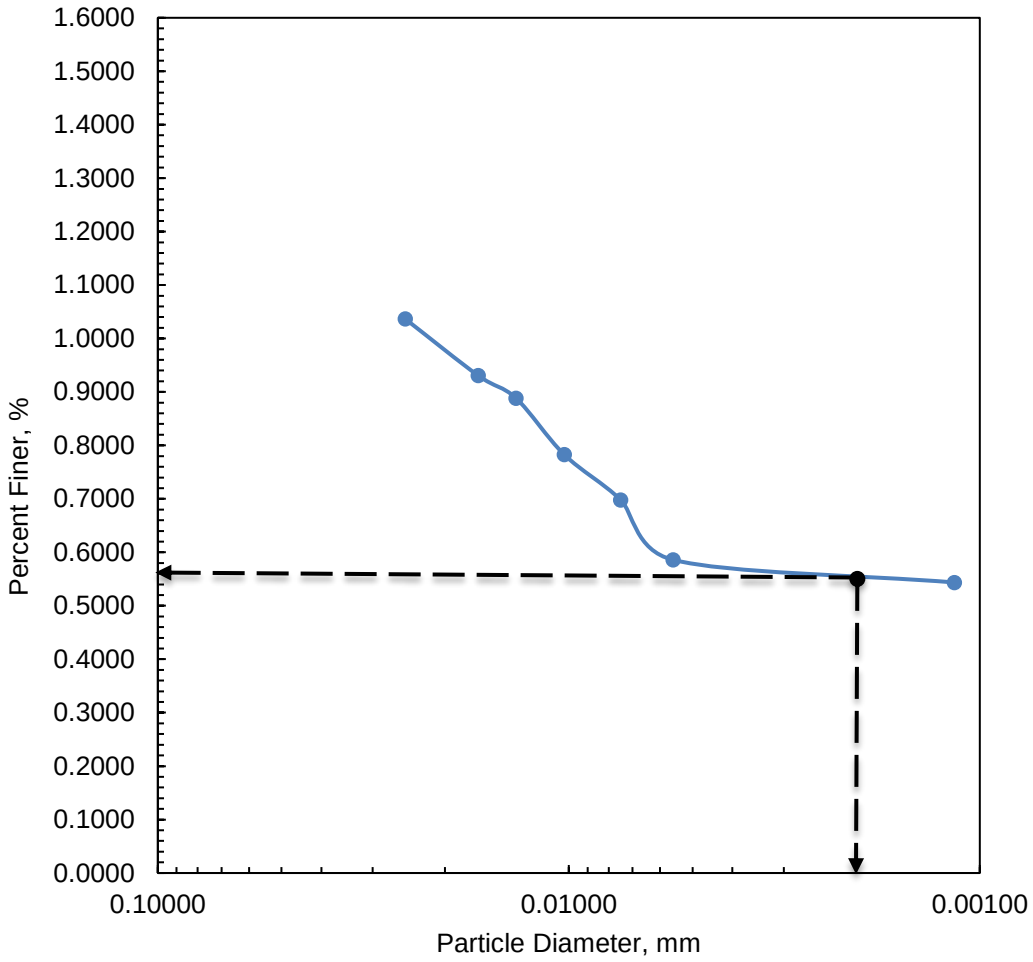

Figure 3-11 Hydrometer Analysis for the Station 3 Site Location

% Silt = 44 corresponding to 6.795 for the total sample.

% Clay = 56 corresponding to 8.648 for the total sample.

3.2.2 Atterberg Limit Test

The Atterberg limits created by Swedish Scientist, Albert Atterberg are a basic measure of the critical water contents of a fine-grained soil: its shrinkage limit, plastic limit and liquid limit. As dry, clayey soil takes on increasing amount of water, it undergoes distinct changes in behavior and consistency. Depending on the water content of the soil, it may appear in four states: solid, semi-solid, plastic and liquid. In each state, the consistency and behavior of a soil is different and consequently so are its engineering properties. Thus, the boundary between each state can be defined based on a change in the soil's behavior.

3.2.2.1 Liquid Limit Test

The liquid limit is conceptually defined as the water content at which the behavior of a clayey soil changes from plastic to liquid. The transition is a gradual process and the shear strength is not zero at this point.

Table 3-10 Liquid Limit Test for Station 1 Location

Item	Test No.				
	1	2	3	4	5
Can No.	1	2	3	4	5
Mass of Can, W_1 (gm)	1.00	1.00	1.00	1.00	1.00
Mass of Can + Moist Soil, W_2 (gm)	8.20	10.70	11.50	8.60	16.90
Mass of Can + Dry Soil, W_3 (gm)	6.90	8.70	9.10	6.80	12.80
Moisture Content, w %	22.03	25.97	29.63	31.03	34.75
Number of Blows, N	35	29	27	24	20

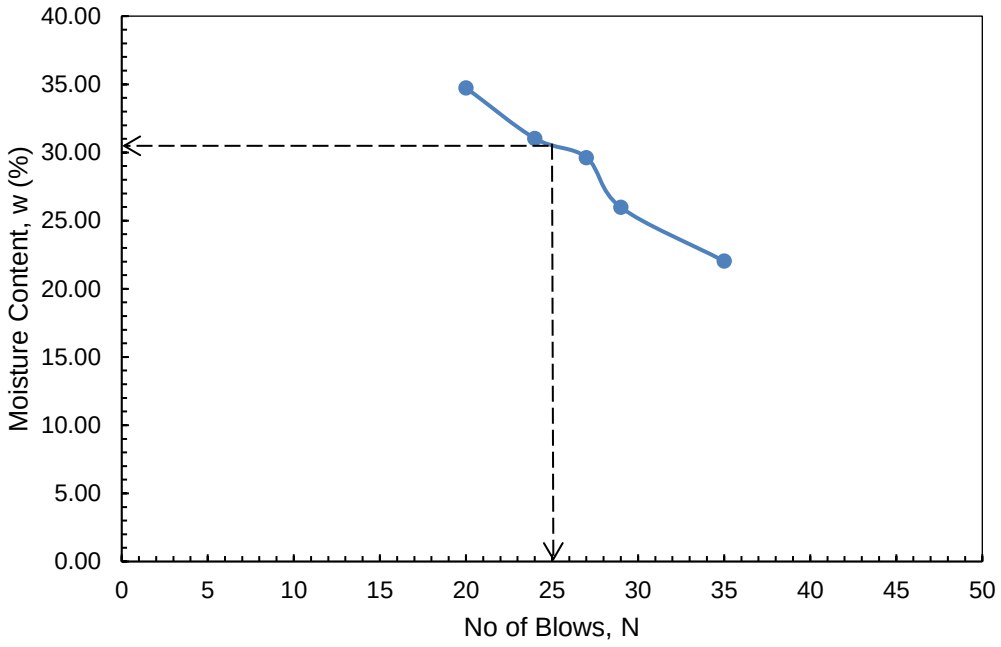

Figure 3-12 Liquid Limit Test for the Station 1 Site Location

Liquid Limit calculated from the graph = 30.5

Table 3-11 Liquid Limit Test for Station 2 Location

Item	Test No.				
	1	2	3	4	5
Can No.	6	7	8	9	10
Mass of Can, W_1 (gm)	1.00	1.00	1.00	1.00	1.00
Mass of Can + Moist Soil, W_2 (gm)	6.70	8.30	11.50	12.30	9.70
Mass of Can + Dry Soil, W_3 (gm)	5.50	6.60	8.90	9.28	7.26
Moisture Content, w %	26.67	30.36	32.91	36.47	38.98
Number of Blows, N	31	28	27	23	21

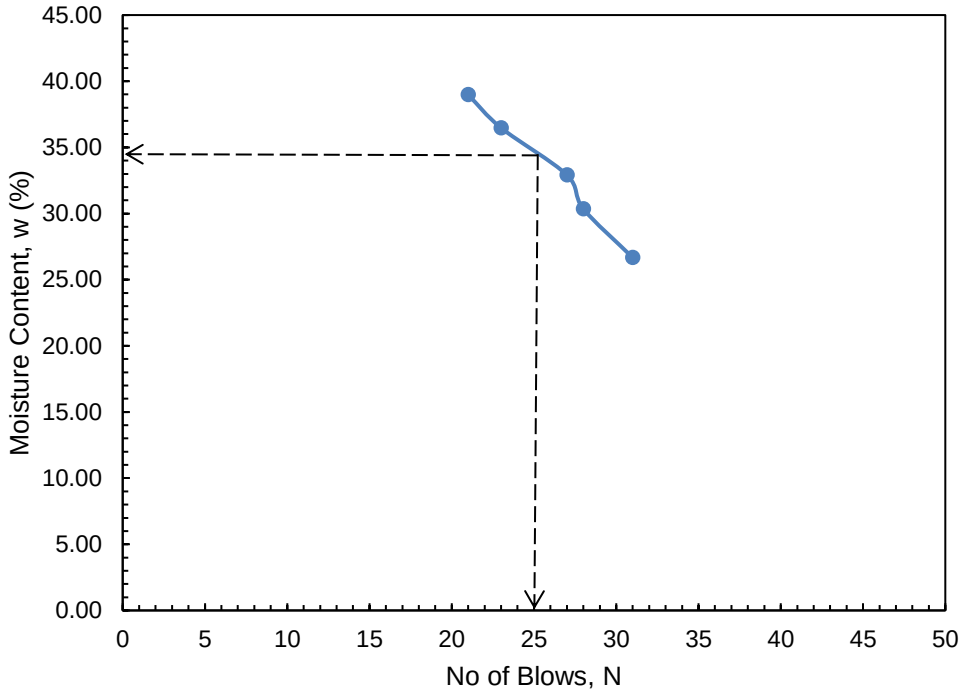

Figure 3-13 Liquid Limit Test for the Station 2 Site Location

Liquid Limit calculated from the graph = 34.5

Table 3-12 Liquid Limit Test for Station 3 Location

Item	Test No.				
	1	2	3	4	5
Can No.	11	12	13	14	15
Mass of Can, W_1 (gm)	1.00	1.00	1.00	1.00	1.00
Mass of Can + Moist Soil, W_2 (gm)	8.50	9.40	8.70	11.20	6.90
Mass of Can + Dry Soil, W_3 (gm)	6.90	7.45	6.85	8.59	5.24
Moisture Content, w %	27.20	30.23	31.62	34.39	39.15
Number of Blows, N	34	30	28	23	19

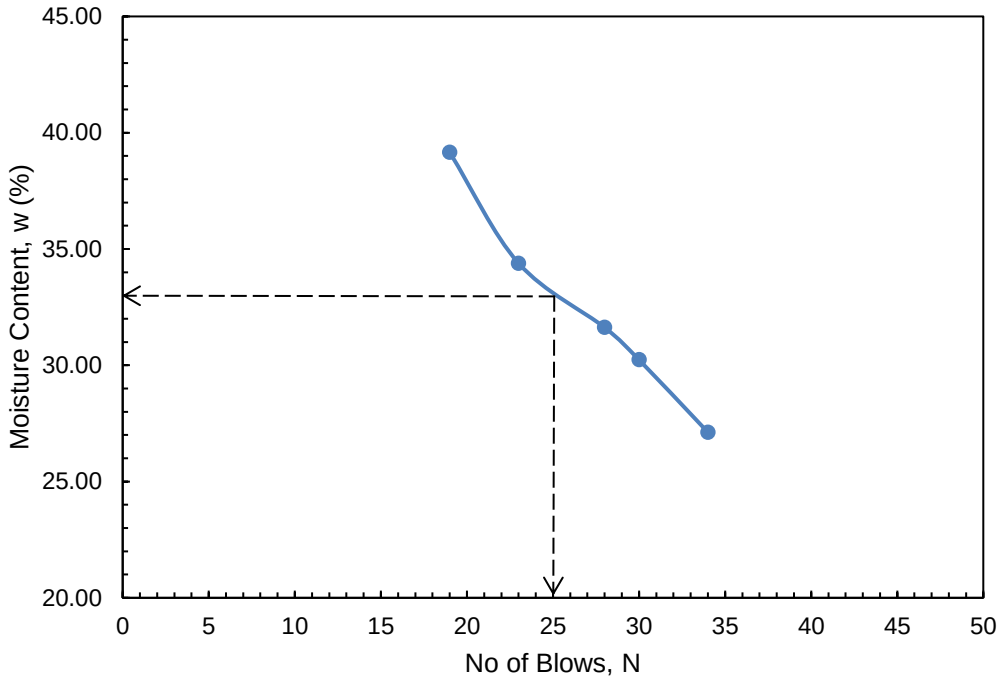

Figure 3-14 Liquid Limit Test for the Station 3 Site Location

Liquid Limit calculated from the graph = 33

3.2.2.2 Plastic Limit Test

The plastic limit is defined as the moisture content at which a soil begins to behave as a plastic material. A plastic material can be molded into a shape and the material will retain that shape.

Table 3-13 Plastic Limit Test for Station 1 Location

Item	Test No.		
	1	2	3
Can No.	1	2	3
Mass of Can, W_1 (gm)	1.00	1.00	1.00
Mass of Can + Moist Soil, W_2 (gm)	1.70	1.60	1.70
Mass of Can + Dry Soil, W_3 (gm)	1.56	1.48	1.58
Moisture Content, w %	25.00	25.00	20.69
Plastic Limit (PL) = Average w %	23.6		
Plasticity Index (PL) = LL- PL	7.0		

Table 3-14 Plastic Limit Test for Station 2 Location

Item	Test No.		
	1	2	3
Can No.	6	7	8
Mass of Can, W_1 (gm)	1.00	1.00	1.00
Mass of Can + Moist Soil, W_2 (gm)	1.80	2.30	1.90
Mass of Can + Dry Soil, W_3 (gm)	1.65	2.18	1.81
Moisture Content, w %	23.08	10.17	11.11
Plastic Limit (PL) = Average w %	14.8		
Plasticity Index (PL) = LL- PL	20.0		

Table 3-15 Plastic Limit Test for Station 3 Location

Item	Test No.		
	1	2	3
Can No.	11	12	13
Mass of Can, W_1 (gm)	1.00	1.00	1.00
Mass of Can + Moist Soil, W_2 (gm)	2.10	2.20	2.20
Mass of Can + Dry Soil, W_3 (gm)	1.92	1.98	2.01
Moisture Content, w %	19.57	22.45	18.81
Plastic Limit (PL) = Average w %	20.3		
Plasticity Index (PL) = LL- PL	13.0		

3.2.2.3 Shrinkage Limit Test

Shrinkage Limit is defined as the water content at which a reduction in water content will not cause a decrease in volume of the soil mass but an increase in water will increase the volume.

It is calculated graphically from the chart when Liquid Limit (LL) and Plasticity Index (PI) is known for the soil sample.

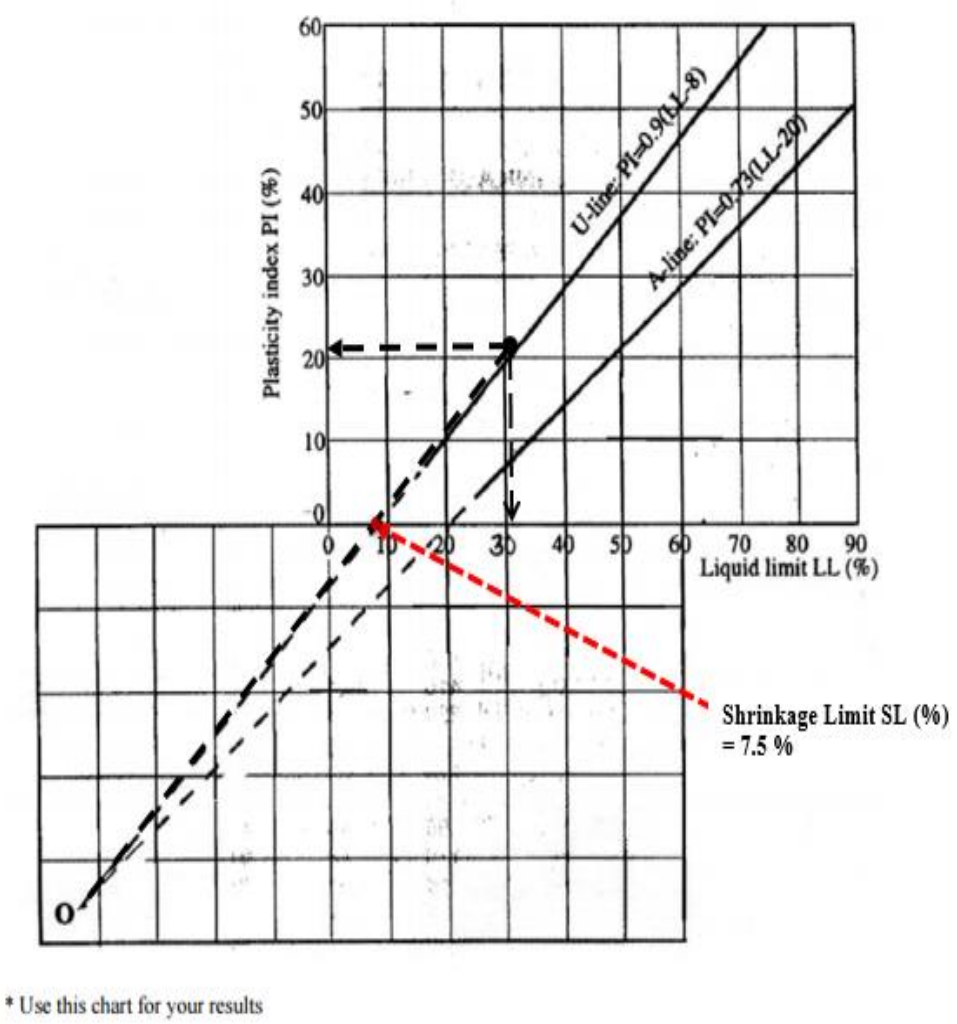

Figure 3-15 Shrinkage Limit determination for Station 1 Site Location

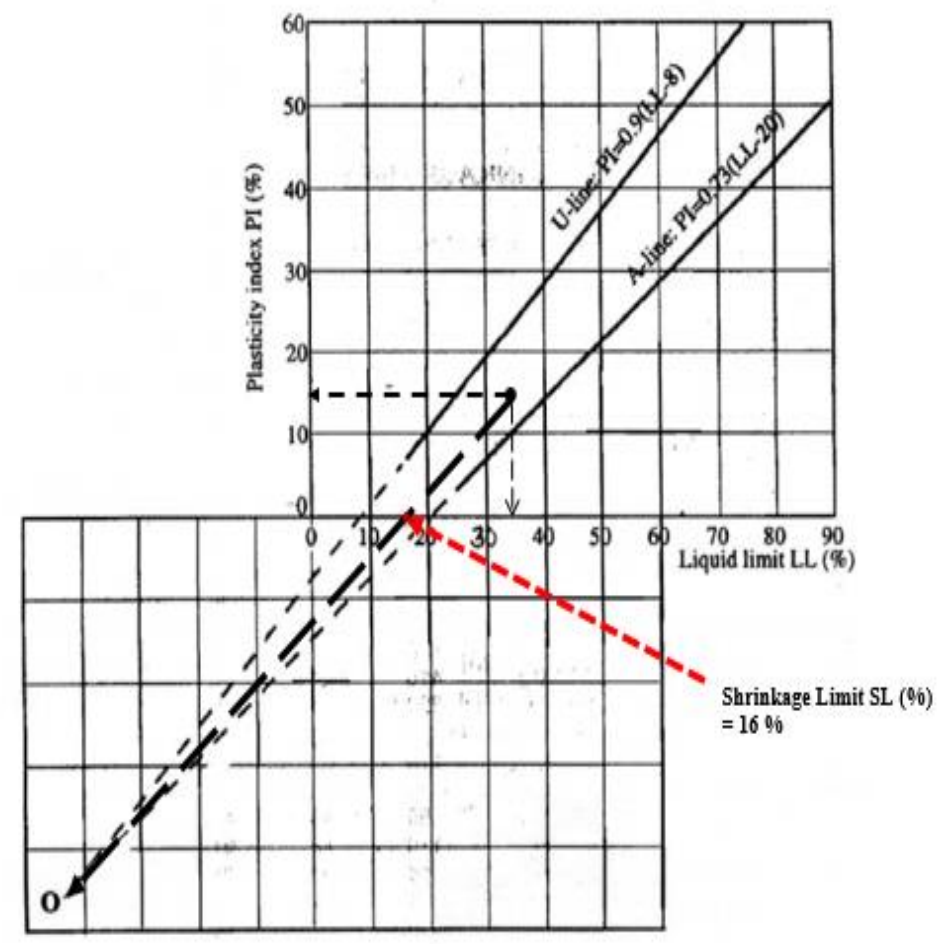

Figure 3-16 Shrinkage Limit determination for Station 2 Site Location

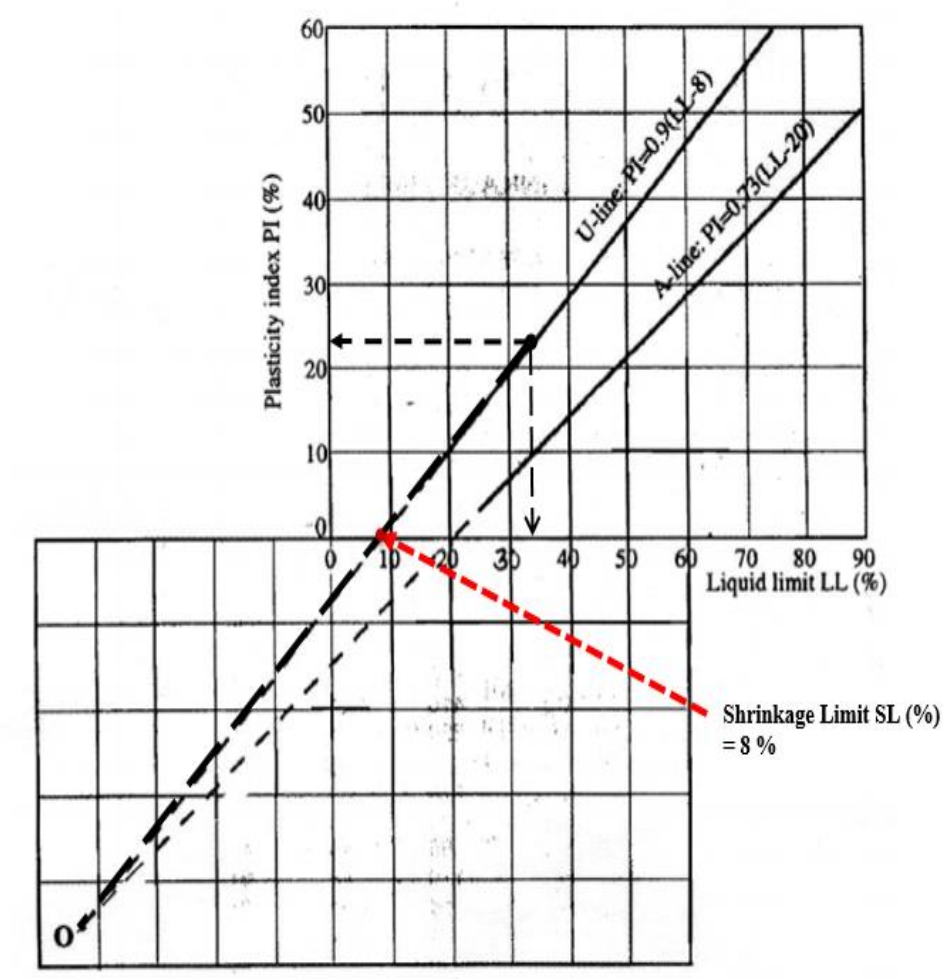

* Use this chart for your results

Figure 3-17 Shrinkage Limit determination for Station 3 Site Location

3.2.3 Sand Cone Test

Sand Cone Method is employed for determining the bulk dry density or in-situ field density for the 3 site location. It is performed in the field according to ASTM Standard D 1556 using Ottawa 20-10 Sand. The data for the results is shown in Table 3-16, 3-17 and 3-18.

Table 3-16 Sand Cone Test for Station 1 Location

Item	Quantity	
Calibration of Unit Weight of Ottawa Sand 20-10		
1. Weight of Proctor Mold, W_1 (lbs.)	9.276	
2. Weight of Proctor Mold + Sand, W_2 (lbs.)	12.448	
3. Volume of mold, V_1 (ft^3)	1/30	
4. Dry unit weight, $g_{d(Sand)} = (W_2 - W_1)/V_1$ (pcf)	95.170	
Calibration Cone		
	1st	2nd
5. Weight of bottle+ cone + sand (before use), W_3 (lbs.)	11.636	11.636
6. Weight of bottle+ cone+ sand (after use), W_4 (lbs.)	7.538	7.519
7. Weight of Sand to fill cone, $W_c = W_3 - W_4$ (lbs.)	4.098	4.117
8. Average of W_c (lbs.)	4.108	
Results from Field Tests		
9. Weight of bottle + cone + sand (before use), W_6 (lbs.)	11.640	
10. Weight of bottle + cone + sand (after use), W_8 (lbs.)	6.341	
11. Volume of hole, $V_2 = (W_6 - W_8 - W_c)/ g_{d(sand)}$ (lbs.)	0.013	
12. Weight of gallon can, W_5 (lbs.)	0.213	
13. Weight of gallon can + moist soil, W_7 (lbs.)	1.520	
14. Weight of gallon can + dry soil, W_9 (lbs.)	1.203	
15. Moist unit weight of soil in field, $g = W_7 - W_5/V_2$ (pcf)	104.395	
16. Moisture Content in field, $w(\%) = ((W_7 - W_9) / (W_9 - W_5))*100$	30.43%	
17. Dry unit weight in field, $g_d = g/1+(w(\%)/100)$ (pcf)	80.041	
18. Dry unit weight in field, $g_d = g/1+(w(\%)/100)$ (g/cm^3)	1.282	

Table 3-17 Sand Cone Test for Station 2 Location

Item	Quantity	
Calibration of Unit Weight of Ottawa Sand 20-10		
1. Weight of Proctor Mold, W_1 (lbs.)	9.316	
2. Weight of Proctor Mold+ Sand, W_2 (lbs.)	12.522	
3. Volume of mold, V_1 (ft^3)	1/30	
4. Dry unit weight, $g_{d(Sand)} = (W_2 - W_1)/V_1$ (pcf)	96.190	
Calibration Cone		
	1st	2nd
5. Weight of bottle+ cone + sand (before use), W_3 (lbs.)	10.096	10.096
6. Weight of bottle+ cone+ sand (after use), W_4 (lbs.)	5.872	5.856
7. Weight of Sand to fill cone, $W_c = W_3 - W_4$ (lbs.)	4.224	4.240
8. Average of W_c (lbs.)	4.232	
Results from Field Tests		
9. Weight of bottle + cone + sand (before use), W_6 (lbs.)	10.090	
10. Weight of bottle + cone + sand (after use), W_8 (lbs.)	4.621	
11. Volume of hole, $V_2 = (W_6 - W_8 - W_c)/ g_{d(sand)}$ (lbs.)	0.013	
12. Weight of gallon can, W_5 (lbs.)	0.161	
13. Weight of gallon can + moist soil, W_7 (lbs.)	1.520	
14. Weight of gallon can + dry soil, W_9 (lbs.)	1.213	
15. Moist unit weight of soil in field, $g = W_7 - W_5/V_2$ (pcf)	105.676	
16. Moisture Content in field, w(%) = $((W_7 - W_9) / (W_9 - W_5))*100$	29.10%	
17. Dry unit weight in field, $g_d = g/1+(w(\%)/100)$ (pcf)	81.859	
18. Dry unit weight in field, $g_d = g/1+(w(\%)/100)$ (g/cm^3)	1.311	

Table 3-18 Sand Cone Test for Station 3 Location

Item	Quantity	
Calibration of Unit Weight of Ottawa Sand 20-10		
1. Weight of Proctor Mold, W_1 (lbs.)	9.008	
2. Weight of Proctor Mold+ Sand, W_2 (lbs.)	12.276	
3. Volume of mold, V_1 (ft^3)	1/30	
4. Dry unit weight, $g_{d(Sand)} = (W_2 - W_1)/V_1$ (pcf)	98.050	
Calibration Cone		
	1st	2nd
5. Weight of bottle+ cone + sand (before use), W_3 (lbs.)	10.462	10.462
6. Weight of bottle+ cone+ sand (after use), W_4 (lbs.)	6.423	6.406
7. Weight of Sand to fill cone, $W_c = W_3 - W_4$ (lbs.)	4.039	4.056
8. Average of W_c (lbs.)	4.048	
Results from Field Tests		
9. Weight of bottle + cone + sand (before use), W_6 (lbs.)	10.460	
10. Weight of bottle + cone + sand (after use), W_8 (lbs.)	4.972	
11. Volume of hole, $V_2 = (W_6 - W_8 - W_c)/ g_{d(sand)}$ (lbs.)	0.015	
12. Weight of gallon can, W_5 (lbs.)	0.161	
13. Weight of gallon can + moist soil, W_7 (lbs.)	1.520	
14. Weight of gallon can + dry soil, W_9 (lbs.)	1.359	
15. Moist unit weight of soil in field, $g = W_7 - W_5/V_2$ (pcf)	92.502	
16. Moisture Content in field, $w(\%) = ((W_7 - W_9) / (W_9 - W_5))*100$	17.44%	
17. Dry unit weight in field, $g_d = g/1+(w(\%)/100)$ (pcf)	78.769	
18. Dry unit weight in field, $g_d = g/1+(w(\%)/100)$ (g/cm^3)	1.262	

3.2.3 Hydraulic Conductivity Test

The falling head permeability test is a common laboratory testing method used to determine the permeability of fine grained soils with intermediate and low permeability such as silts and clays. Falling head test was performed in the laboratory according to the ASTM standard and the data for the respective soil samples are shown in Table 3-19, 3-20 and 3-21.

Table 3-19 Laboratory Hydraulic Conductivity Test for Station 1 Location

Item	Test No.		
	1	2	3
Diameter of the Specimen, D (cm)	10.160	10.160	10.160
Diameter of area of burette, d (cm)	3.175	3.175	3.175
Length of Specimen, L (cm)	10.000	10.000	10.000
Area of the specimen, A (cm^2)	81.032	81.032	81.032
Beginning head difference, h_1 (cm)	50	40	60
Ending head difference, h_2 (cm)	40	30	50
Test duration, t (s)	540	780	480
Inside cross-sectional area of burette, a (cm^2)	7.91	7.91	7.91
$k = 2.303\ \frac{aL}{At}\log\frac{h_1}{h_2}\ (\frac{cm}{s})$	4.04E-04	3.60E-04	3.71E-04
$k_{20°C} = k_{T°C}\ \frac{n_{T°C}}{n_{20°C}}\ (\frac{cm}{s})$	3.76E-04	3.28E-04	3.38E-04
Average $k_{20°C} = k_{T°C}\ \frac{n_{T°C}}{n_{20°C}}\ (\frac{cm}{s})$	3.47E-04		
Average $k_{20°C} = k_{T°C}\ \frac{n_{T°C}}{n_{20°C}}\ (\frac{m}{s})$	3.47E-06		

Table 3-20 Laboratory Hydraulic Conductivity Test for Station 2 Location

Item	Test No.		
	1	2	3
Diameter of the Specimen, D (cm)	10.160	10.160	10.160
Diameter of area of burette, d (cm)	3.175	3.175	3.175
Length of Specimen, L (cm)	10.000	10.000	10.000
Area of the specimen, A (cm^2)	81.032	81.032	81.032
Beginning head difference, h_1 (cm)	50	40	60
Ending head difference, h_2 (cm)	40	30	50
Test duration, t (s)	1679	1705	1713
Inside cross-sectional area of burette, a (cm^2)	7.91	7.91	7.91
$k = 2.303\ \frac{aL}{At}\log\frac{h_1}{h_2}\ (\frac{cm}{s})$	1.30E-04	1.65E-04	1.04E-04
$k_{20°C} = k_{T°C}\ \frac{n_{T°C}}{n_{20°C}}\ (\frac{cm}{s})$	1.15E-04	1.50E-04	9.46E-05
Average $k_{20°C} = k_{T°C}\ \frac{n_{T°C}}{n_{20°C}}\ (\frac{cm}{s})$	1.20E-04		
Average $k_{20°C} = k_{T°C}\ \frac{n_{T°C}}{n_{20°C}}\ (\frac{m}{s})$	1.19992E-06		

Table 3-21 Laboratory Hydraulic Conductivity Test for Station 3 Location

Item	Test No.		
	1	2	3
Diameter of the Specimen, D (cm)	10.160	10.160	10.160
Diameter of area of burette, d (cm)	3.175	3.175	3.175
Length of Specimen, L (cm)	10.000	10.000	10.000
Area of the specimen, A (cm^2)	81.032	81.032	81.032
Beginning head difference, h_1 (cm)	50	40	60
Ending head difference, h_2 (cm)	40	30	50
Test duration, t (s)	849	980	920
Inside cross-sectional area of burette, a (cm^2)	7.91	7.91	7.91
$k = 2.303\ \frac{aL}{At}\log\frac{h_1}{h_2}\ (\frac{cm}{s})$	2.57E-04	2.87E-04	1.94E-04
$k_{20°C} = k_{T°C}\ \frac{n_{T°C}}{n_{20°C}}\ (\frac{cm}{s})$	2.39E-04	2.61E-04	1.76E-04
Average $k_{20°C} = k_{T°C}\ \frac{n_{T°C}}{n_{20°C}}\ (\frac{cm}{s})$	2.25E-04		
Average $k_{20°C} = k_{T°C}\ \frac{n_{T°C}}{n_{20°C}}\ (\frac{m}{s})$	2.25356E-06		

3.2.4 Field Capacity and Permanent Wilting Point Test

Field Capacity is the water content of the soil two or three days after a rain or irrigation event when the remainder of water has been removed by the downward forces of gravity. The soil is considered to be at field capacity when the water potential in the soil is at -33 kPa.

Permanent Wilting Point is when the water potential in the soil is at or below -1.5 MPa, so the permanent plant wilting will occur when the volumetric water content is too low for the plant's root to extract water.

The important concept about field capacity and permanent wilting point is field capacity is not the same as saturation and soil at permanent wilting point is not necessarily dry. The difference between field capacity and permanent wilting point is termed the available water storage. Moisture content, Field capacity and Permanent Wilting Point is termed as Soil Moisture Characteristics.

Field Capacity is calculated by observing the moisture content reading obtained from the TDR and TDT sensors after the rainfall event when it is stabilized to a constant value as shown in the figures 3-18, 3-19, 3-20, 3-21, 3-22, 3-23, 3-24, 3-25, 3-26, 3-27, 3-28, 3-29, 3-30, 3-31 and 3-32 for the observation period of 08/26/2015 to 12/31/2015.

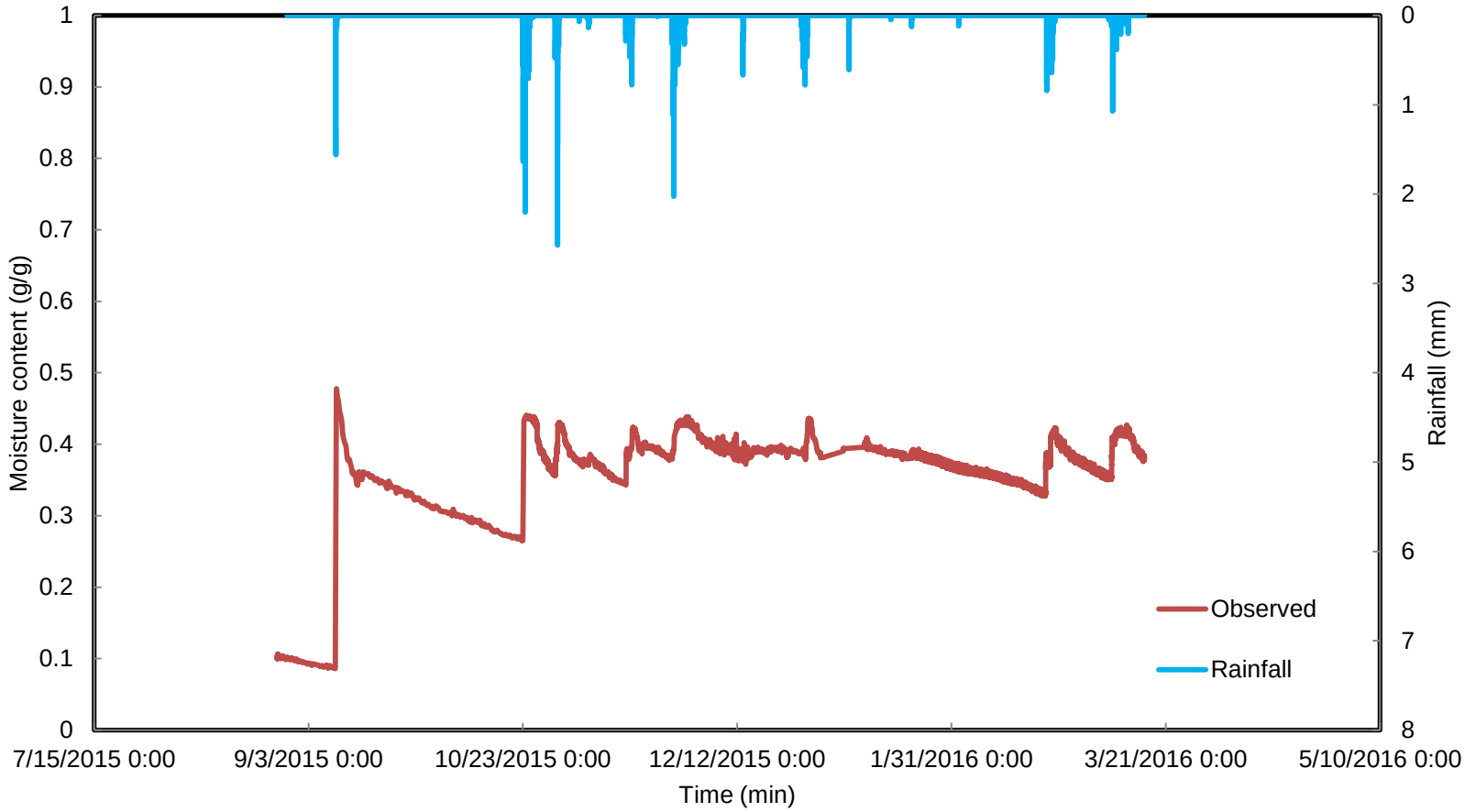

Figure 3-18 Field Capacity for the Sensor-1 at a depth of 5 cm at Station 1

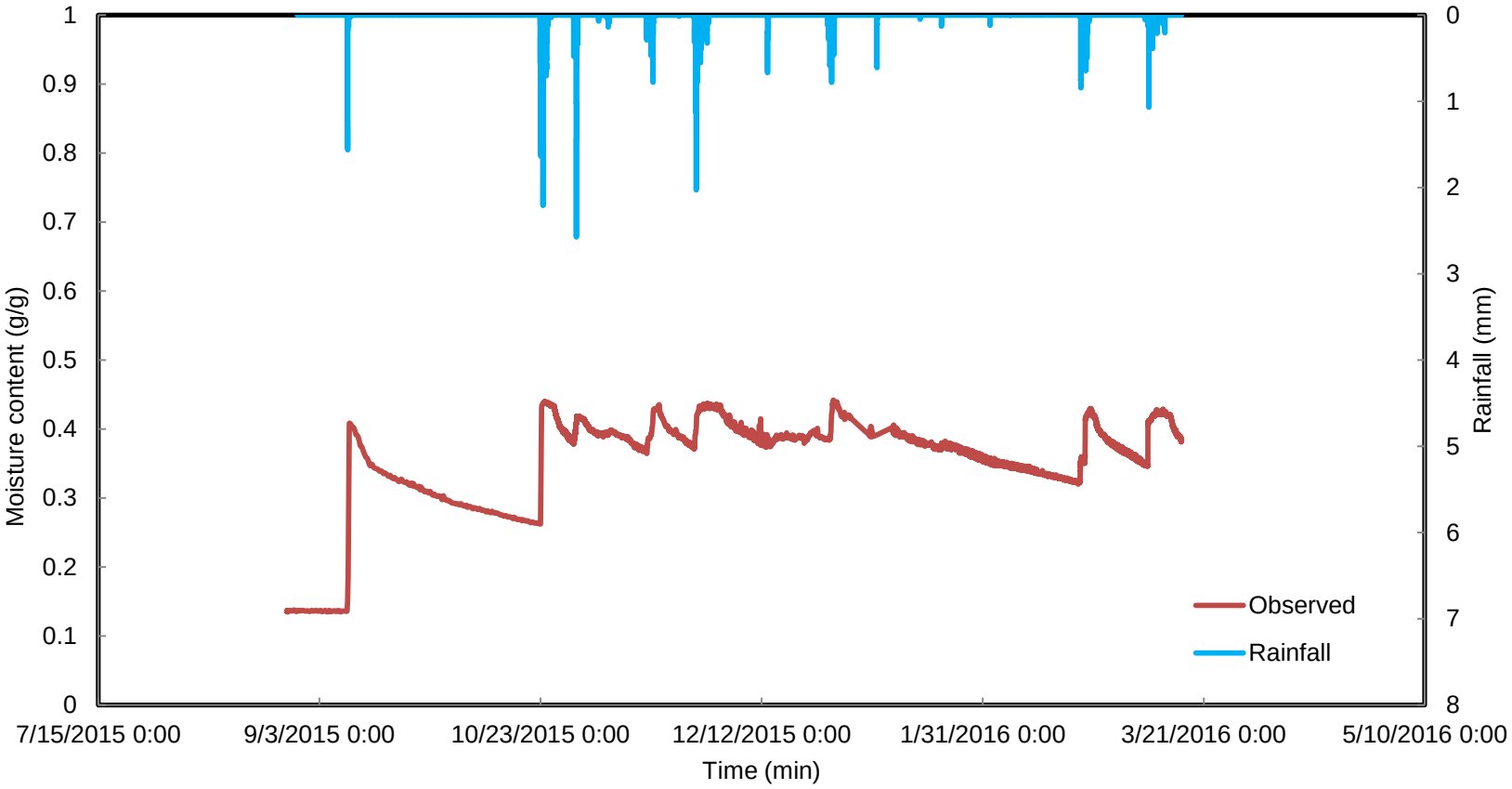

Figure 3-19 Field Capacity for the Sensor-2 at a depth of 10 cm at Station 1

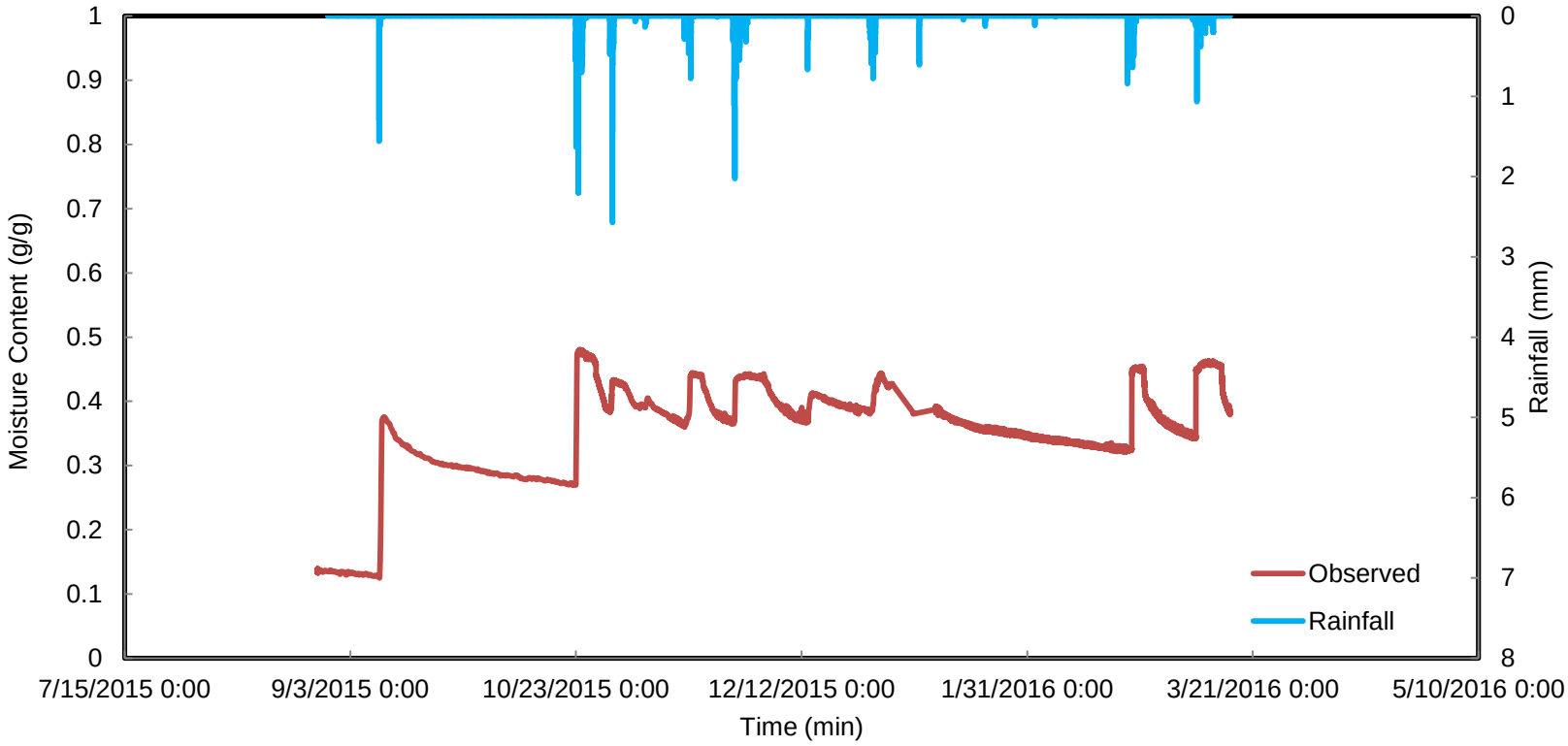

Figure 3-20 Field Capacity for the Sensor-3 at a depth of 25 cm at Station 1

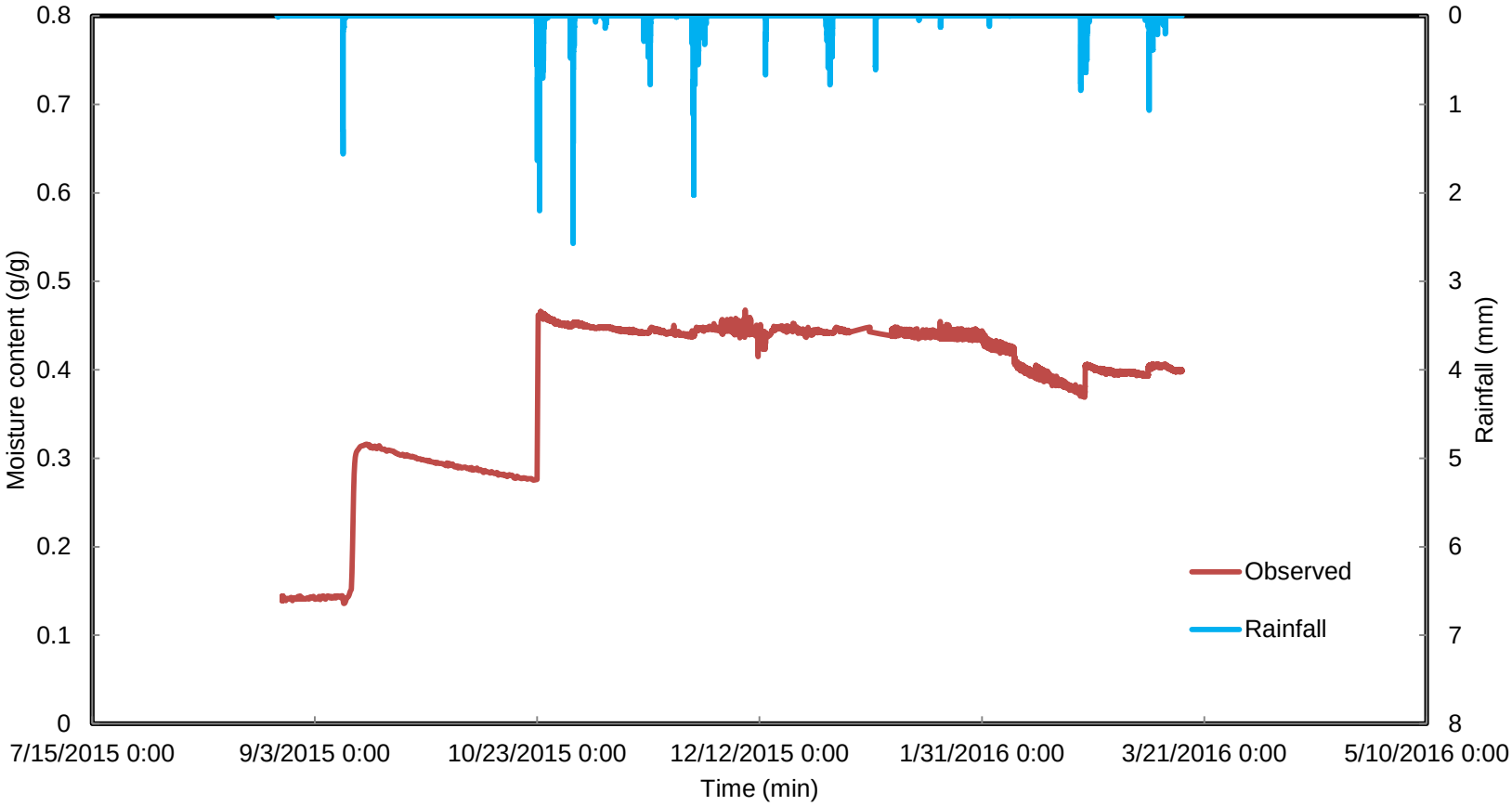

Figure 3-21 Field Capacity for the Sensor-4 at a depth of 50 cm at Station 1

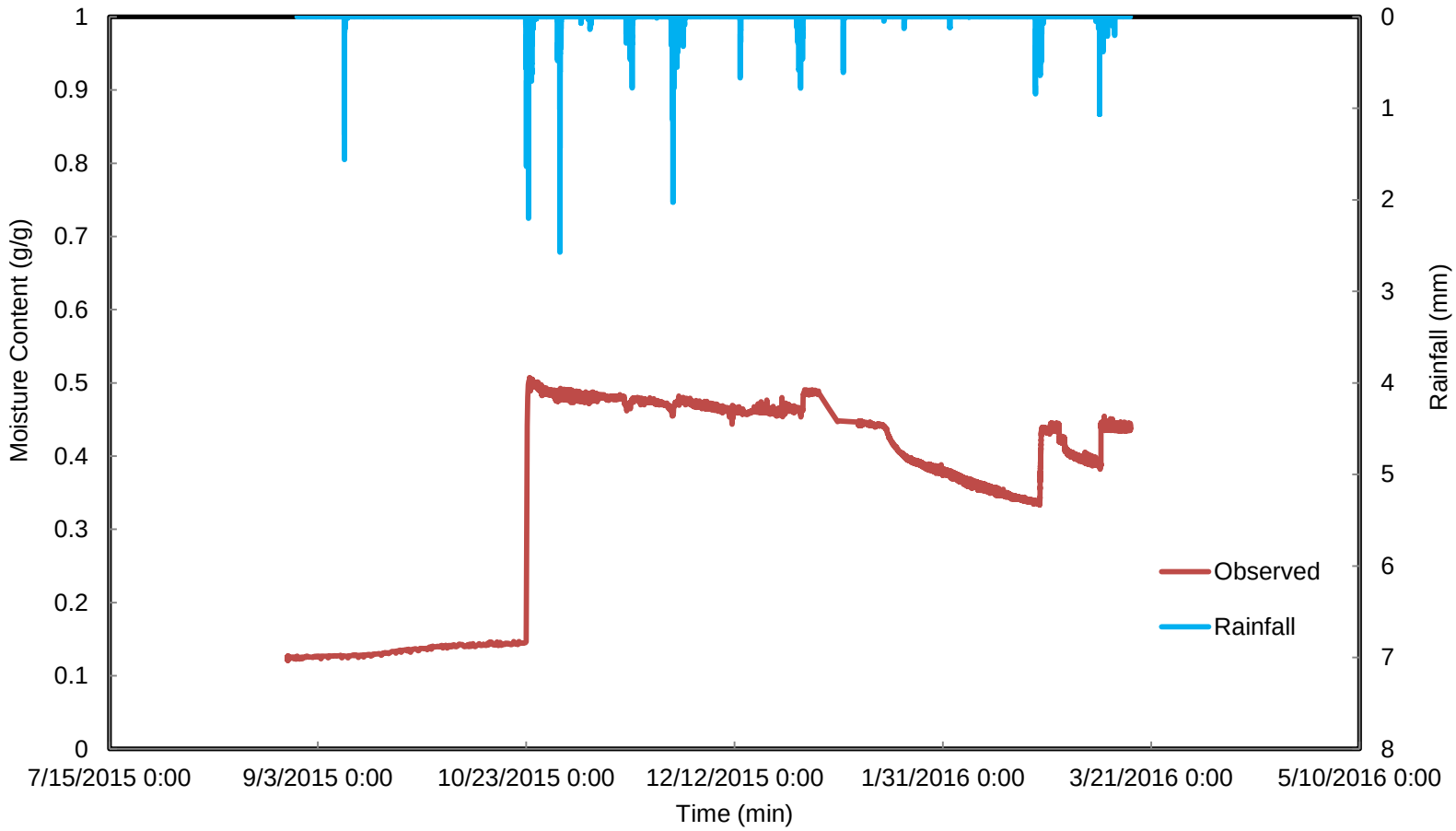

Figure 3-22 Field Capacity for the Sensor-5 at a depth of 1 m at Station 1

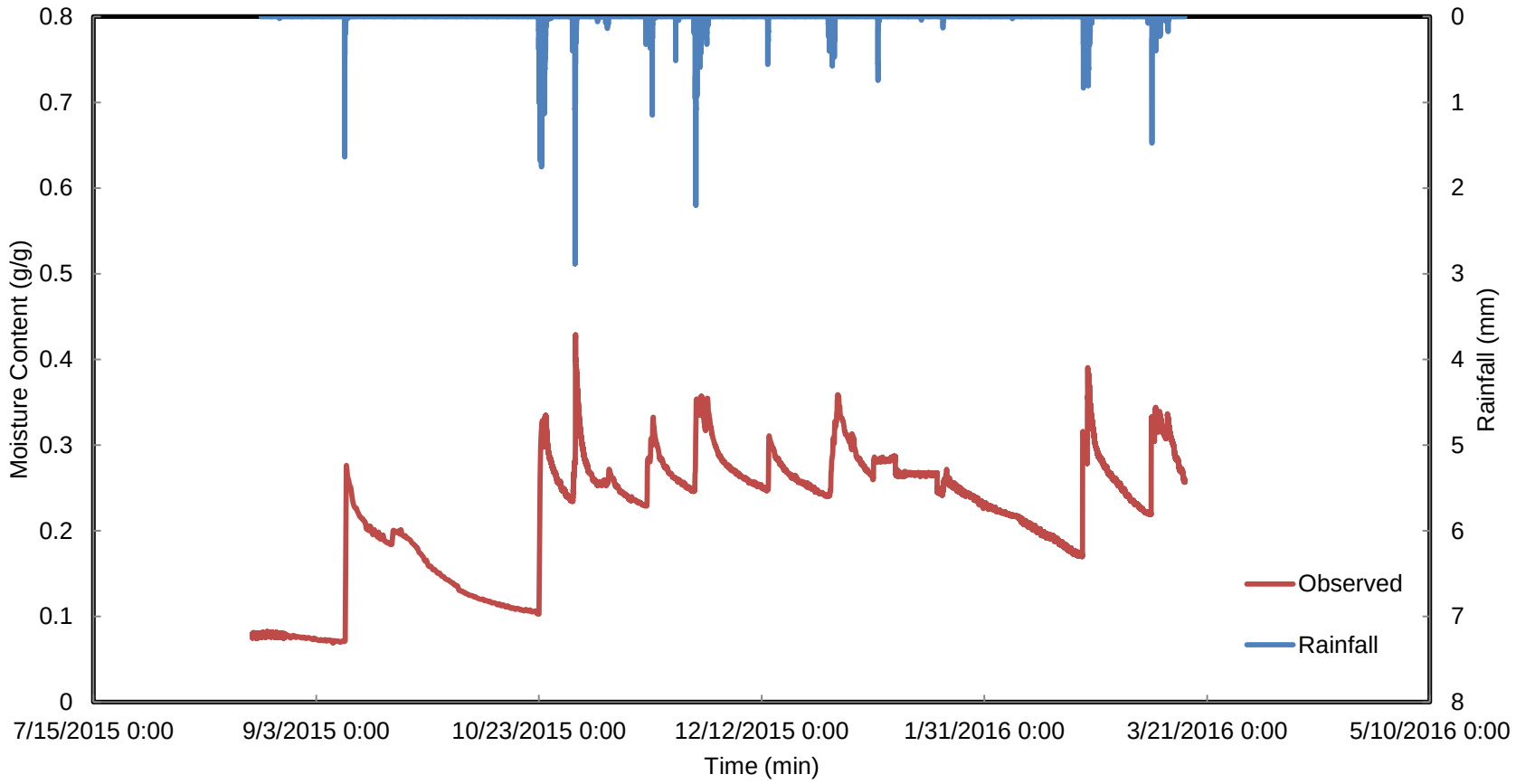

Figure 3-23 Field Capacity for the Sensor-6 at a depth of 5 cm at Station 2

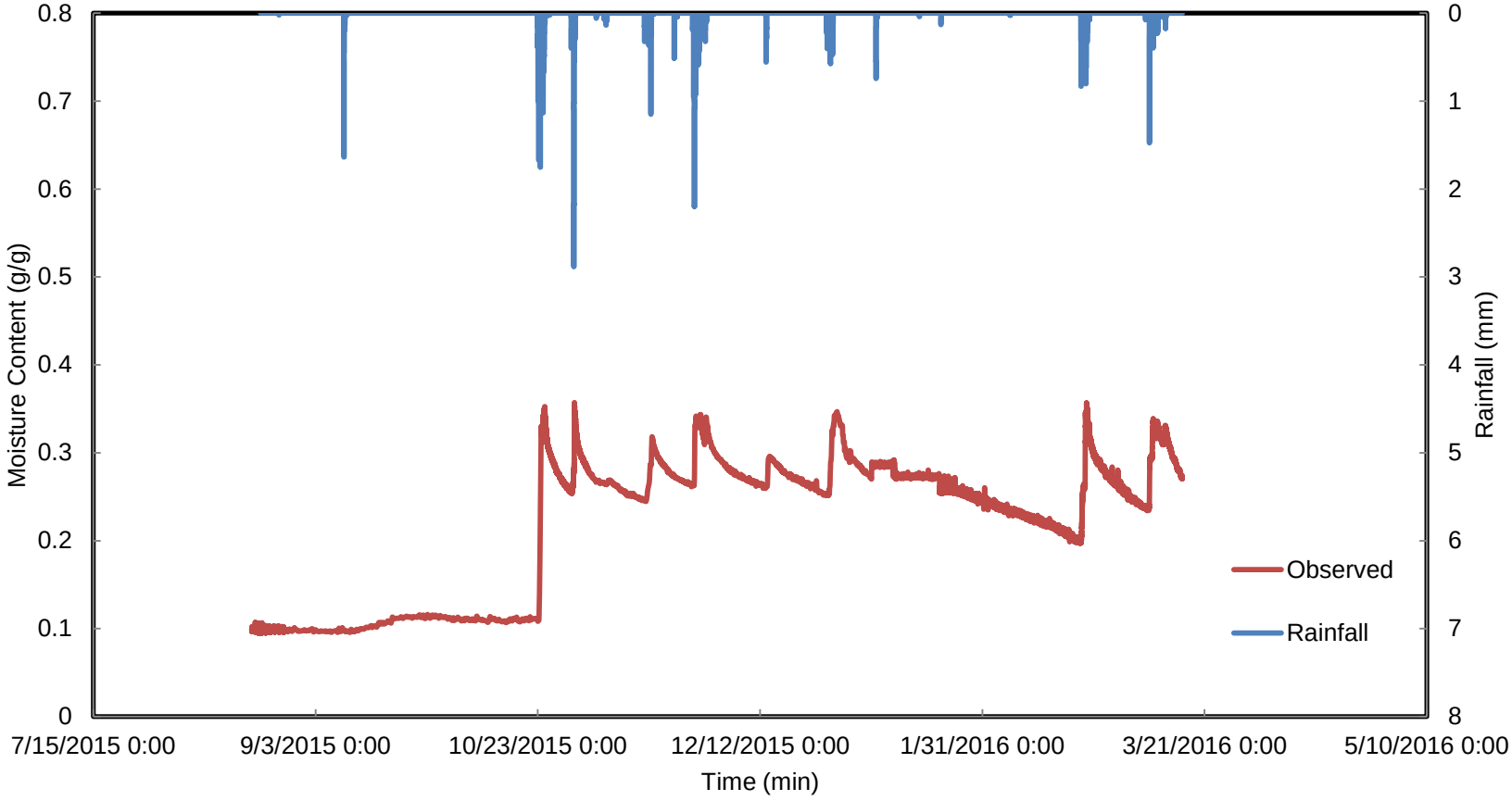

Figure 3-24 Field Capacity for the Sensor-7 at a depth of 10 cm at Station 2

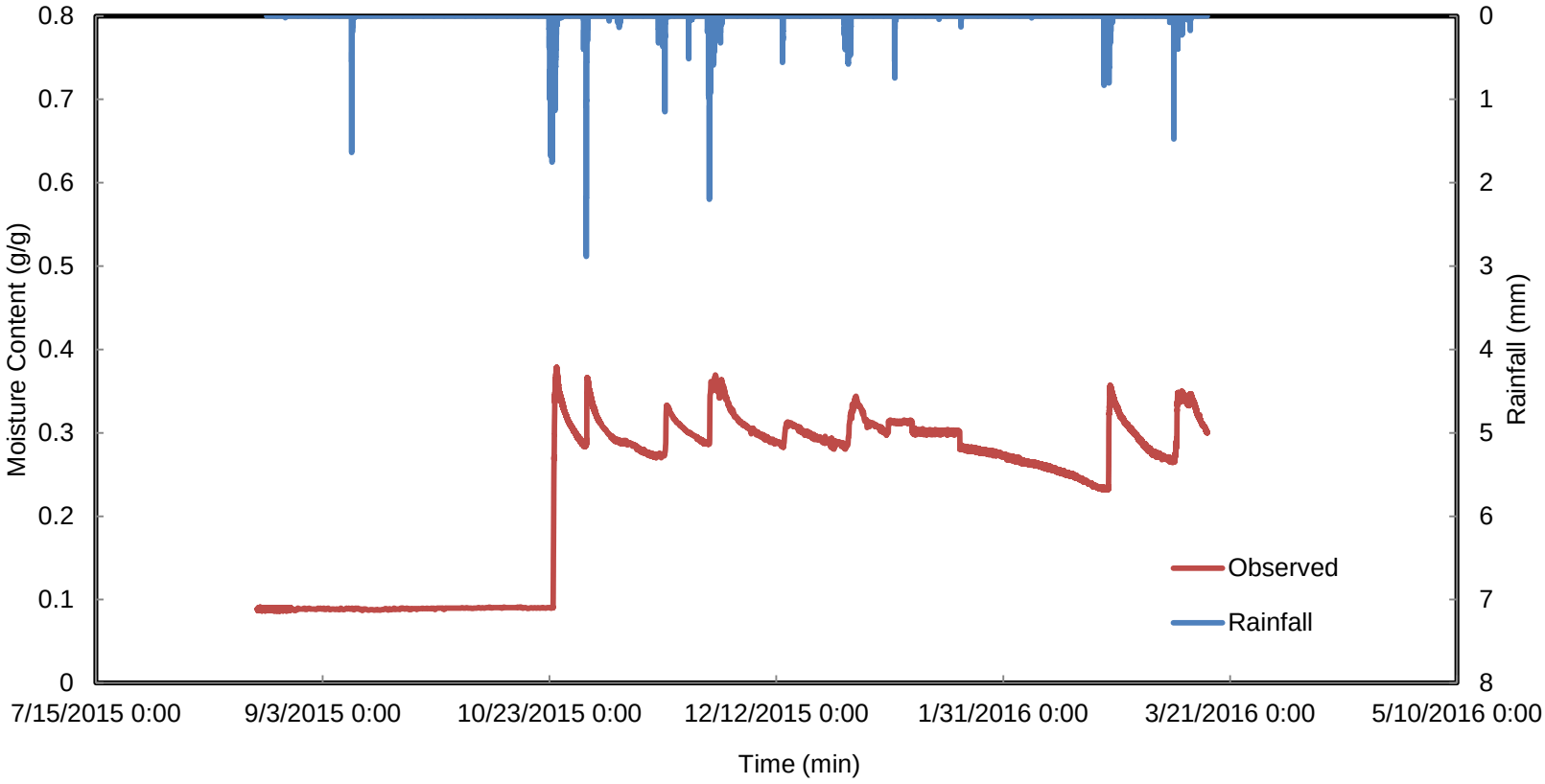

Figure 3-25 Field Capacity for the Sensor-8 at a depth of 25 cm at Station 2

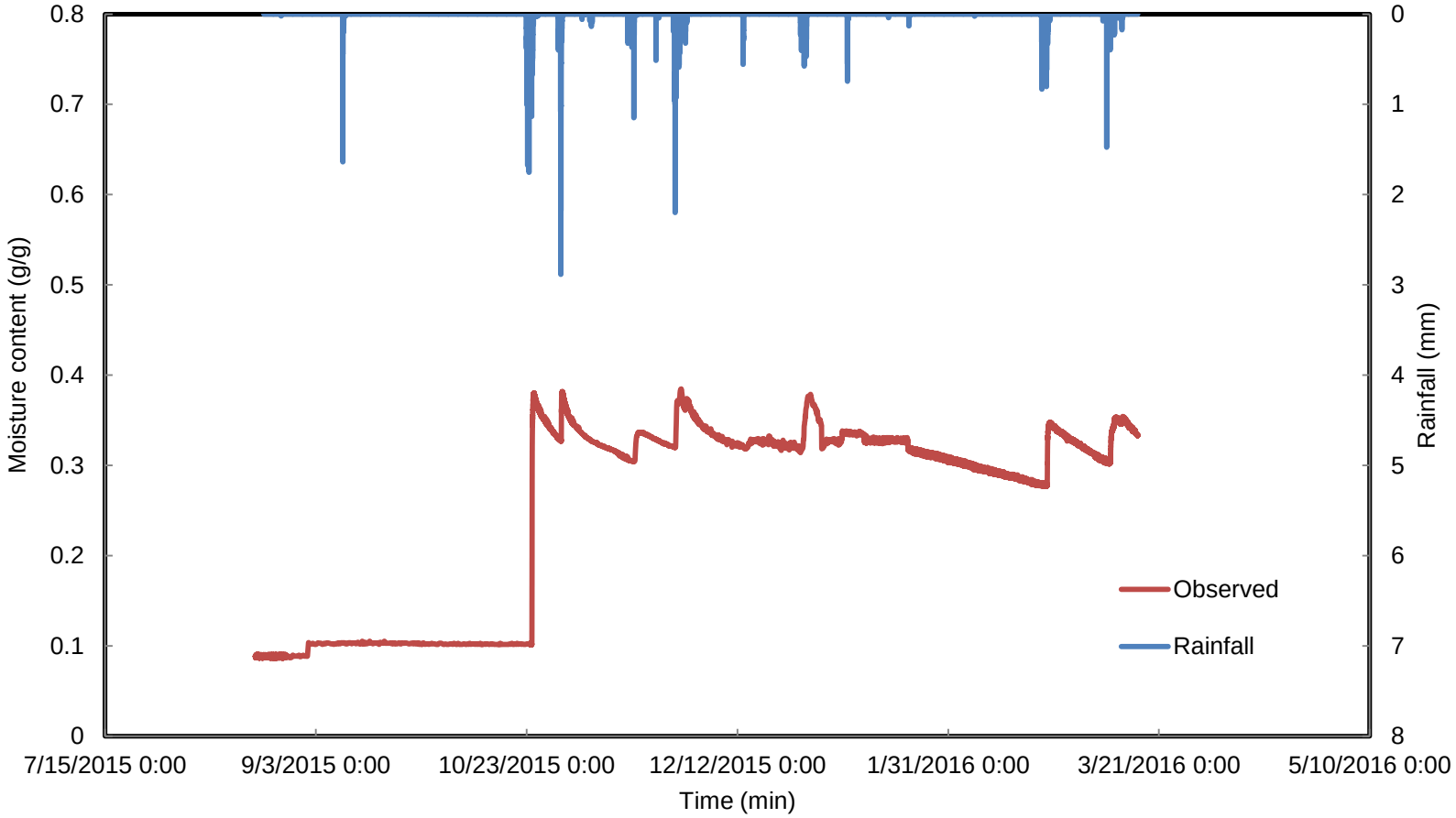

Figure 3-26 Field Capacity for the Sensor-9 at a depth of 50 cm at Station 2

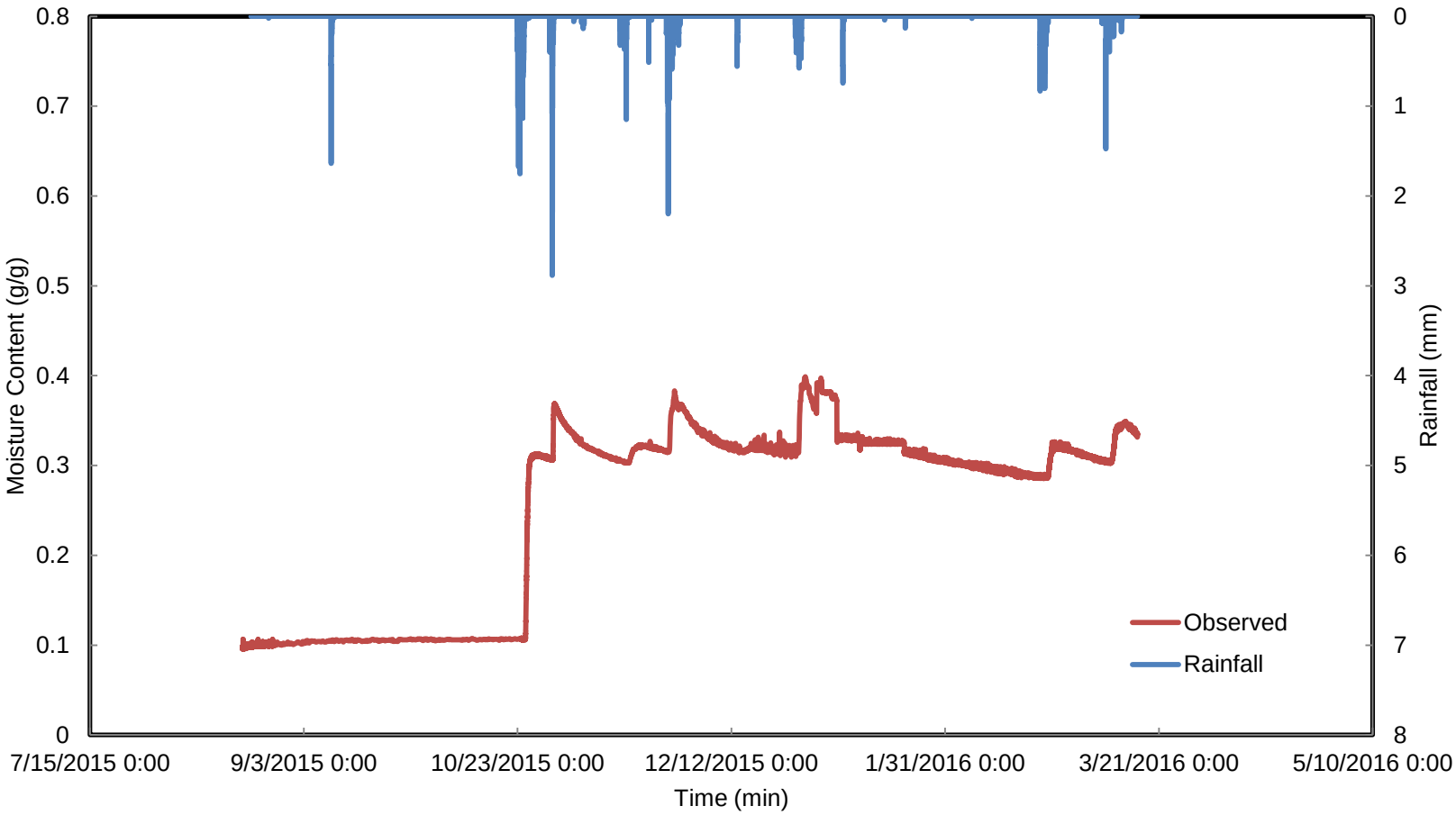

Figure 3-27 Field Capacity for the Sensor-10 at a depth of 1 m at Station 2

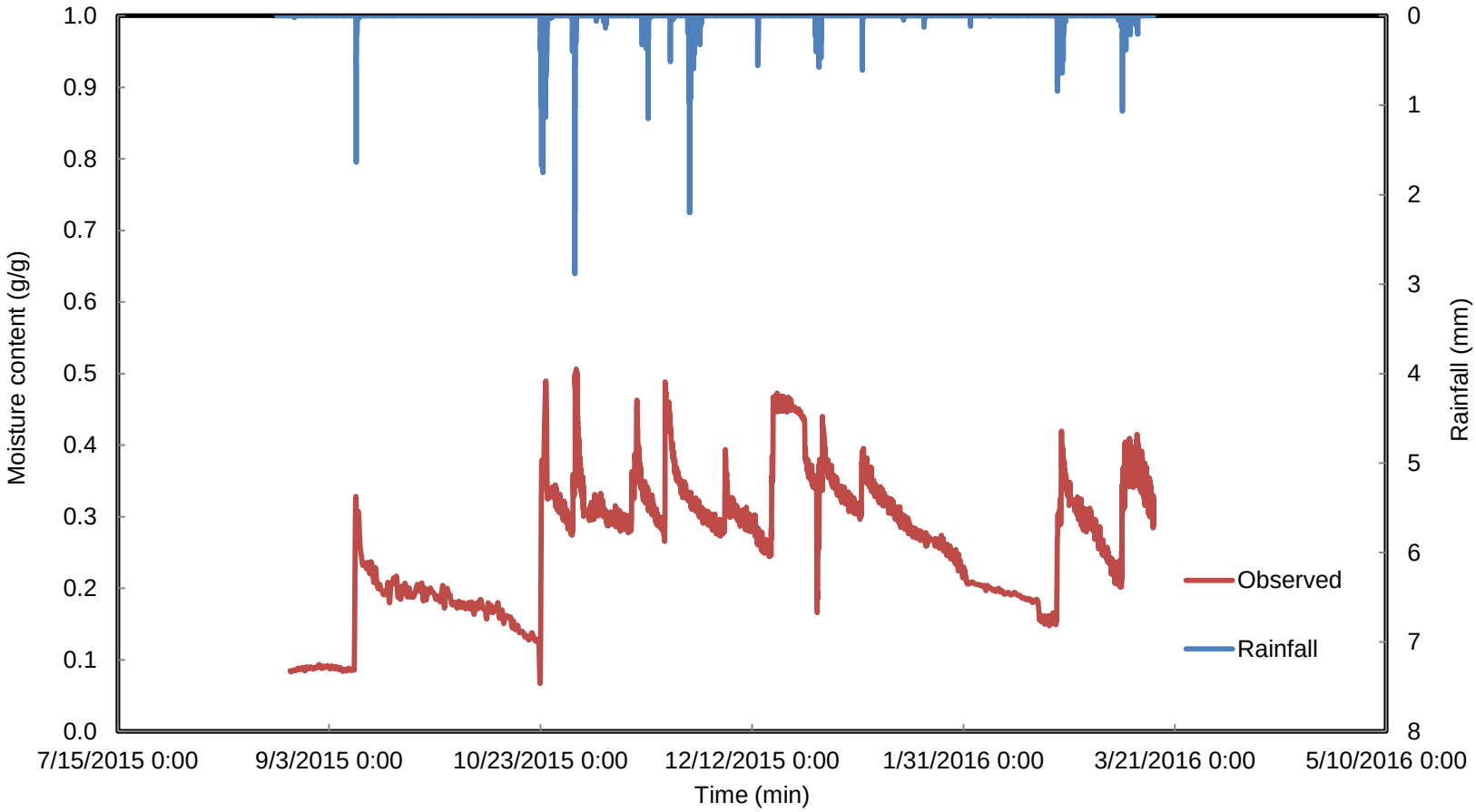

Figure 3-28 Field Capacity for the Sensor-1 at a depth of 5 cm at Station 3

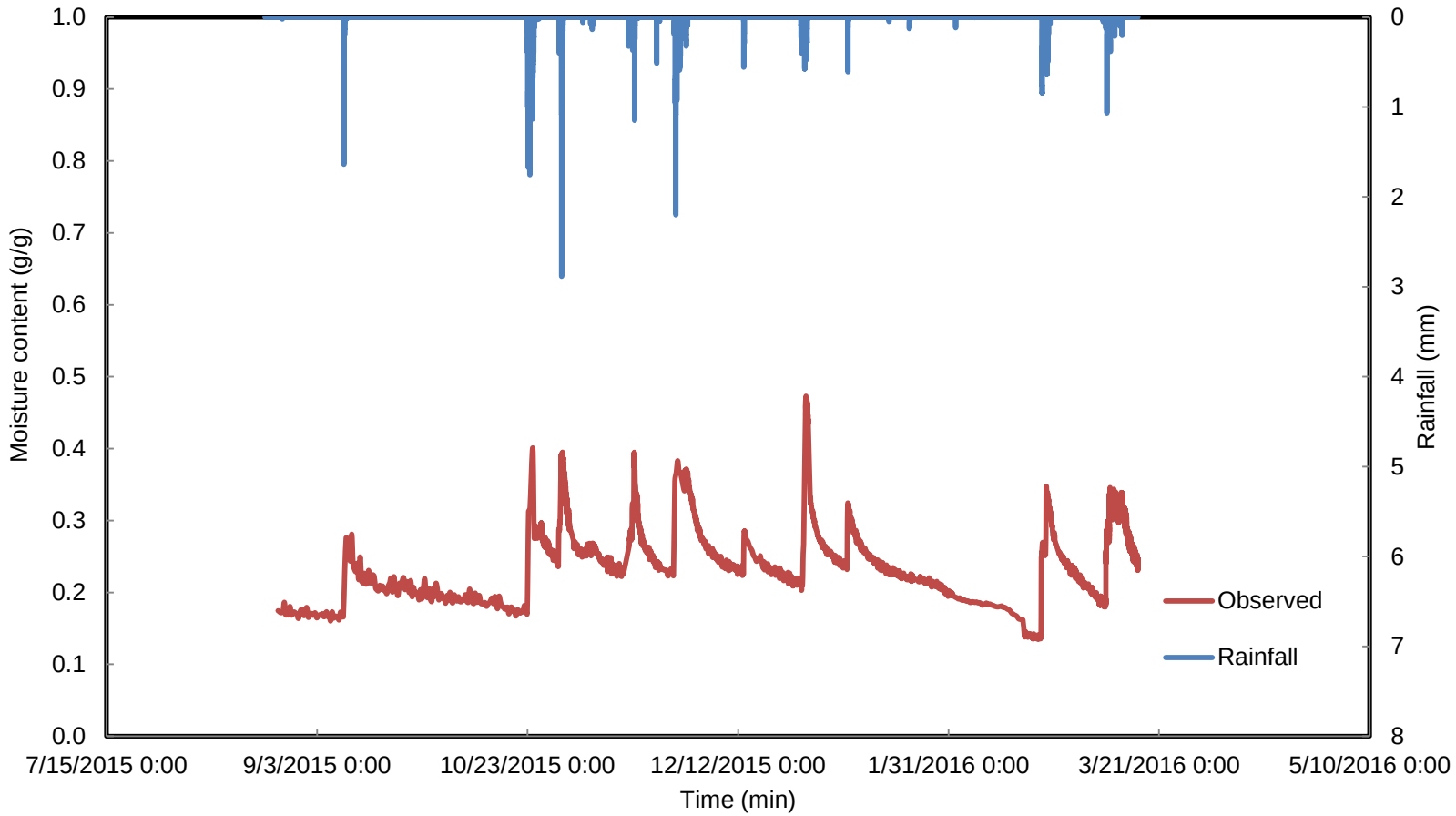

Figure 3-29 Field Capacity for the Sensor-2 at a depth of 10 cm at Station 3

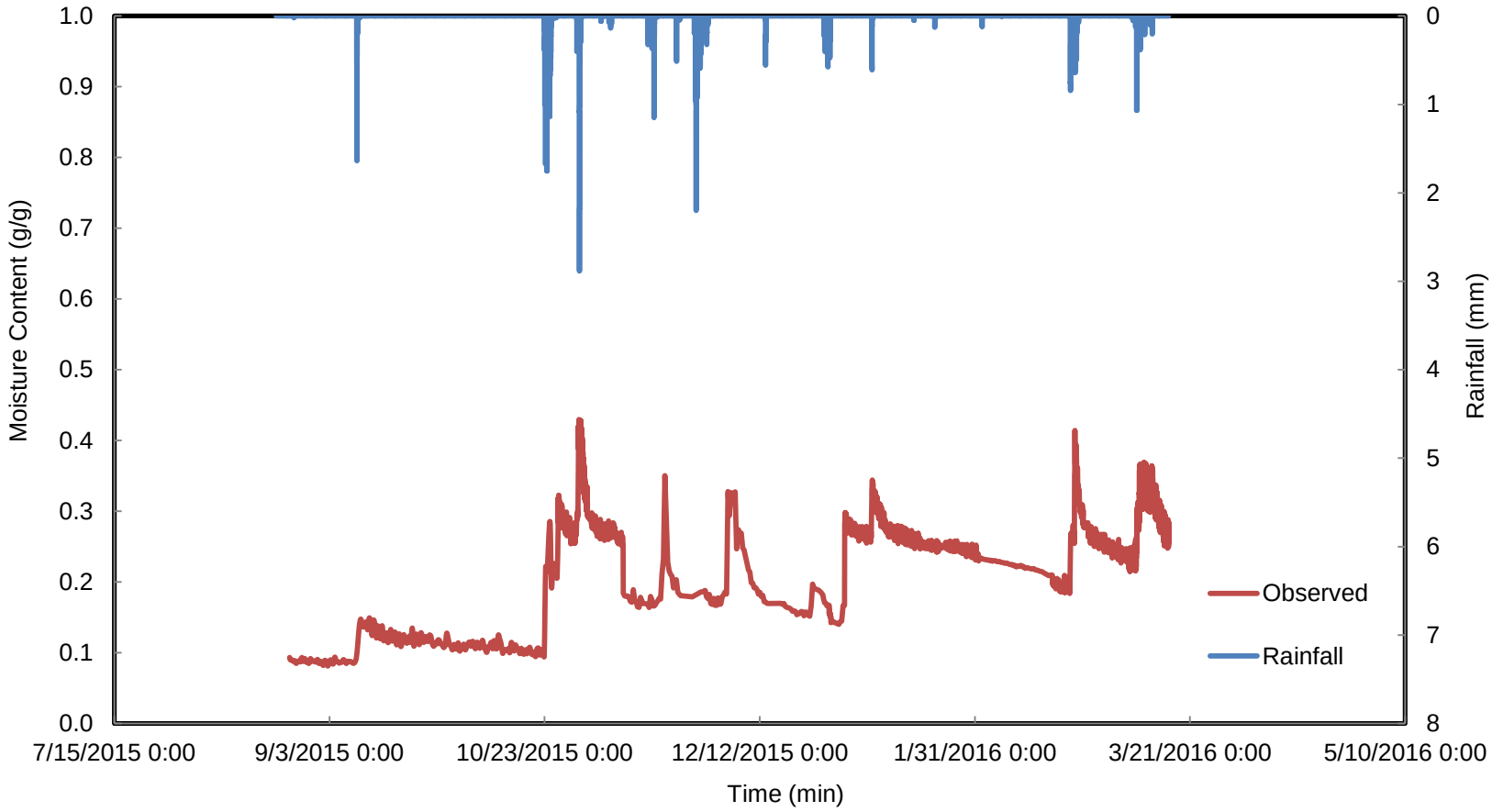

Figure 3-30 Field Capacity for the Sensor-3 at a depth of 25 cm at Station 3

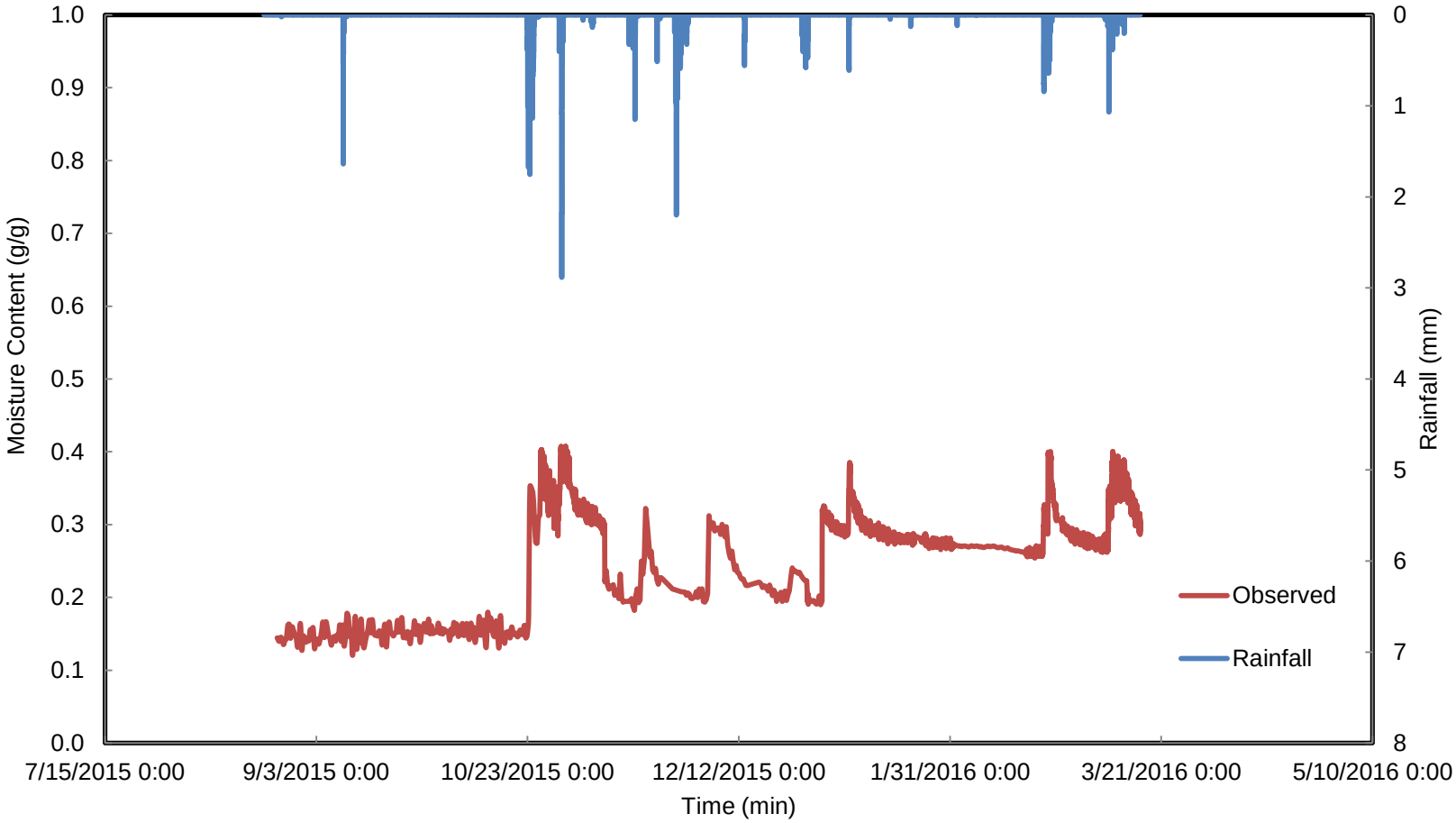

Figure 3-31 Field Capacity for the Sensor\-4 at a depth of 50 cm at Station 3

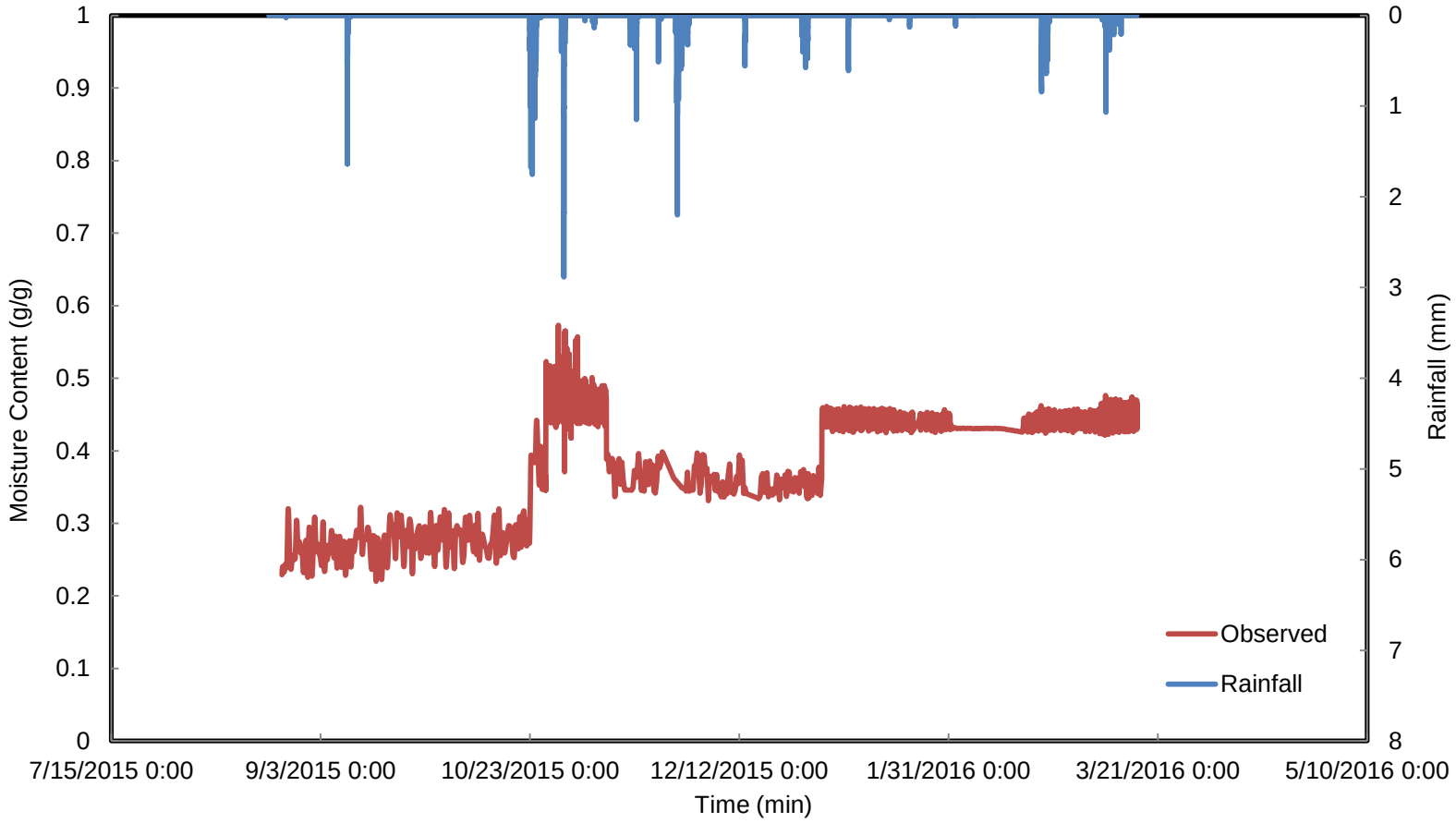

Figure 3-32 Field Capacity for the Sensor-5 at a depth of 100 cm at Station 3

Permanent Wilting Point is measured by Decagon Devices WP4C Dew Point Potentiometer in the laboratory. A 100 gm of air-dry soil sample is taken and 6.29 gm of water are added to it. Now, the sample is thoroughly mixed and placed in a sealed container overnight to equilibrate. At the end of the equilibration period a subsample of the soil is placed in a stainless steel cup and its water potential determined with the WP4C. The stainless steel cup is oven dried at 105° C, and reweighted to determine the water content on the sample. The water content is computed as the mass of the water (change in sample mass on drying) divided by the mass of the oven dry soil (dry mass of the sample and container minus the mass of the container).

Having obtained the water content – water potential information for the soil sample, the -1.5 MPa value is obtained by extrapolation or interpolation. This is easy to do since the moisture characteristic, between about -1 MPa (pF 4.01) and oven dry (-1000 MPa, pF 7.01) is linear in pF or logarithm of water potential. From a single value of water content and potential near the wilting point, the -1.5 MPa or pF 4.18 water content is computed as follows:

$$w_{-1.5} = w_m \frac{\ln\left(\frac{-1000}{-1.5}\right)}{\ln\left(\frac{-1000}{\psi_m}\right)} \tag{19}$$

Where w_m is the measured water content corresponding to the water potential ψ_m or pF_m.

The volumetric water content is then calculated as in the field, volume is the basis for computing water storage, not mass. The equation is:

$$\theta_{-1.5} = w_{-1.5} \frac{\rho_b}{\rho_w} \tag{20}$$

Where $\theta_{-1.5}$ is the volumetric water content ($m^3\ m^{-3}$), ρ_b is the soil bulk density and ρ_w is the density of water.

Table 3-22 Moisture content for the sample prepared for Station 1 Location

Wt. of Sampler (g)	Wt. of sampler + moist soil (g)	Wt. of sampler + oven dry soil (g)	Wt. of water (g)	Wt. of dry soil (g)	Gravimetric Water Content determined by Oven Dried Method (w)
1.0	16.98	14.38	2.6	13.38	19.43

w	ψ_m MPa	pF
0.194	-1.13	4.06

Where $\rho_b = 1.282$ g/cm^3 , $w_{-1.5} = 0.186$ kg/kg, $\theta_{-1.5} = 0.2383$ kg/kg ~ 23.83 %

Similarly, Table 3-23 and Table 3-24 shows the calculation for Station 2 and Station 3

Table 3-23 Moisture content for the sample prepared for Station 2 Location

Wt. of Sampler (g)	Wt. of sampler + moist soil (g)	Wt. of sampler + oven dry soil (g)	Wt. of water (g)	Wt. of dry soil (g)	Gravimetric Water Content determined by Oven Dried Method (w)
1.0	15.46	13.27	2.19	12.27	17.85

w	ψ_m MPa	pF
0.178	-1.18	4.08

Where $\rho_b = 1.311$ g/cm^3, $w_{-1.5} = 0.178$ kg/kg, $\theta_{-1.5} = 0.2251$ kg/kg ~ 22.51 %

Table 3-24 Moisture content for the sample prepared for Station 3 Location

Wt. of Sampler (g)	Wt. of sampler + moist soil (g)	Wt. of sampler + oven dry soil (g)	Wt. of water (g)	Wt. of dry soil (g)	Gravimetric Water Content determined by Oven Dried Method (w)
1.0	14.86	12.35	2.51	11.35	22.11

w	ψ_m MPa	pF
0.221	-1.23	4.10

Where ρ_b = 1.262 g/cm^3, $w_{-1.5}$ = 0.214 kg/kg, $\theta_{-1.5}$ = 0.2706 kg/kg ~ 27.06 %

Figures 3-33 and 3-34 shows the use of WP4C instrument for measurement of permanent wilting point.

Figure 3-33 Samples prepared at different moisture content for testing with WP4C

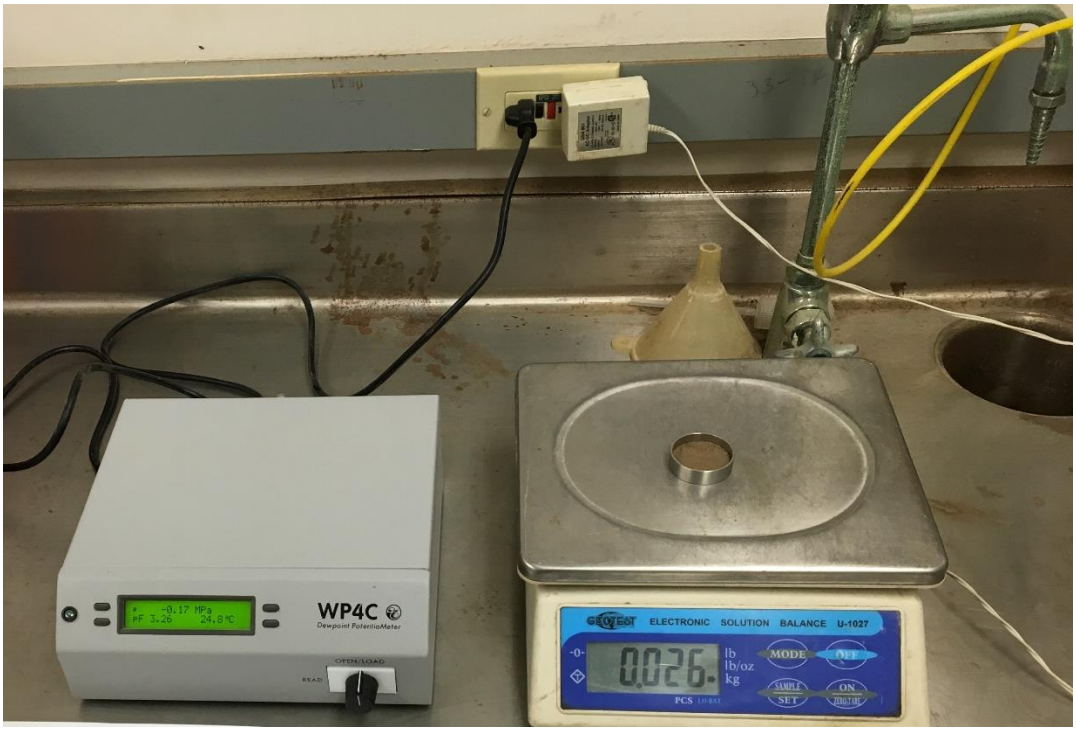

Figure 3-34 Samples being weighed at different moisture content for testing with WP4C

3.3 Installation of Sensors at Site Locations

The main intent of this task to install the sensors in the field by excavating the soil to the required depth. Two holes were made by excavating the soil with the Drill Augers as shown in Figure 3-35, 3-36, 3-37 and 3-38. First hole was dug 1.5 m deep and 1 m wide in dimension for the TDR and TDT sensors to be installed and second hole 0.5 m deep and 1 m wide was dug only on TDT sensors Site location for the Valve Box to be installed. Relatively, the sensors were placed at a bottom depth starting from 1 m, 0.5 m, 0.25 m, 0.10 m and 0.05 m. Each sensor placed had a different orientation as compared to the other for the different flow pattern of water through the soil layers. After placing the sensor at a particular depth, some backfill excavated soil was put over and compacted according to the field standards. Soil Samples were collected at three different levels i.e. Top at 0.05 m, Middle at 0.50 m and Bottom at 1.0 m for three different stations to have a cross-evaluation of actual moisture content obtained after oven-drying method to the moisture content obtained from the instrument.

Figure 3-35 Rotatory Drill Auger Excavator employed for excavation

Figure 3-36 Soil Excavation using Rotatory Drill Auger Excavator

Figure 3-37 Soil Excavation using Rotatory Drill Auger Excavator

Figure 3-38 Hand Augers and Auger Drills operated by DG in sloping ground

3.3.1 Installation of TDT (Time Domain Transmissometry) Sensor

Before proceeding onto the field, the TDT sensors were tested in the laboratory for proper functionality. TDT sensors were labelled according to the depth of their installation and were programmed to the Data Snap with which they were connected. A total of five nos. of TDT sensors were installed at each station. The detailed field installation process has been illustrated in the Figure 3-39, 3-40, 3-41, 3-42, 3-43 and 3-44. Each Acclima Digital TDT sensors comes with the irrigation 3 wire line cable (Red, Blue, and White) of 25 feet. The detailed installation diagram for the TDT sensors are as shown in Figure 3-45.

Figure 3-39 TDT sensor placed at 1 m depth after leveling the ground

Figure 3-40 Backfill excavated soil is filled till the next depth layer and compacted with the help of tamper

Figure 3-41 All the TDT sensors are installed and the ground surface is compacted and levelled

Figure 3-42 A trench of length 5 m is excavated for the irrigation wires running through to connect to the Valve Box

Figure 3-43 The second hole is filled with gravel and the water tight box is installed within the Valve Box with wire connection at CELB Site Location

Figure 3-44 The sensors are validated and set at fixed interval for recording the data

Each of these sensors were placed at different depth levels and at different orientation as mentioned above. The cable lengths were tied together to run along a length of 5 m (or 16 feet approximately) to reach to the Valve Box. The Valve Box is kept in the small excavated pit surrounded from all sides with gravel to avoid the stagnation of water around it. Inside the Valve Box, two water-tight box is kept connected to each other by a non-metallic connector insulated by all sides with the rubber sealant. On one side all the 3 wire line cables for the five sensors are individually connected to waterproof wire connectors to make the connection waterproof and finally connected to the SDI -12 data snap which records four soil parameters i.e. Moisture Content, Temperature, Permittivity and Conductivity. Initially, the time is set to take down readings every 1 minute based on the weather forecast for rain. Later on, for an optimum and uniform rate of measurement of data, the readings can be noted at an interval of 6-8 hours.

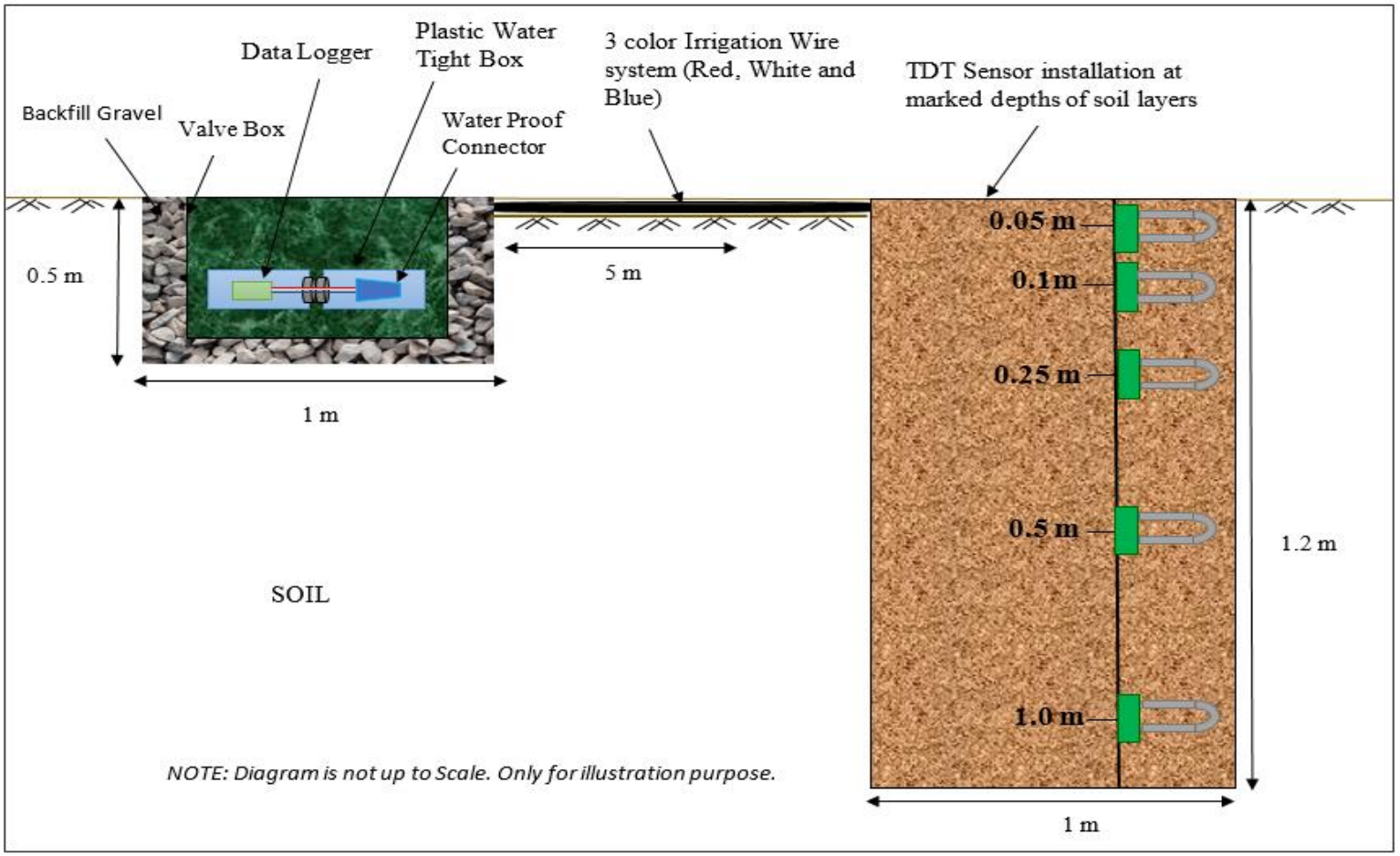

Figure 3-45 Schematic Diagram for the Installation of Acclima Digital TDT Moisture Sensors at Station 1 and Station 2

3.3.2 Installation of TDR (Time Domain Reflectometry) Sensor

TDR Sensors installation follows a similar procedure as that of TDT sensor but is more complex and sensitive to operate and analyze. A total 5 nos. of Campbell Scientific TDR sensors are tested for functionality i.e. 4 Nos. of CS 610 TDR Probe with a co-axial cable of 30 feet length and 1 no of CS 605 TDR Probe with a co-axial cable of 20 feet length. The TDR sensors are installed at a depth starting from 1 m from the ground level to 0.5 m, 0.25 m, 0.1 m and 0.05 m which is shown in Figure 3-46, 3-47, 3-48, 3-49, 3-50 and 3-51. In the field installation, it is ensured that each sensor has a different orientation as compared to the other. CS 605 TDR Probe is placed at 0.05 m from the ground level owing to a shorter length of co-axial cable.

All the co-axial cables are connected to the Campbell Scientific Weather Box which houses the Data Logger CR 1000, Multiplexer SDMX 50, TDR 100, and Power source PS 100. All the co-axial cables are labelled according to the depth in the descending order of their depth from the ground level i.e. the CS 605 being on the top labelled as 1. All the co-axial cables are run into the set up at the pier of the bridge. The co-axial cables inside the box are connected to the multiplexer serially in accordance to the channels to which they are programmed. At the end, the box is grounded or earthed to protect it from lightening. The Earthing or Grounding process involves 8 conductor gauge Bare Copper Wire (8 feet long) attached to the earthing slot provided at the bottom of the box. Copper Ground Rod (5/8 inch diameter and 8 feet long) is inserted into the ground and the bare copper wire is attached to it with the help of bronze clamp rod completing the circuit as shown in Figure 3-52, 3-53, 3-54, and 3-55. The TDR is switched in ON position and the program code is sent to the data logger through the laptop. The program has been designed as such to note down the readings at an interval of 8 hours. A detailed schematic diagram is shown in Figure 3-56 to illustrate the installation of the TDR Cables and the working methodology.

Figure 3-46 The excavated soil is leveled and compacted. Soil samples are collected at the bottom level.

Figure 3-47 TDR sensor is placed at 1 m below the ground level facing the N-W direction.

Figure 3-48 TDR sensor is placed at 0.05 m below the ground level facing the S direction as the orientation of the TDR Probe for each level need to be different.

Figure 3-49 The co-axial cables are inserted into the PVC Pipe to insulate it against weathering.

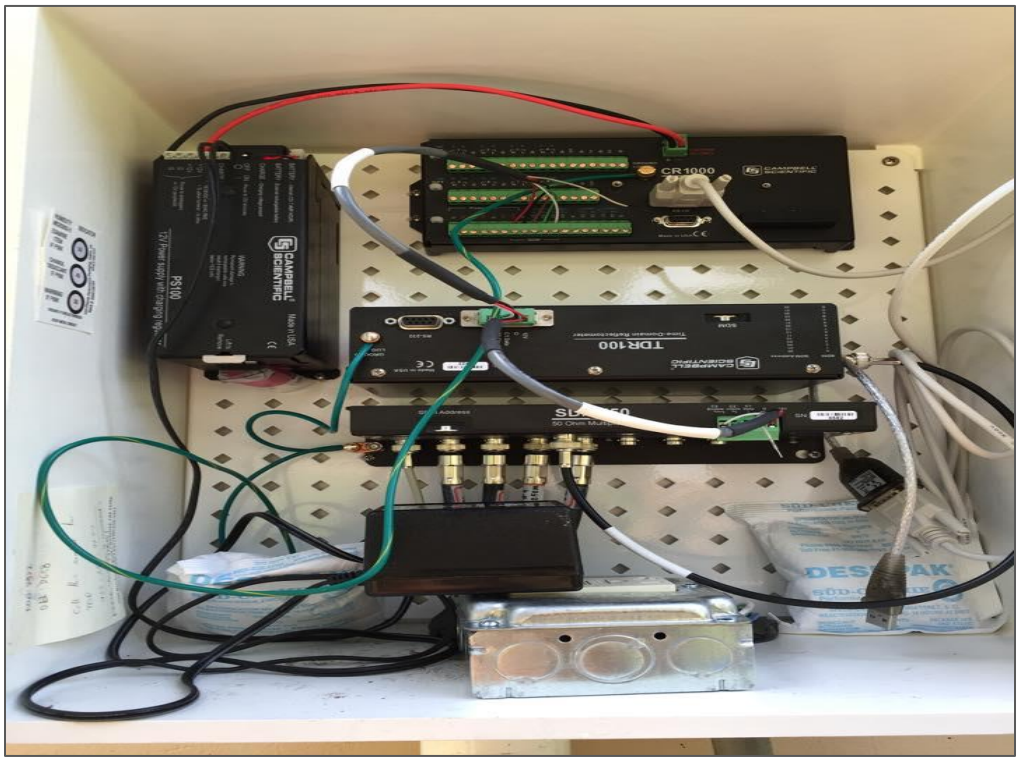

Figure 3-50 The Weather Proof box containing the components of TDR Assembly. The co-axial cables are connected to the multiplexer channels in accordance to the program code. Desiccant packs are kept inside to absorb any moisture and a humidity indicator is kept to check for the moisture level in the box. The two outlet have been sealed with a sealing putty to prevent any insects or reptiles crawling into the enclosure.

Figure 3-51 The whole assembly for the TDR installation and measurement is complete.

Figure 3-52 Copper Ground Rod of 5/8 inch in diameter and 8 feet long in diameter is pushed into the soil after wetting the soil

Figure 3-53 The bare copper wire is inserted into the PVC Pipe to prevent it from corroding by being exposed to the atmosphere.

Figure 3-54 The bare copper wire is connected to the copper rod with the help of bronze clamp rod and the grounding operation is complete for the Weathering Box.

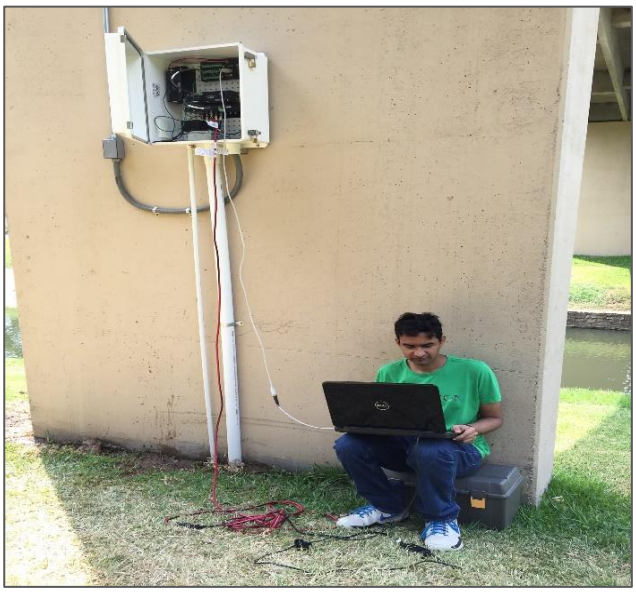

Figure 3-55 Program code uploaded to the data logger and time interval is set for the continuous measurement of data.

The data obtained from the field is analyzed to find the di-electric constant, electrical conductivity, bulk dry density and moisture content. Laboratory calibration is performed to obtain the calibration parameters specific to the soil type for subsequent field measurements. Generally, bulk electrical conductivity provides us an estimate of soil salinity and soil pore-fluid conductivity. Pore fluid conductivity plays a very important role. The calibration equations needs to be adjusted to the standard pore fluid conductivity as di-electric constant and electrical conductivity have variable effects with pore fluid conductivity. Different methods are followed to analyze the waveforms obtained from the data points but the 'Method of Tangents' and the 'Method of Peak' are the most popular ones that we are going to use to find the first reflection point and the second reflection point. Topp et al. 1980 method is used to calculate the apparent di-electric constant of the soil. Giese and Tiemann 1975 Method is employed to calculate the apparent electrical conductivity of the soil. The water content calculated here is gravimetric water content in comparison to volumetric water content obtained from the TDT sensors. Gravimetric water content is a better measure and representation of water content in the soil owing to the mass change being more sensitive to volume change.

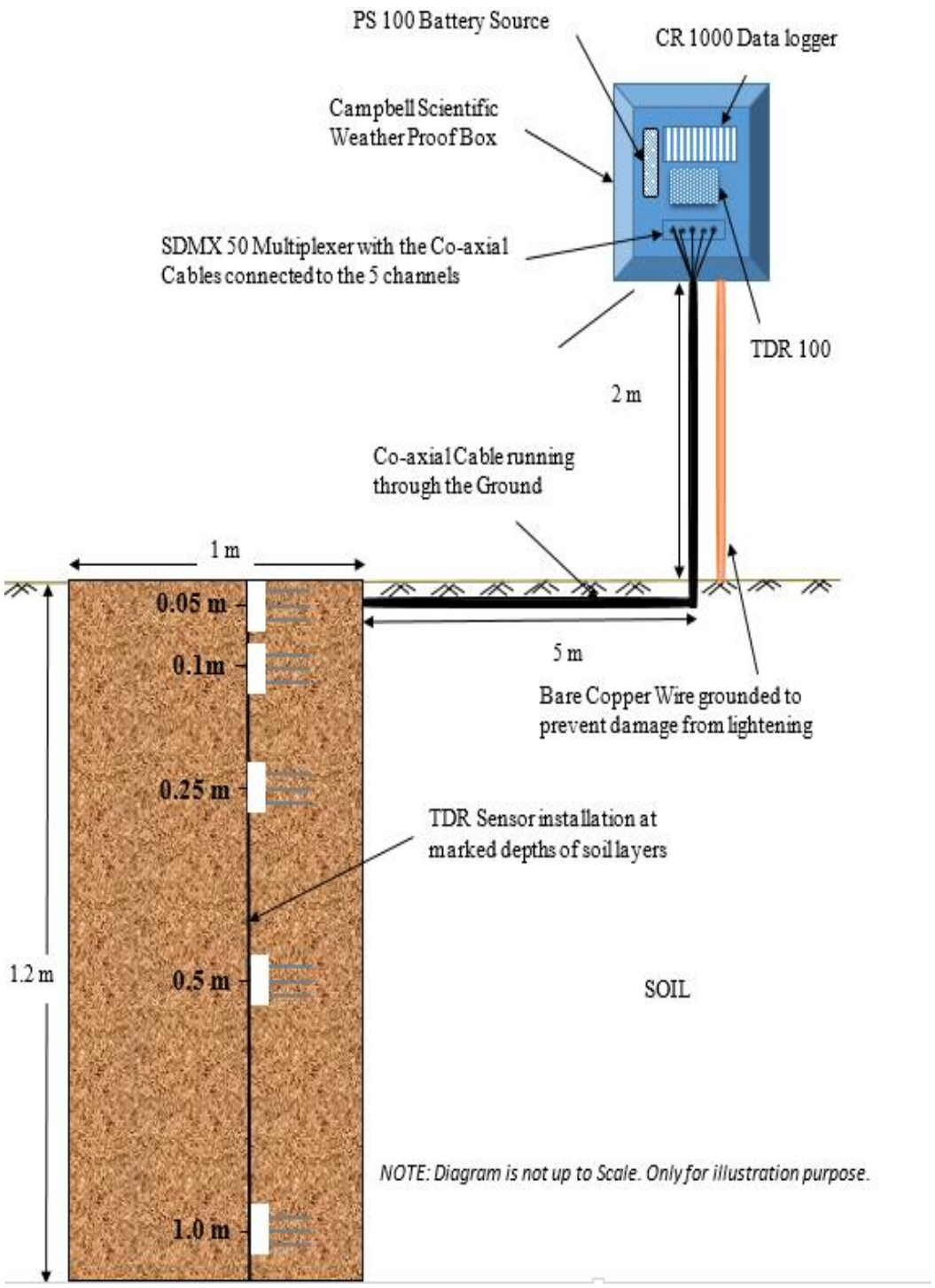

Figure 3-56 Schematic diagram for installation of Campbell Sci. TDR Probe at Station 3

3.4 Field Monitoring of Data at Site Locations

3.4.1 Field Monitoring of TDT (Time Domain Transmissometry) Sensor

The field data monitoring is continuing from the month of August 2015 to till date and all the light, medium and heavy rainfall events were captured for having a better representation of infiltration data for the respective field locations Station 1 and Station 2.

The figures 3-57,3-58,3-59,3-60,3-61,3-62,3-63 and 3-64 corresponds to the rainfall events held in between 10/26/2015-12 AM to 11/02/2015-7:10 PM , 12/27/2015-12 AM to 12/31/2015-11:00 PM, 02/10/16-12 AM to 02/25/2016-5:50 PM, and 03/08/2016-12:00 AM to 03/15/2016-11:55 PM.

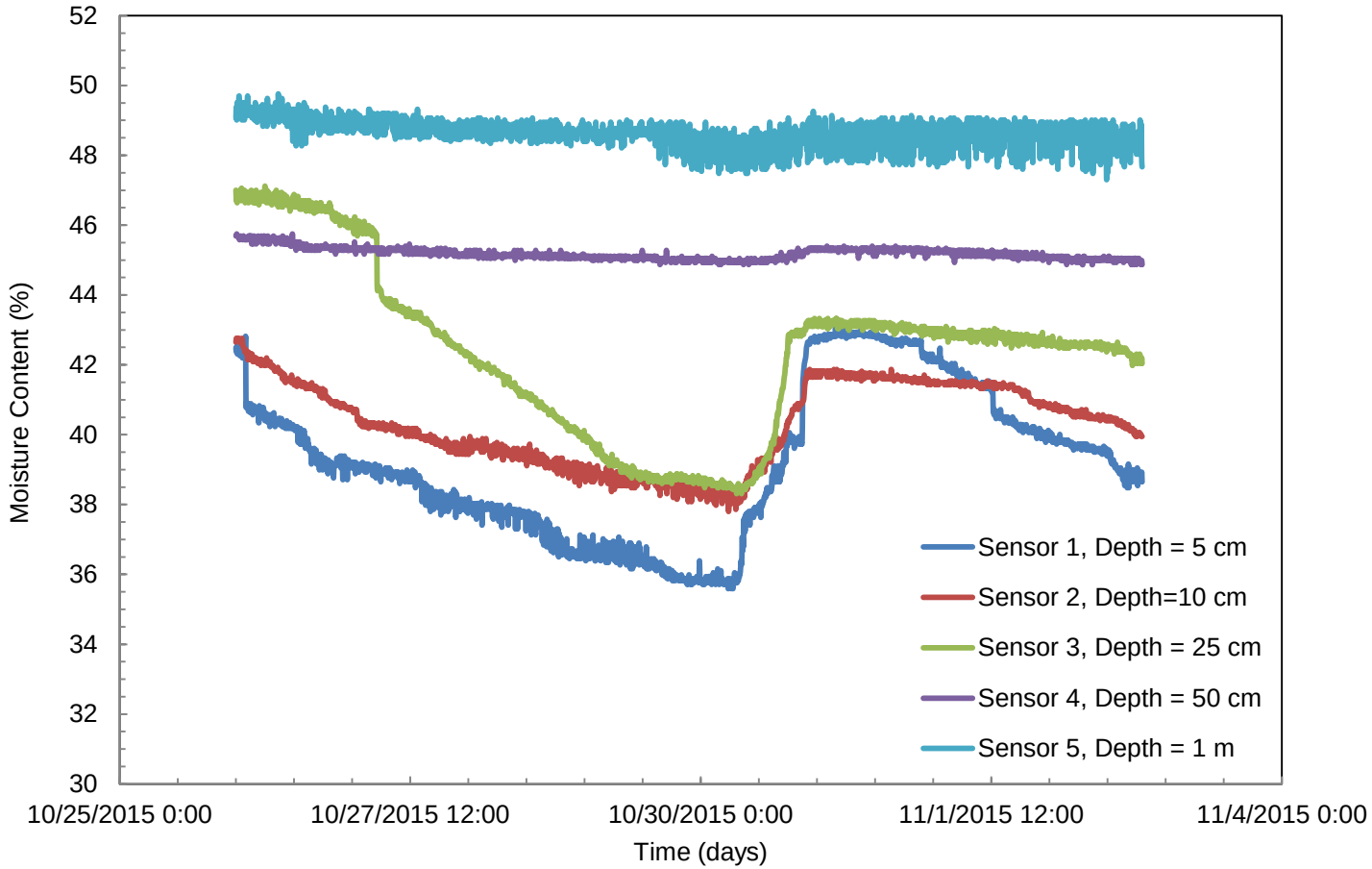

Figure 3-57 Moisture Variation for Rainfall Event held in between 10/26/2015-12 AM to 11/02/2015-7:10 PM at Station 1 Site Location

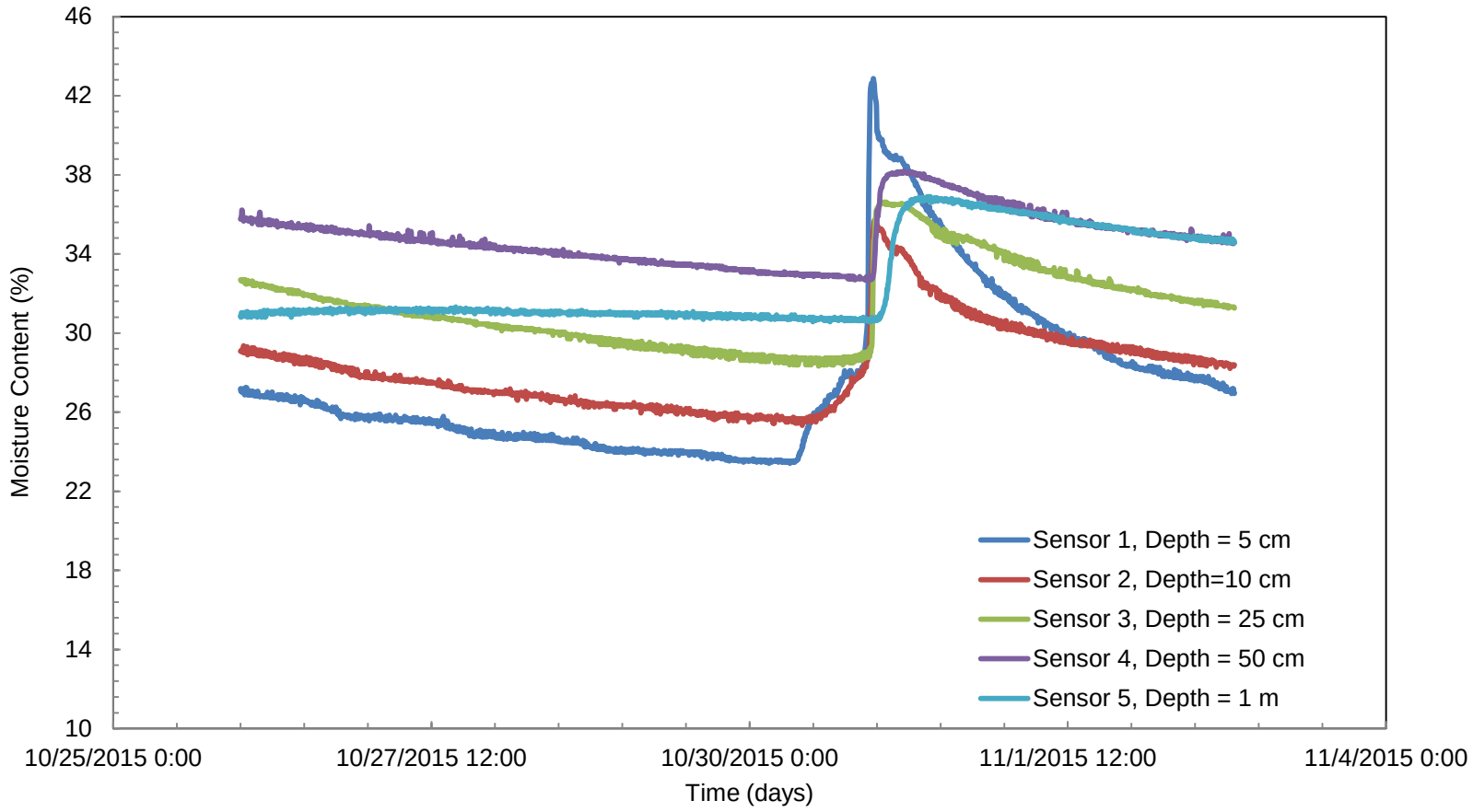

Figure 3-58 Moisture Variation for Rainfall Event held in between 10/26/2015-12 AM to 11/02/2015-7:10 PM at Station 2 Site Location

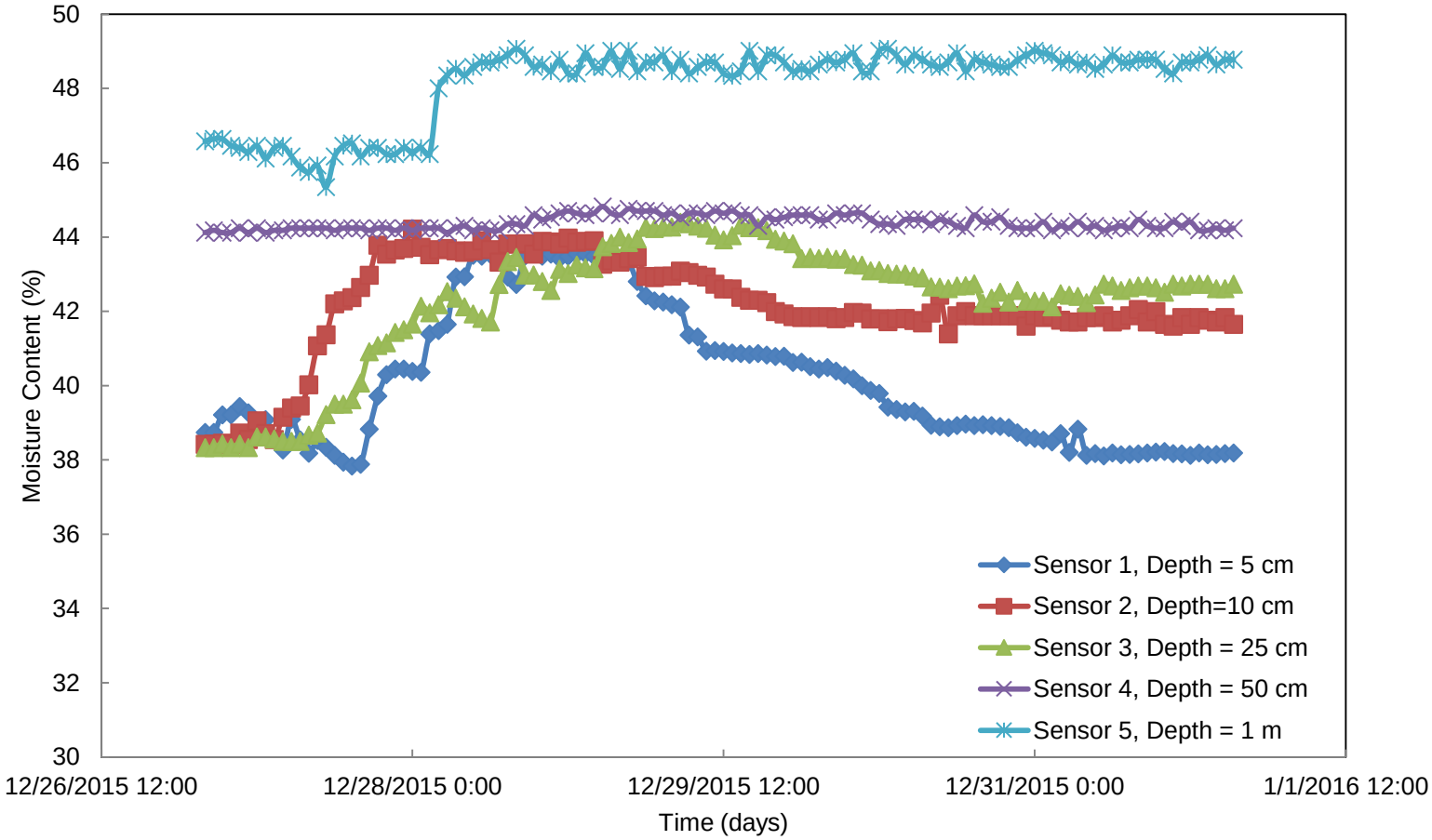

Figure 3-59 Moisture Variation for Rainfall Event held in between 12/27/2015-12 AM to 12/31/2015-11:00 PM at Station 1 Site Location

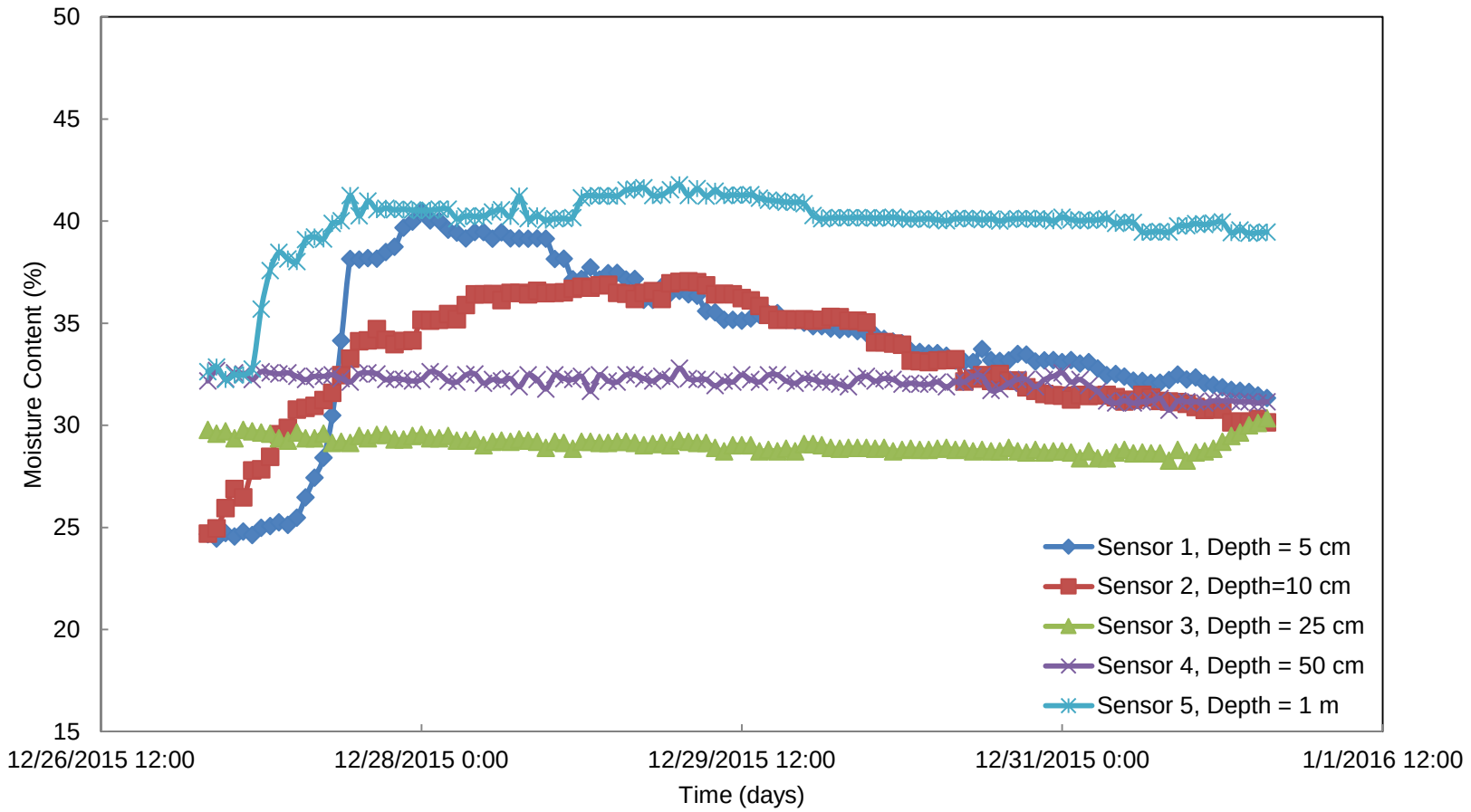

Figure 3-60 Moisture Variation for Rainfall Event held in between 12/27/2015-12 AM to 12/31/2015-11:00 PM at Station 2 Site Location

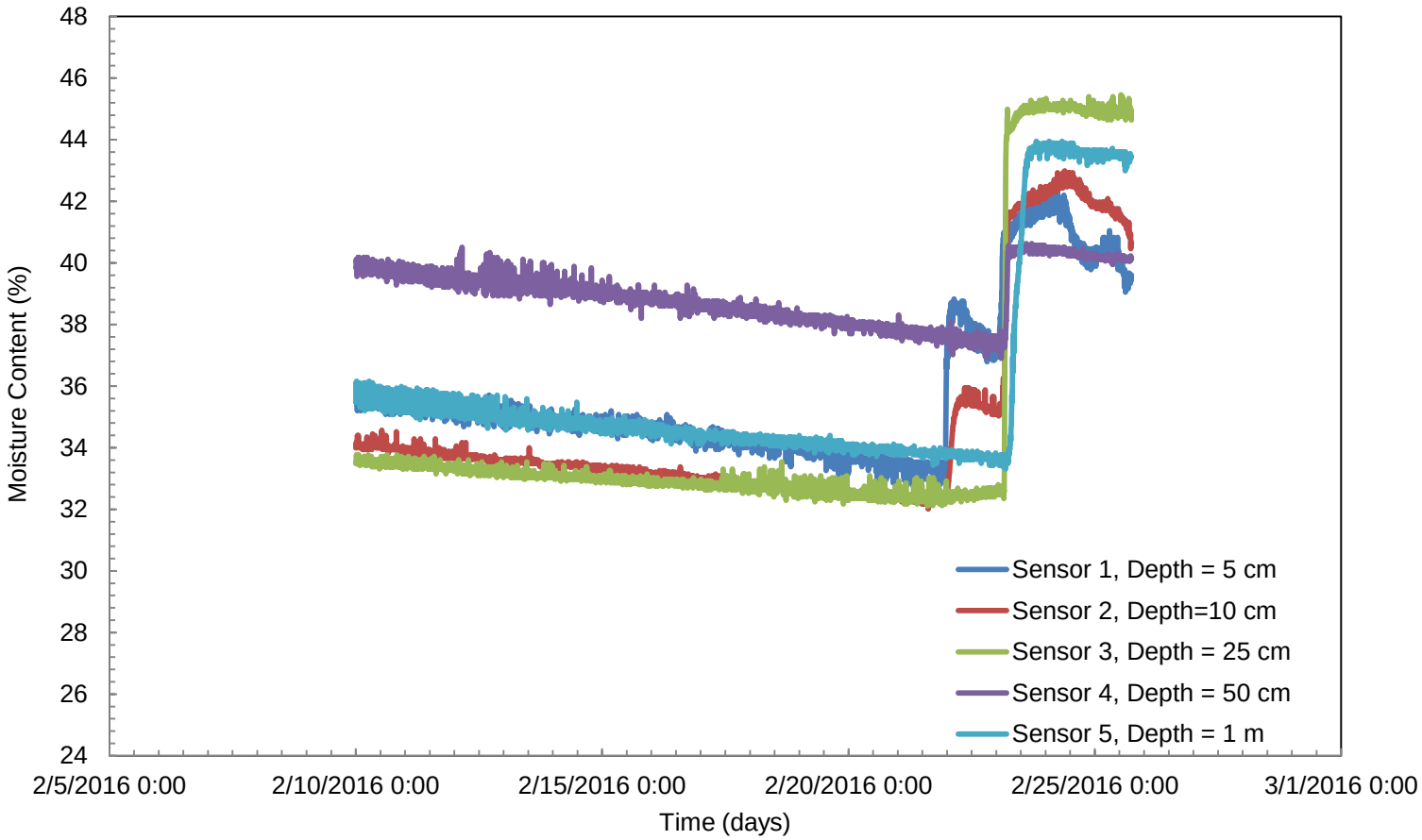

Figure 3-61 Moisture Variation for Rainfall Event held in between 02/10/16-12 AM to 02/25/2016-5:50 PM at Station 1 Site Location

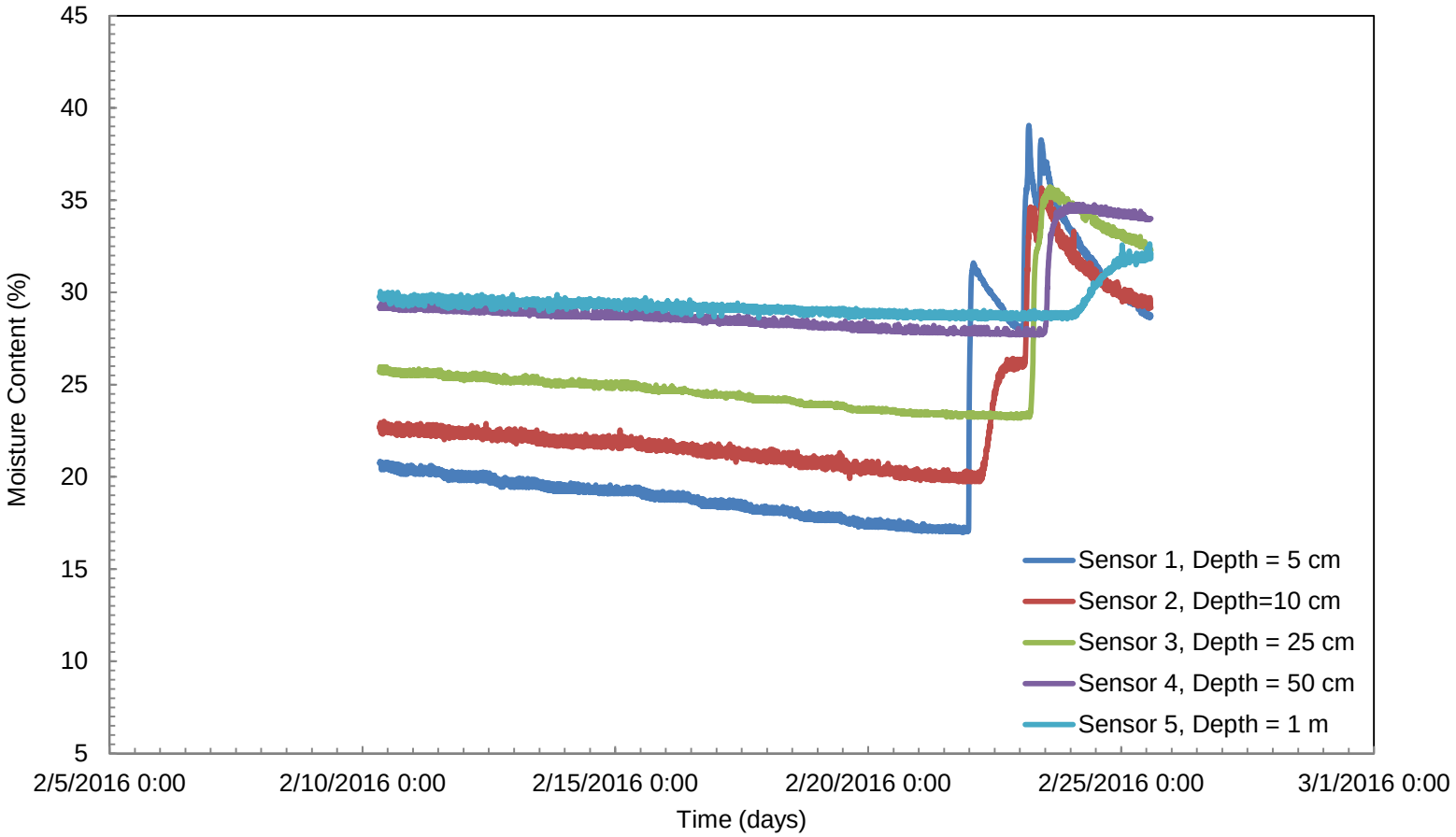

Figure 3-62 Moisture Variation for Rainfall Event held in between 02/10/16-12 AM to 02/25/2016-5:50 PM at Station 2 Site Location

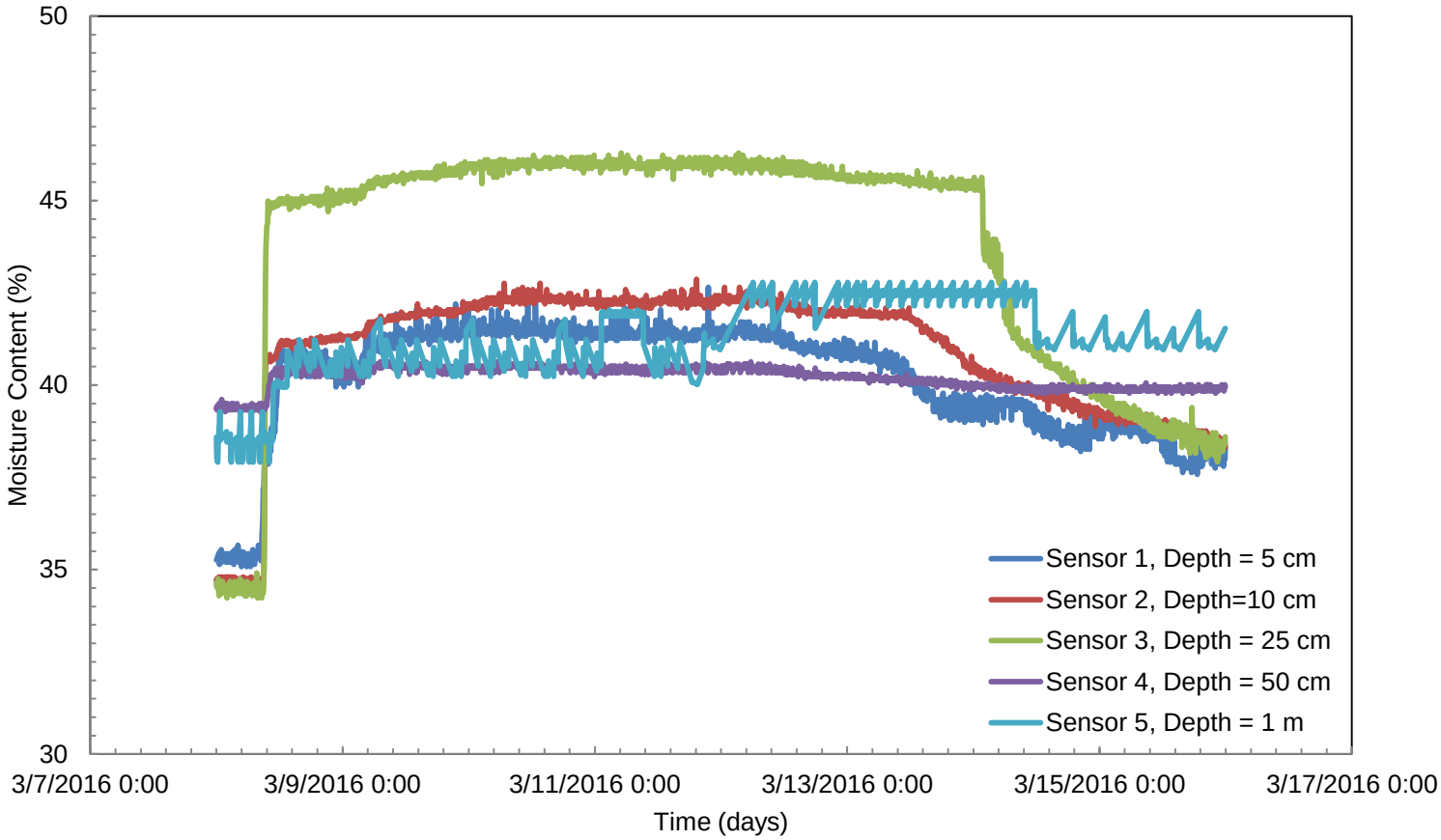

Figure 3-63 Moisture Variation for Rainfall Event held in between 03/08/2016-12:00 AM to 03/15/2016-11:55 PM at Station 1 Site Location

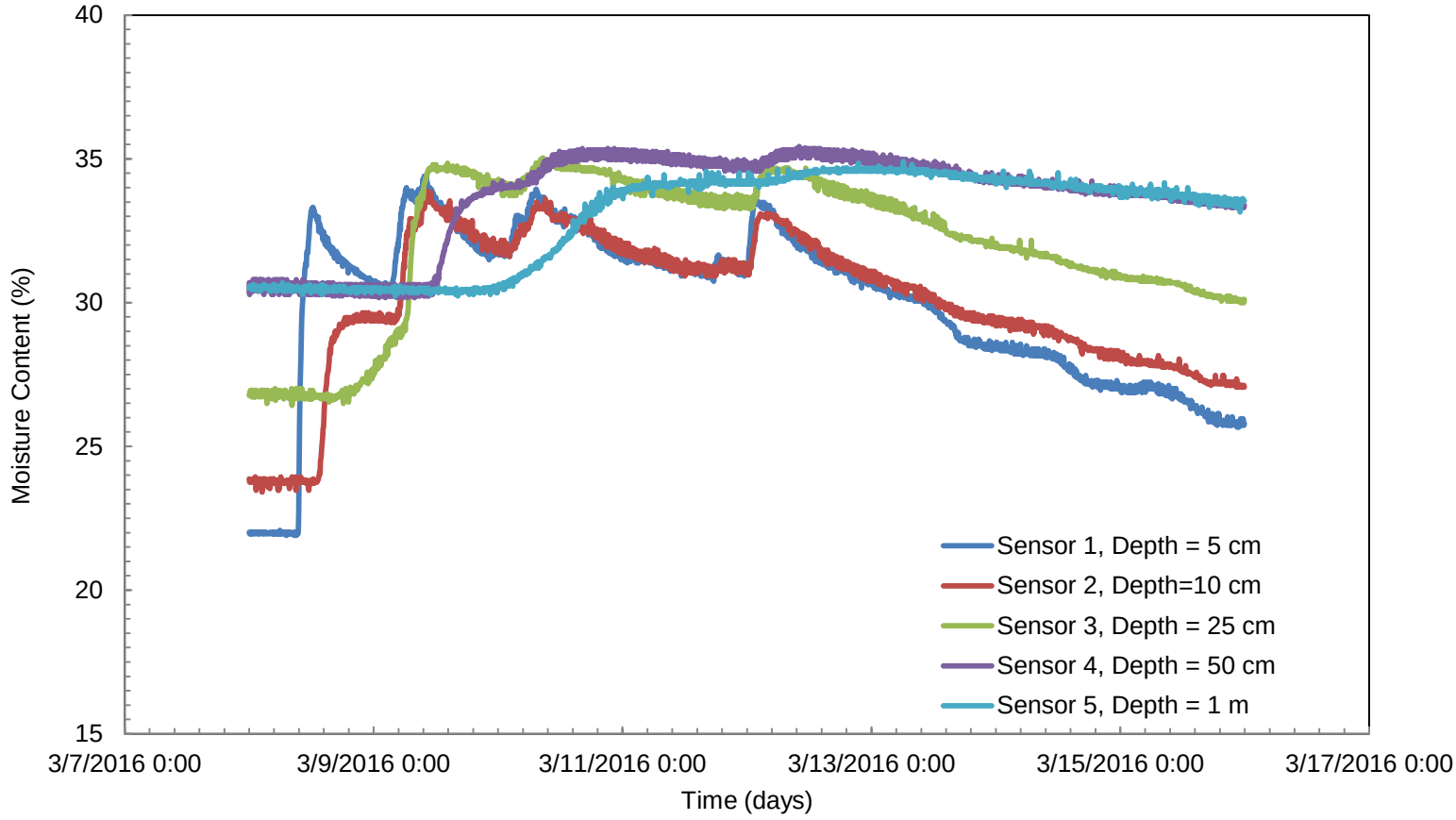

Figure 3-64 Moisture Variation for Rainfall Event held in between 03/08/2016-12:00 AM to 03/15/2016-11:55 PM at Station 2 Site Location

3.4.2 Field Monitoring of TDR (Time Domain Reflectometry) Sensor

The field data monitoring is continuing from the month of August 2015 to till date and all the light, medium and heavy rainfall events were captured for having a better representation of infiltration data for the respective field locations Station 1 and Station 2.

The figures 3-65,3-66,3-67, and 3-68 corresponds to the rainfall events held in between 10/26/2015-12 AM to 11/02/2015-7:10 PM , 12/27/2015-12 AM to 12/31/2015-11:00 PM, 02/10/16-12 AM to 02/25/2016-5:50 PM, and 03/08/2016-12:00 AM to 03/15/2016-11:55PM.

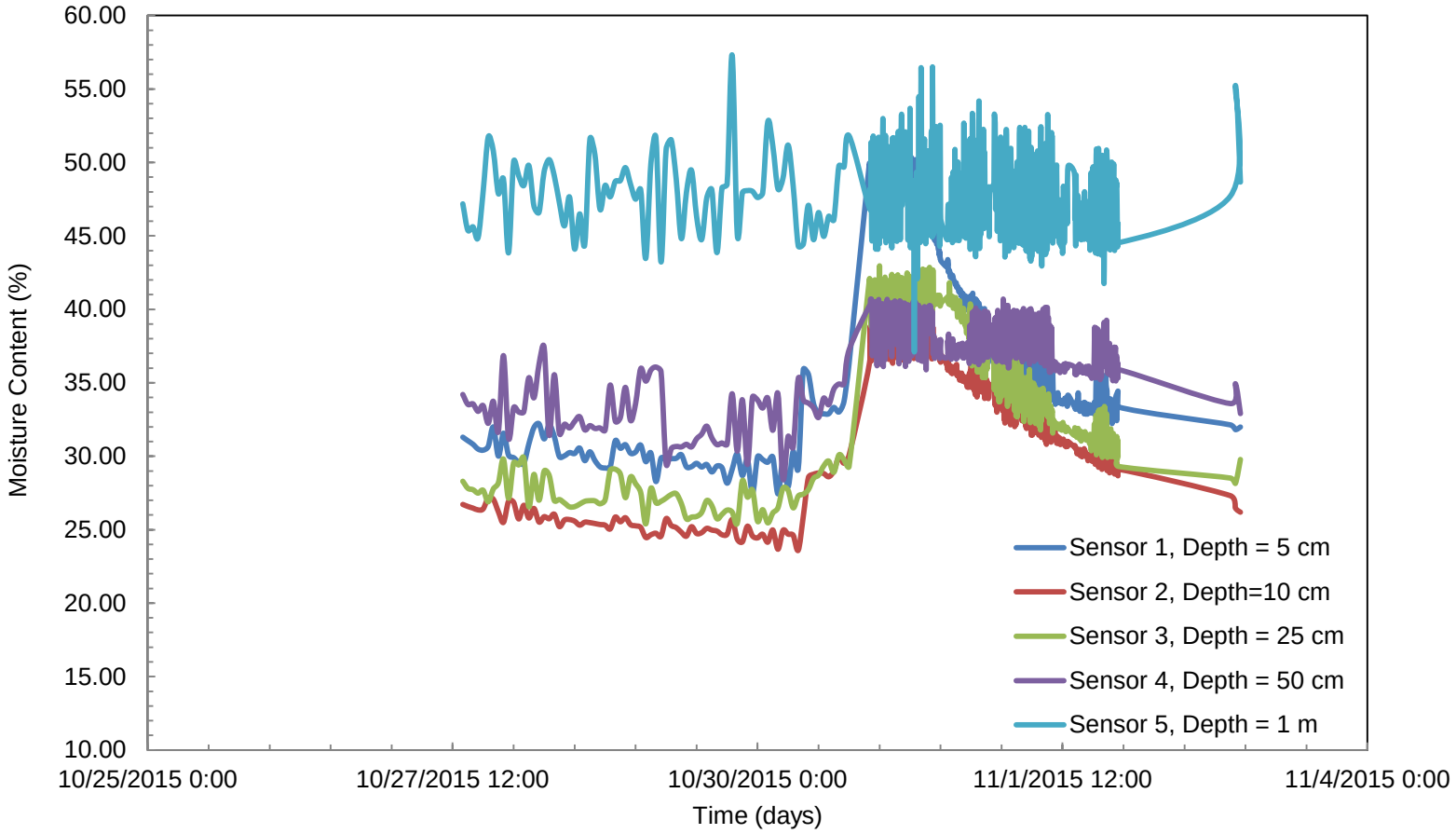

Figure 3-65 Moisture Variation for Rainfall Event held in between 10/26/2015-3:40 AM to 11/02/2015-11:00 PM at Station 3 Site Location

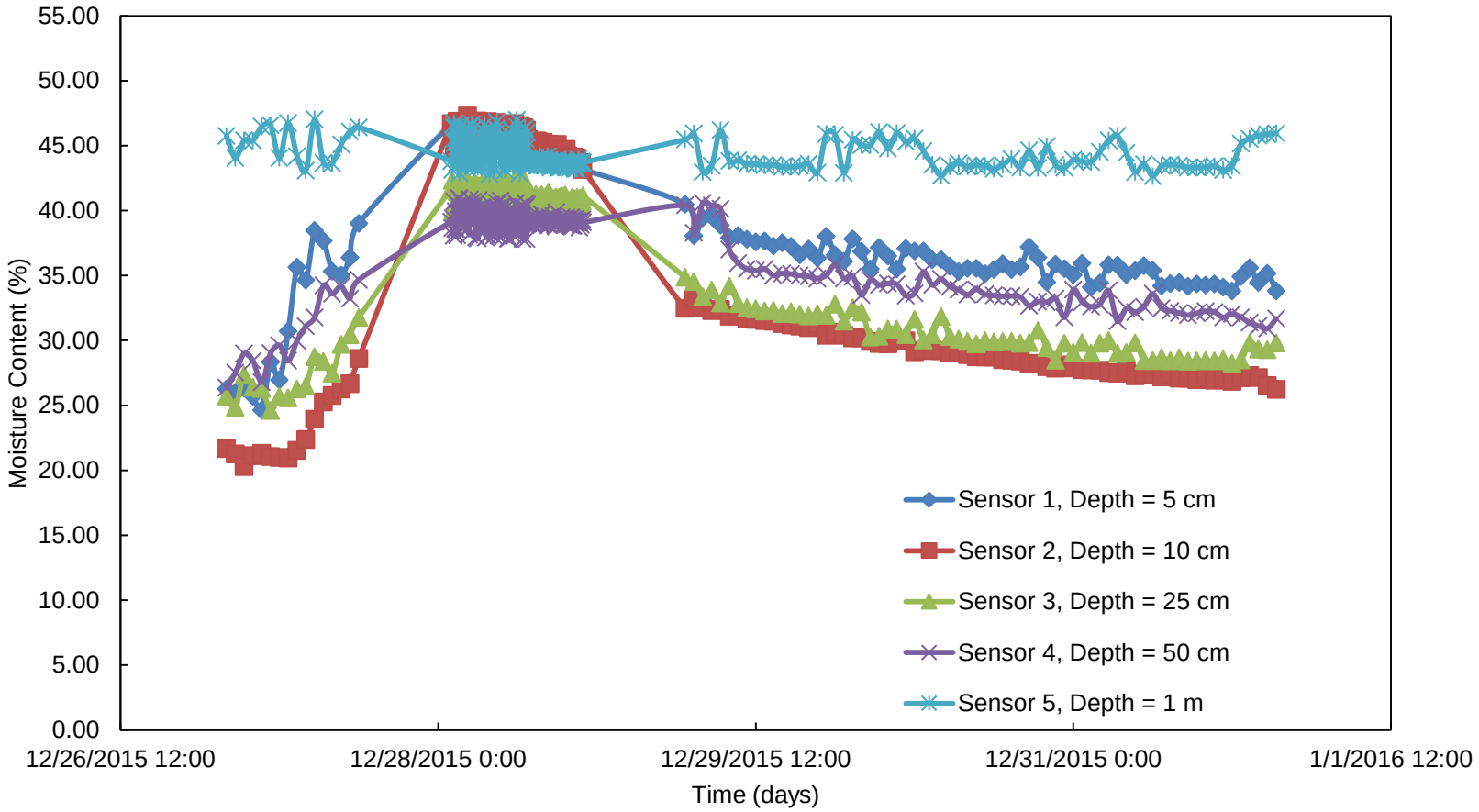

Figure 3-66 Moisture Variation for Rainfall Event held in between 12/27/2015-12 AM to 12/31/2015-11:00 PM at Station 3 Site Location

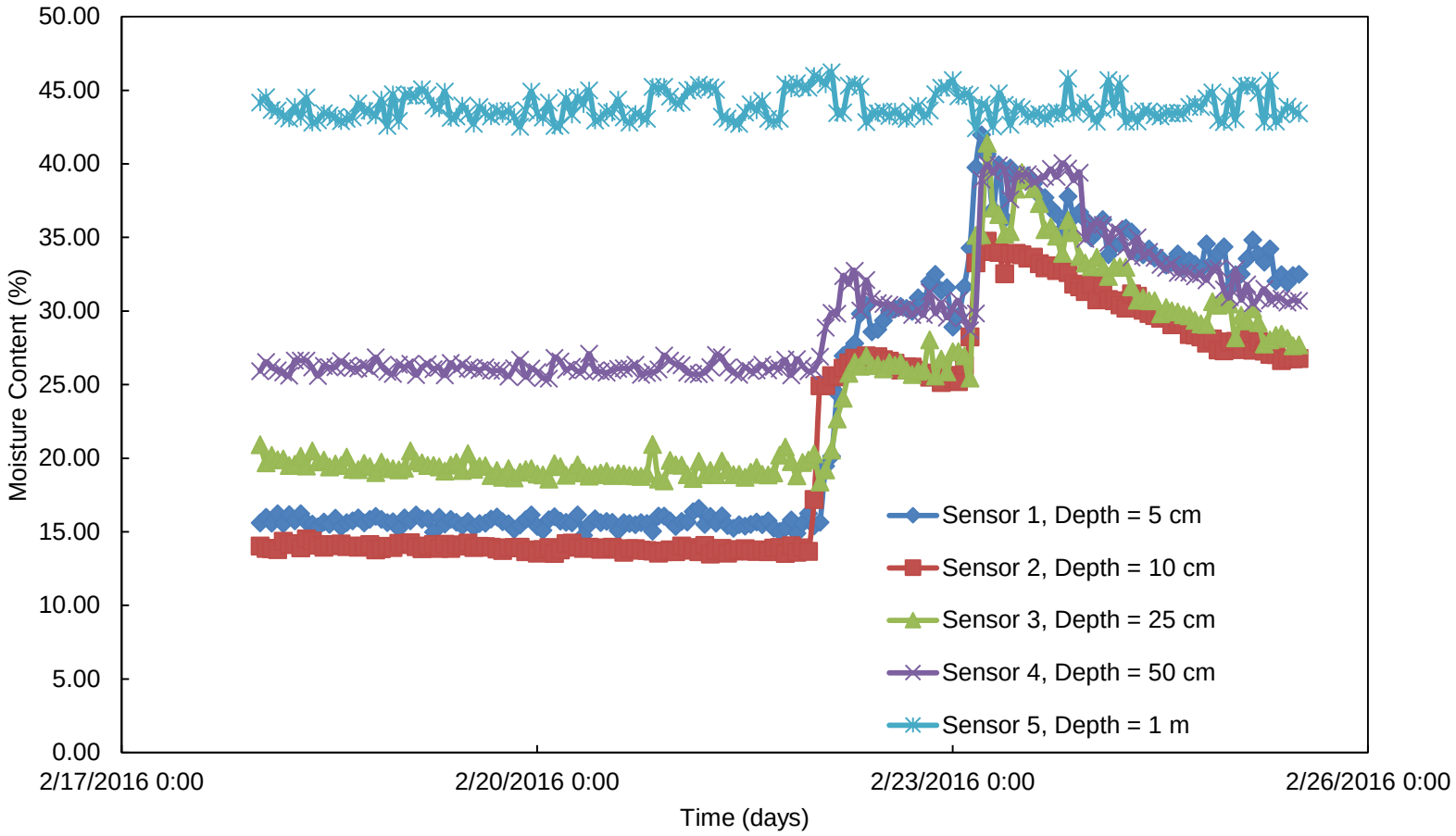

Figure 3-67 Moisture Variation for Rainfall Event held in between 02/18/16-12 AM to 02/25/2016-12 Noon at Station 3 Site Location

Figure 3-68 Moisture Variation for Rainfall Event held in between 03/08/2016-12:00 AM to 03/15/2016-11:55 PM at Station 2 Site Location

3.4 Field Testing using Turf Tec Infiltrometer

3.4.1 Field Monitoring of Saturated Hydraulic Conductivity

Turf Tec Infiltrometer is specifically designed to give infiltration readings directly on site as shown in Figure 3-69. The turf tec infiltrometer consists of a stop watch, a ring and a meter scale. It is fixed onto the ground directly in contact with the soil that needs to be tested. Then, the hole at the center bottom is filled up to the top so that the ring is floating above the water. Slowly, the water drains out to the ground and simultaneously the ring's position is also lowered.

The ring is attached to a vertical scale which has a pointer which shows the reading with the stop watch being operated from the time the experiment is performed. The readings in the meter scale is noted for the time lapse which gives us the infiltration rate. The infiltrometer experiment is performed at three different points for every site location and the best one is chosen for the calculation of saturated hydraulic conductivity using Philips equation as shown in Figure 3-70, 3-71 and 3-72. Philip's Equation is a better way of solving for the transient flow in a porous medium with vertical infiltration.

Figure 3-69 Turf Tec Infiltrometer installed at Station 3 TDR location

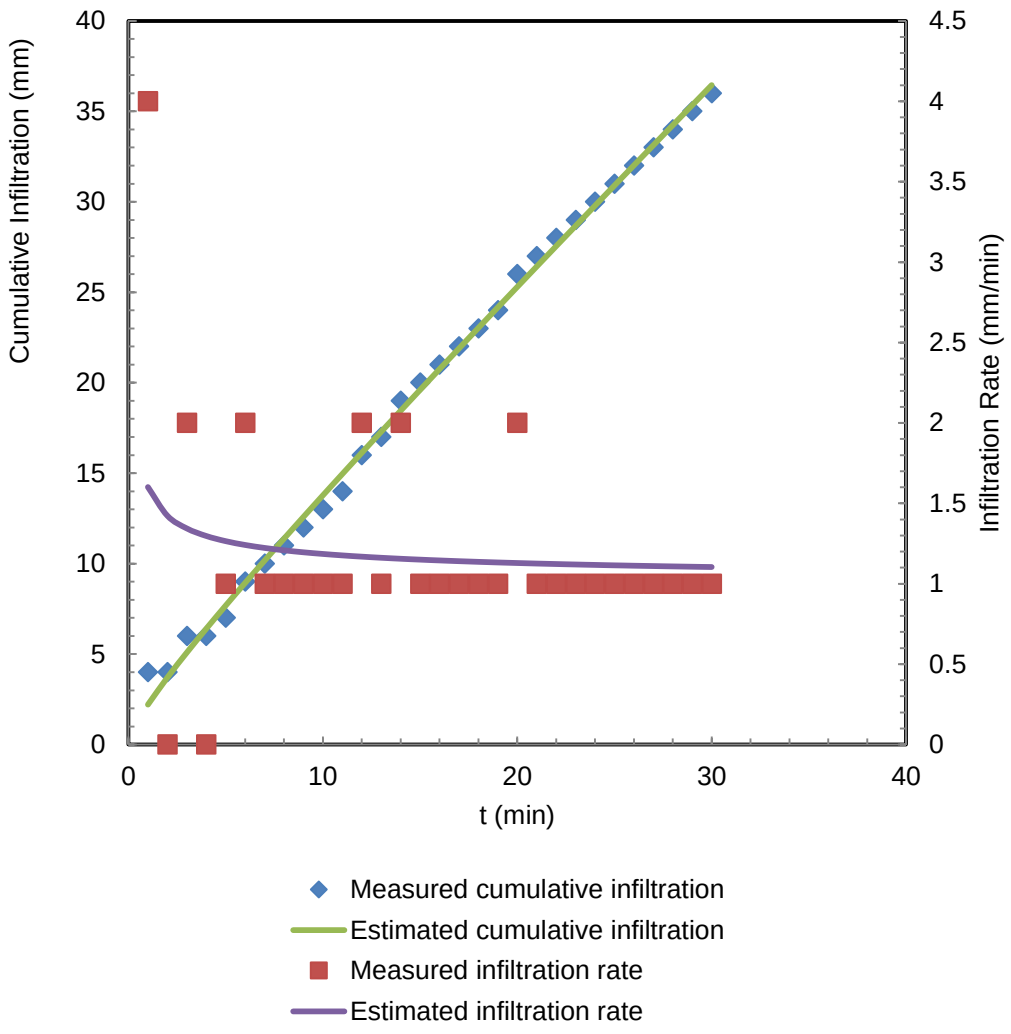

Figure 3-70 Philips Curve Fitting for the Infiltration data at Station 1

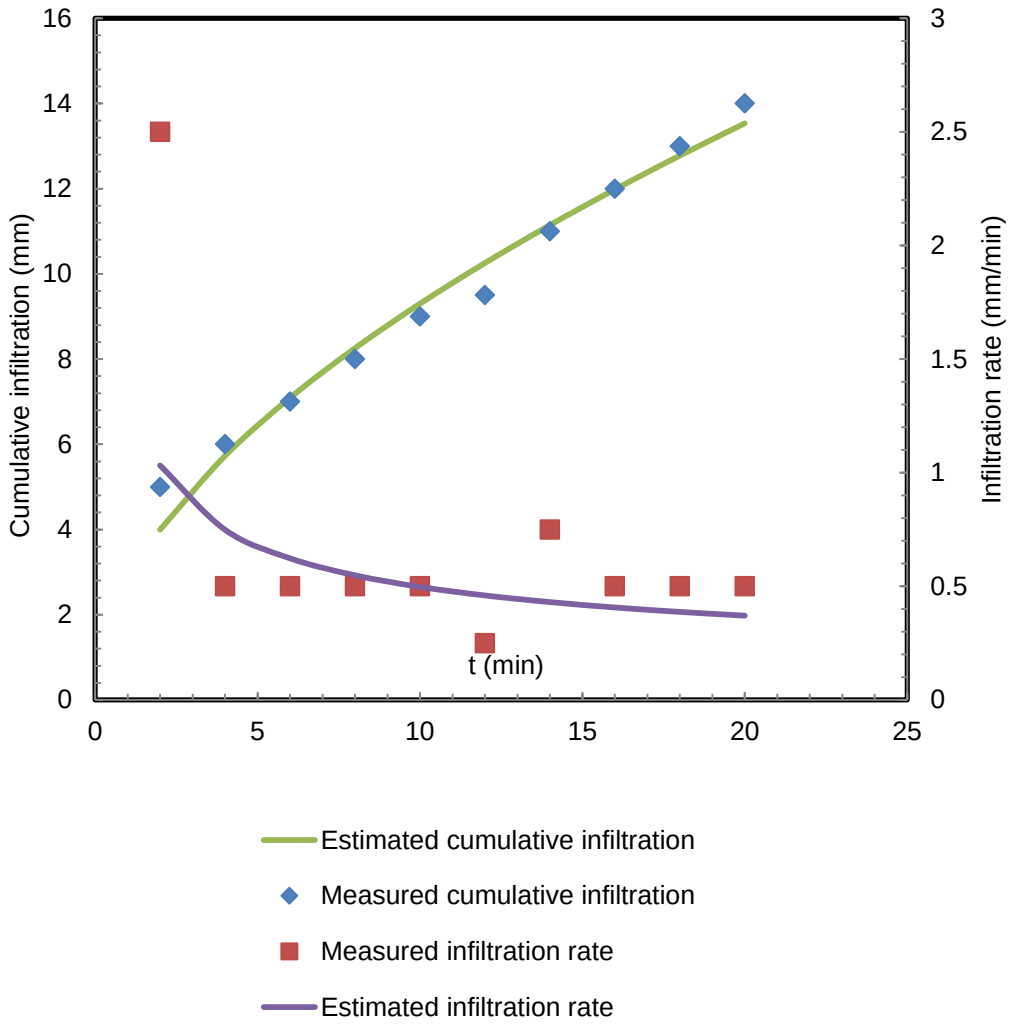

Figure 3-71 Philips Curve Fitting for the Infiltration data at Station 2

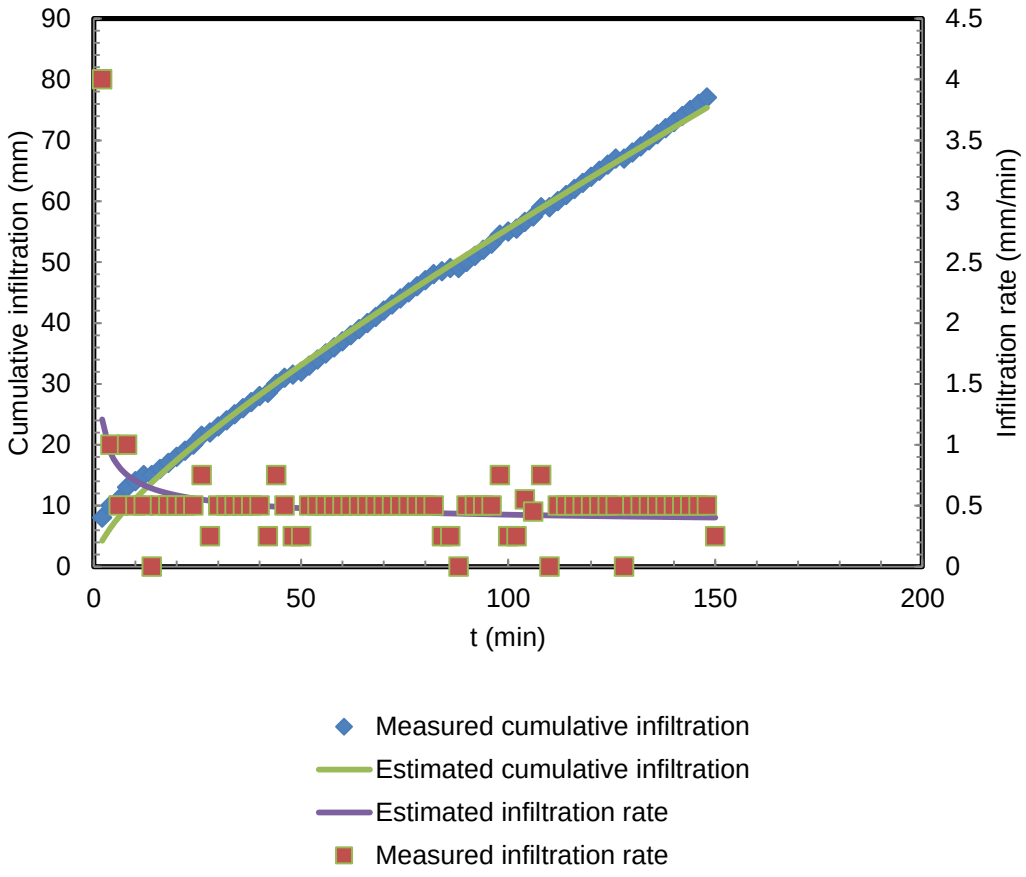

Figure 3-72 Philips Curve Fitting for the Infiltration data at Station 3

Table 3-25 Saturated Hydraulic Conductivity (K_{sat}) calculated from Infiltrometer readings

Location	K_{sat} from Field Test (m/s)
Station 1	7.06×10^{-6}
Station 2	1.09×10^{-6}
Station 3	4.95×10^{-6}

3.5 Summary

The following results obtained from the soil tests are abridged in Table 3-26 and 3-27.

Table 3-26 Atterberg Limits for the soils at Station 1, Station 2 and Station 3

Location	Station 1	Station 2	Station 3
Liquid Limit (LL)	30.5 %	34.5 %	33.0 %
Plastic Limit (PL)	23.6 %	14.8 %	20.3 %
Plasticity Index (PI)	7.0	20.0	13.0
Shrinkage Limit (SL)	7.50 %	16.00 %	8.00 %

Table 3-27 Soil Classification for Station 1, Station 2 and Station 3

Location	Station 1	Station 2	Station 3
Sieve Analysis	% Gravel = 0.000	% Gravel = 0.231	% Gravel = 0.000
	% Sand = 85.747	% Sand = 85.681	% Sand = 84.557
	% Fines = 14.253	% Fines = 14.319	% Fines = 15.443
	D_{10} = 0.068 mm	D_{10} = 0.065 mm	D_{10} = 0.061 mm
	D_{30} = 0.125 mm	D_{30} = 0.120 mm	D_{30} = 0.140 mm
	D_{60} = 0.308 mm	D_{60} = 0.265 mm	D_{60} = 0.405 mm
	C_u = 4.485	C_u = 4.077	C_u = 6.639
	C_c = 0.753	C_c = 0.836	C_c = 0.793
Specific Gravity	2.68	2.66	2.70
Hydrometer Test	% Silt = 10.405	% Silt = 3.723	% Silt = 6.795
	% Clay = 3.848	% Clay = 10.596	% Clay = 8.648
Soil Group	Coarse Grained Soil	Coarse Grained Soil	Coarse Grained Soil
	SC-SM	SC	SC

Table 3-28 Field Capacity at different depths of soil layers at Station 1, 2 and 3

Station 1	Depth- 5 cm	Depth- 10 cm	Depth- 25 cm	Depth- 50 cm	Depth- 1 m
Field Capacity	36 %	38 %	38 %	44 %	NA
Station 2	Depth- 5 cm	Depth- 10 cm	Depth- 25 cm	Depth- 50 cm	Depth- 1 m
Field Capacity	27 %	27 %	28 %	33 %	30 %
Station 3	Depth- 5 cm	Depth- 10 cm	Depth- 25 cm	Depth- 50 cm	Depth- 1 m
Field Capacity	20 %	15 %	18 %	28 %	NA

Table 3-29 Permanent Wilting Point for Station 1, 2 and 3

Location	Station 1	Station 2	Station 3
Permanent Wilting Point	23.83 %	22.51 %	27.06 %

The field capacity calculated here is a short term field capacity of the soil assuming the water has drained due to gravity and there is no loss due to evaporation or transpiration. The field capacity for depth at 1 m for Station 1 and Station 3 cannot be calculated owing to the soil being in a continuous state of saturation. The field capacity at Station 3 is less as the sensors are placed in a slope. So, most of the water is drained out.

Further validation of the field results required the measurement of hydraulic conductivity of the soil. The movement of water in the soil is spatially variable. A comparison of hydraulic conductivity is a good measure to describe the ease with which the water can move through the pore spaces in the soil. The saturated hydraulic conductivity of the soil in the laboratory was tested using Falling Head Permeameter. To have an assessment for the in-situ saturated hydraulic conductivity, Turf-Tec Infiltrometer

was mobilized at the three site locations. Table 3-30 shows the comparison of saturated hydraulic conductivity obtained at the field and the lab and the results are close enough.

Table 3-30 Validation of hydraulic conductivity at Station 1, Station 2 and Station 3

Location	K_{sat} from Lab Test (m/s)	K_{sat} from Field Test (m/s)
Station 1	3.47×10^{-6}	7.06×10^{-6}
Station 2	1.19×10^{-6}	1.09×10^{-6}
Station 3	2.25×10^{-6}	4.95×10^{-6}

Field Cone Test was performed on the three site locations to determine the in-situ field density and moisture content in the soil as shown in Table 3-31 to compare with that obtained from the TDR and TDT locations. The di-electric constant readings from the TDR sensors are converted to the volumetric water content scale using Topp's empirical formula. But, in case of TDT sensors, the readings obtained are already in volumetric water content scale. For the validation of the TDT and TDR sensors, samples are augered at three different depths i.e. at 5 cms, 10 cms and 25 cms for the three site locations.

The reason that we are taking samples at upper three depths for validation was based on the larger variability in moisture content over a period of time noted while monitoring the data. The field samples are properly sealed immediately after being retrieved to avoid any loss of moisture. Now, the moisture content for the field samples are tested in the laboratory in-accordance with the ASTM Standard. In-situ density obtained from the sand cone test is used for conversion of gravimetric water content determined in the laboratory to volumetric water content scale to have a comparison with the moisture content obtained in the same scale from TDR and TDT sensor locations as shown in Table 3-32, 3-33, and 3-34.

The results seems to be in-congruence with that of the field with an allowance variation of + 2 % or – 2% due to the errors owing to sampling in the field and disturbance in the waveform evaluation technique of the sensors.

Table 3-31 Sand Cone Test performed at Station 1, Station 2 and Station 3

Location	Station 1	Station 2	Station 3
Moist Unit Weight (pcf)	104.395	105.676	92.502
Moisture Content (%)	30.430	29.100	17.440
Dry Unit Weight (pcf)	80.041	81.859	78.769
Dry Unit Weight (g/cm^3)	1.282	1.311	1.262

Table 3-32 Validation of Moisture Content data for the TDT Sensor at Station 1

Sample Depth	Gravimetric Water Content (%)	Volumetric Water Content (%)	Water Content determined by TDR Sensor (%)
1st Layer – 5 cms	27.783	35.562	35.540
2nd Layer – 10 cms	27.705	35.463	35.140
3rd Layer – 25 cms	26.060	33.357	34.750

Table 3-33 Validation of Moisture Content data for the TDT Sensor at Station 2

Sample Depth	Gravimetric Water Content (%)	Volumetric Water Content (%)	Water Content determined by TDR Sensor (%)
1st Layer – 5 cms	18.272	23.936	22.310
2nd Layer – 10 cms	19.654	25.747	23.990
3rd Layer – 25 cms	21.932	28.731	26.950

Table 3-34 Validation of Moisture Content data for the TDT Sensor at Station 3

Sample Depth	Gravimetric Water Content (%)	Volumetric Water Content (%)	Water Content determined by TDR Sensor (%)
1st Layer – 5 cms	13.364	16.839	15.769
2nd Layer – 10 cms	10.652	13.422	12.680
3rd Layer – 25 cms	13.369	16.845	15.790

The monitoring of data for the 3 site locations for different rainfall event and their effects were captured for the infiltration analysis of the soil.

A light rainfall of 0.56 mm (0.022 inch) per hour was observed on 12/13/2015 and the data interval time was set to 1 hour to capture the variation of moisture content. The TDR sensors located at a depth of 5 cm, 10 cm, 25 cm, 50 cm at Station 3 showed an increase in moisture content up to 8%; followed by an increase of 6%, 2% and 4% respectively as shown in Figure 3-73. With light rainfall, the top layer absorbs most of the water to get saturated after which through capillary action, the other subsequent layers slowly absorbs rest of the water infiltrating at a much lower pace in subsequent days.

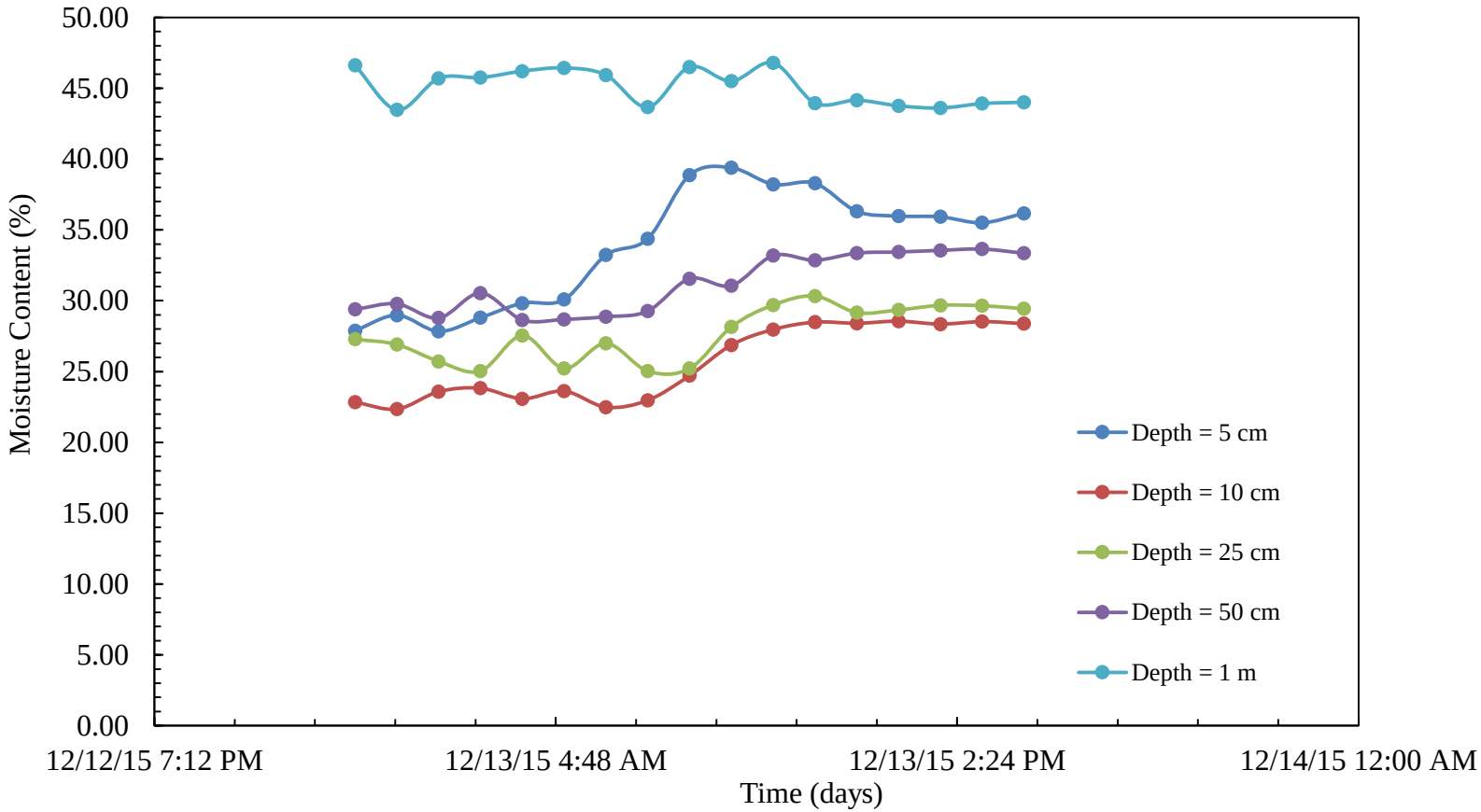

Figure 3-73 Light Rainfall Event for the period (Date: 12/13/2015 - 12 AM to 4 PM) at Station 3

A heavy rainfall of 7.87 mm (0.31 inch) per hour was observed in between the time period 12/30/2015 to 12/31/2015 and the data interval was set to 5 minutes to capture the variation of moisture content. The TDT sensor located at a depth of 5 cm, 10 cm, 25 cm, 50 cm showed an increase in moisture content up to 11 %; followed by an increase of 7 %, 8 %, 5 % and 1 % respectively. With heavy continuing rainfall the surface soil nearly reached saturation which led to infiltration being homogeneous which is the reason for steady constant change in moisture content for the a subsequent deeper two layers. Preferential flow was also reported at depths of 10 cm and 25 cm due to presence of organic matter in the soil as depicted in Figure 3-74.

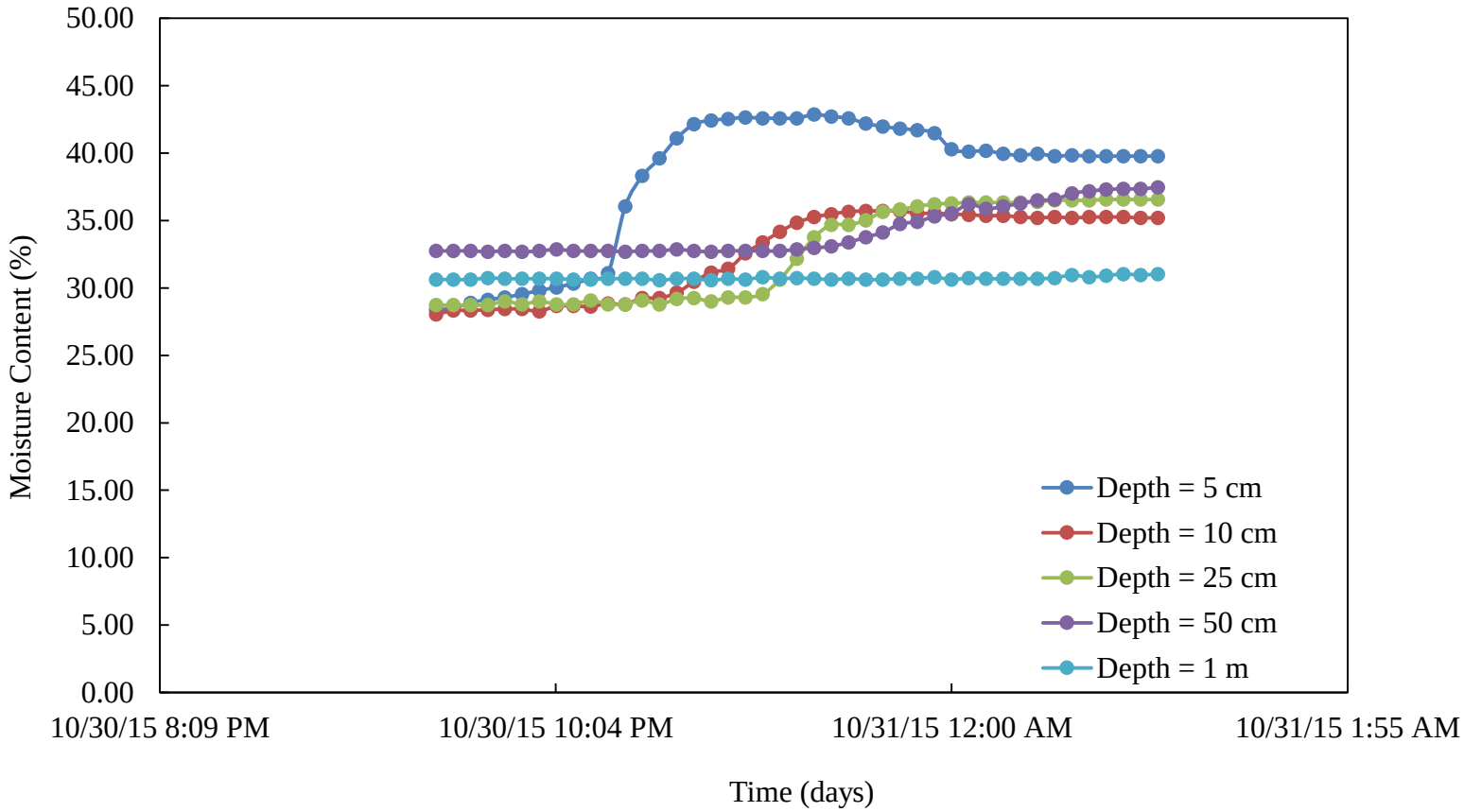

Figure 3-74 Heavy Rainfall Event for the period (Date: 12/30/2015 – 9:30 PM to 12/31/2015 – 1:00 AM) at Station 2

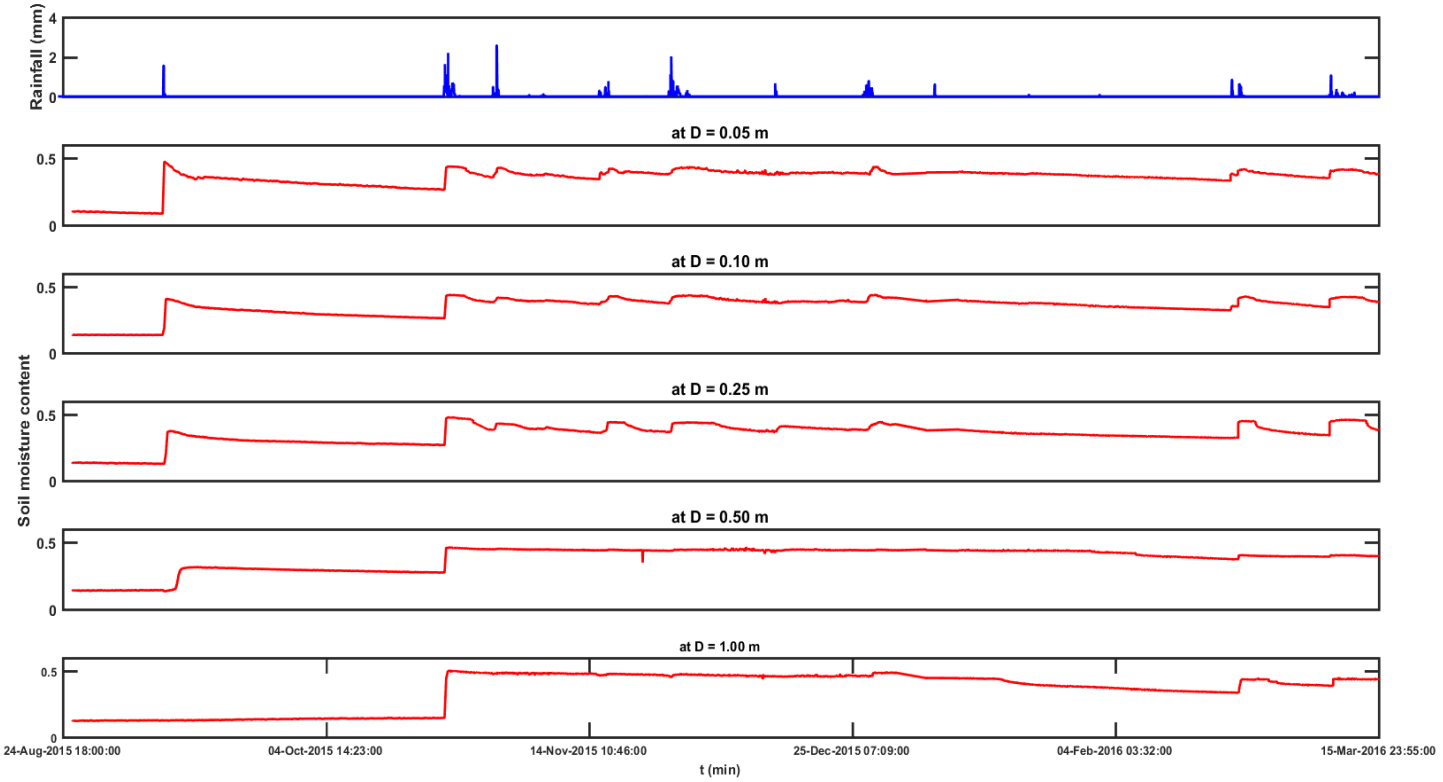

Figure 3-75 Time Series for rainfall vs moisture content variation throughout the depth of the soil profile at Station 1

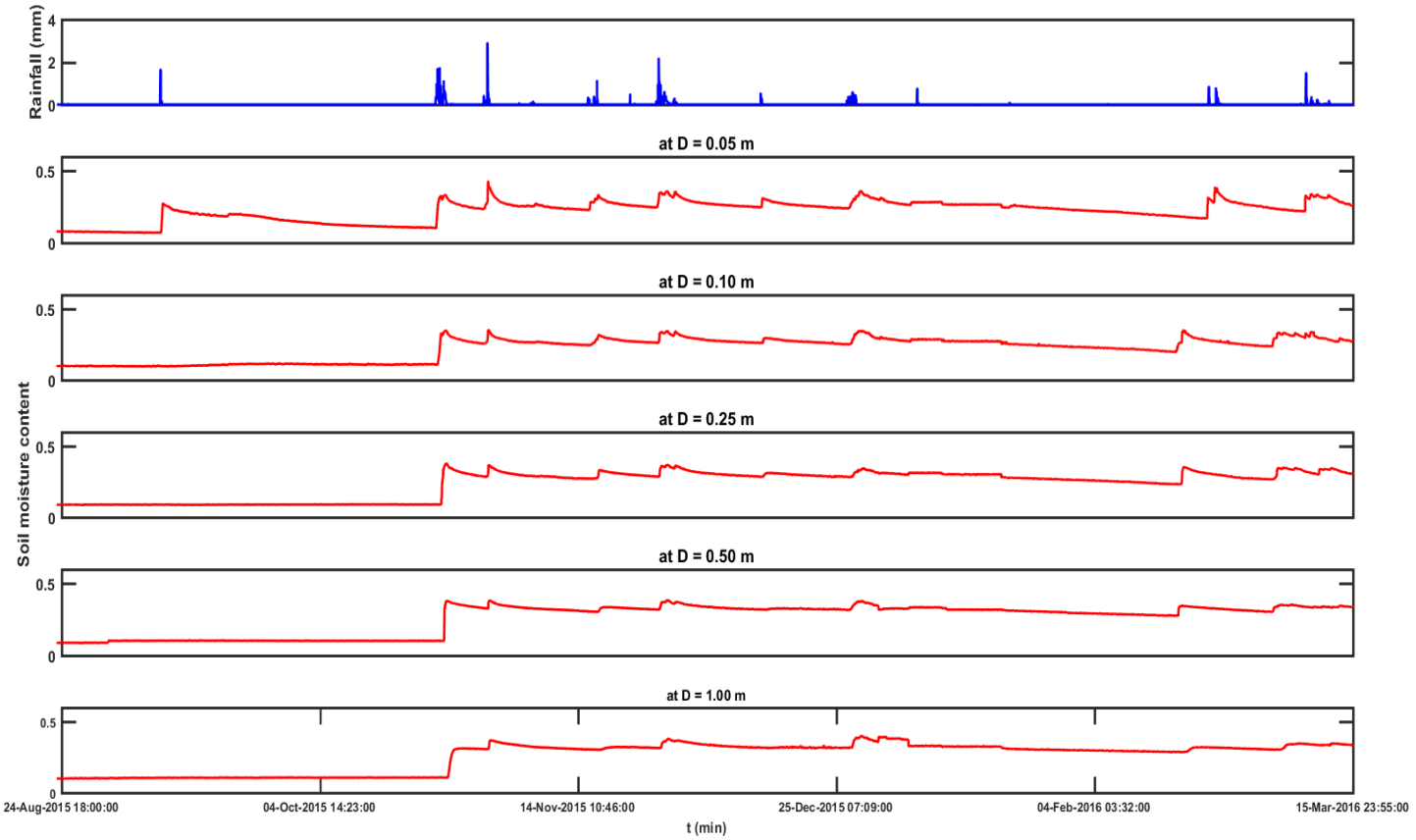

Figure 3-76 Time Series for rainfall vs moisture content variation throughout the depth of the soil profile at Station 2

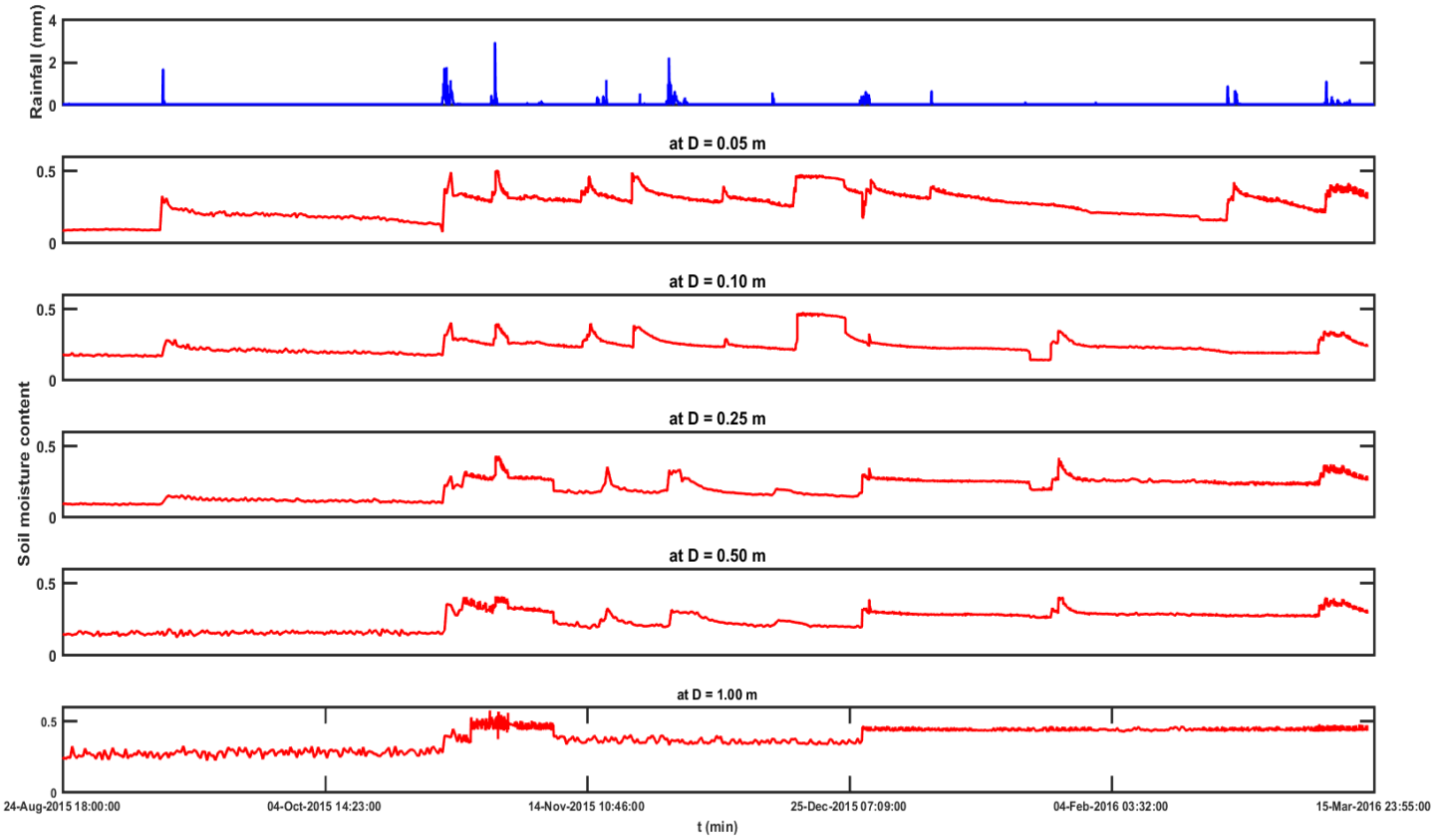

Figure 3-77 Time Series for rainfall vs moisture content variation throughout the depth of the soil profile at Station 3

Chapter 4

INFILTRATION STUDY IN LABORATORY

4.1 Introduction

4.2 Single sensor infiltration study

4.2.1 Materials and Methods

Three rod stainless steel probe TDR sensor was fabricated in the laboratory with the probe needle of dimension (210 mm x 3.15 mm) and a probe head of dimension (109.3 mm x 50 mm x 30 mm) as shown in Figure 4-1. A rectangular model was designed using hard acrylic plastic of dimension (240 mm x 260 mm) with the TDR sensor being placed at the bottom. ASTM Graded Sand was the material selected to fill up the model with 25 blows of equal compaction being applied at every one-third of the height of the model with the help of a tamping rod as shown in Figure 4-2.

A rainfall simulator was fabricated to cover up the whole length of the model with fine pores of diameter 3 mm at an equal spacing of 30 mm. The water to the top of the rainfall simulator was supplied through the means of a constant overhead container placed at a height of 600 mm managed through a valve for a uniform flow as shown in Figure 4-3. The waveforms are recorded using PMTDR program and saved to be later analyzed through an Excel algorithm.

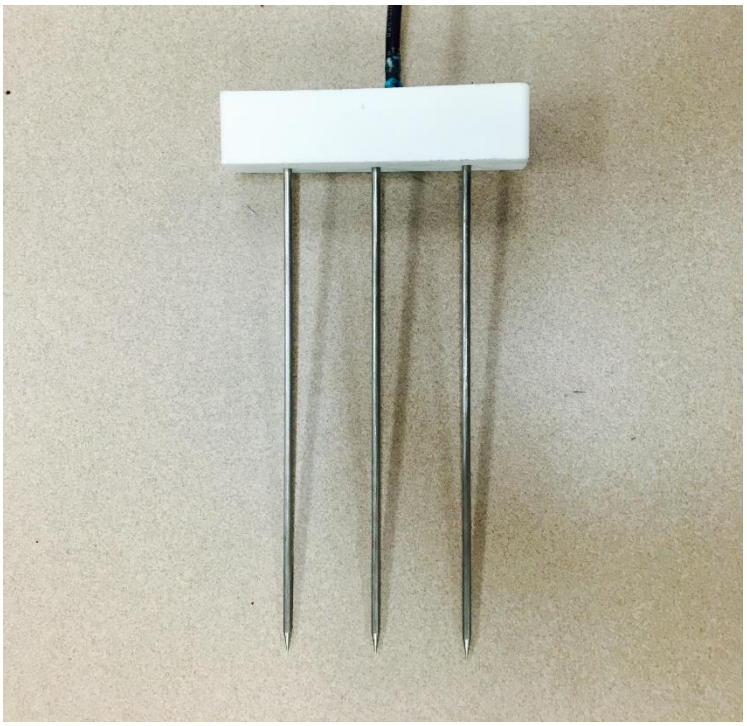

Figure 4-1 TDR Probe of length 21 cm fabricated at the lab

Figure 4-2 Compaction being applied to the ASTM Graded Sand

Figure 4-3 Infiltration Model for the Laboratory testing

4.2.2 Analysis of Results

The infiltration model was run with the uniform flow of water through it with readings being recorded at every 1 minute. The total duration of time for the soil sample to get completed saturated was 9 minutes. The TDR waveforms for every one minute interval is shown in Figure 4-4 and the corresponding change in dielectric constant and electrical conductivity are shown in Figure 4-5 and 4-6.

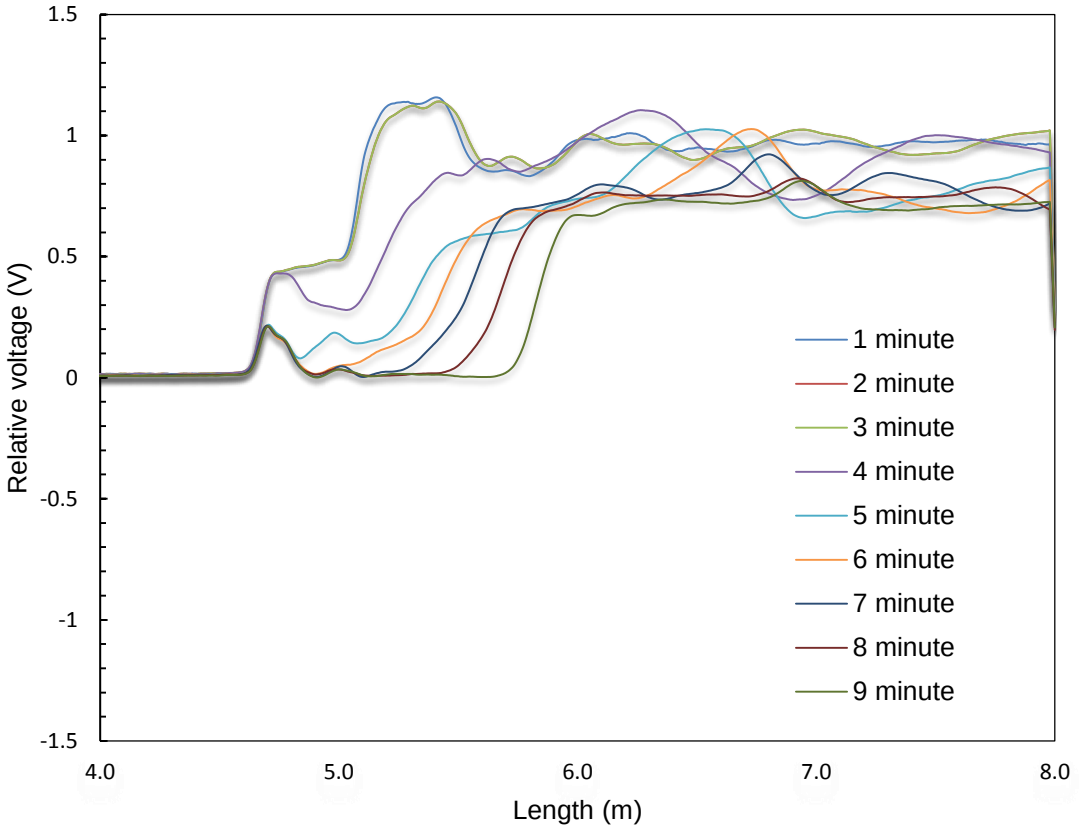

Figure 4-4 Time Variation of Waveform with Infiltration Rate

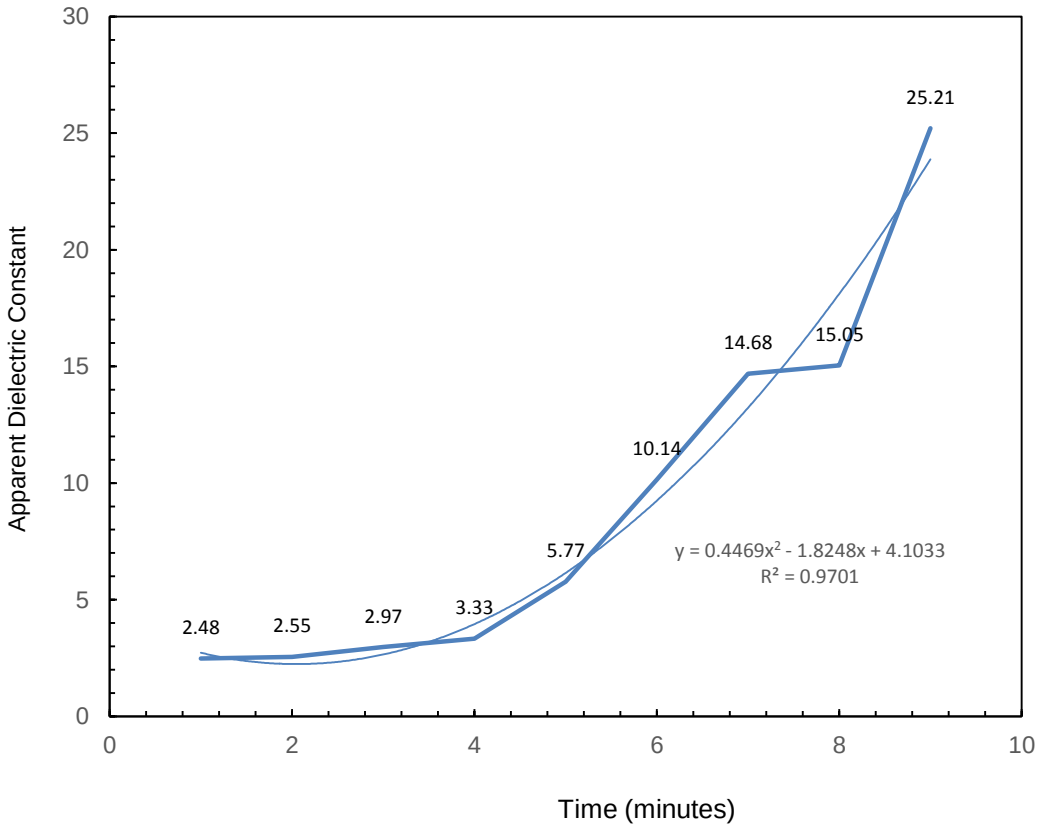

Figure 4-5 Time Variation of Dielectric constant with Infiltration Rate

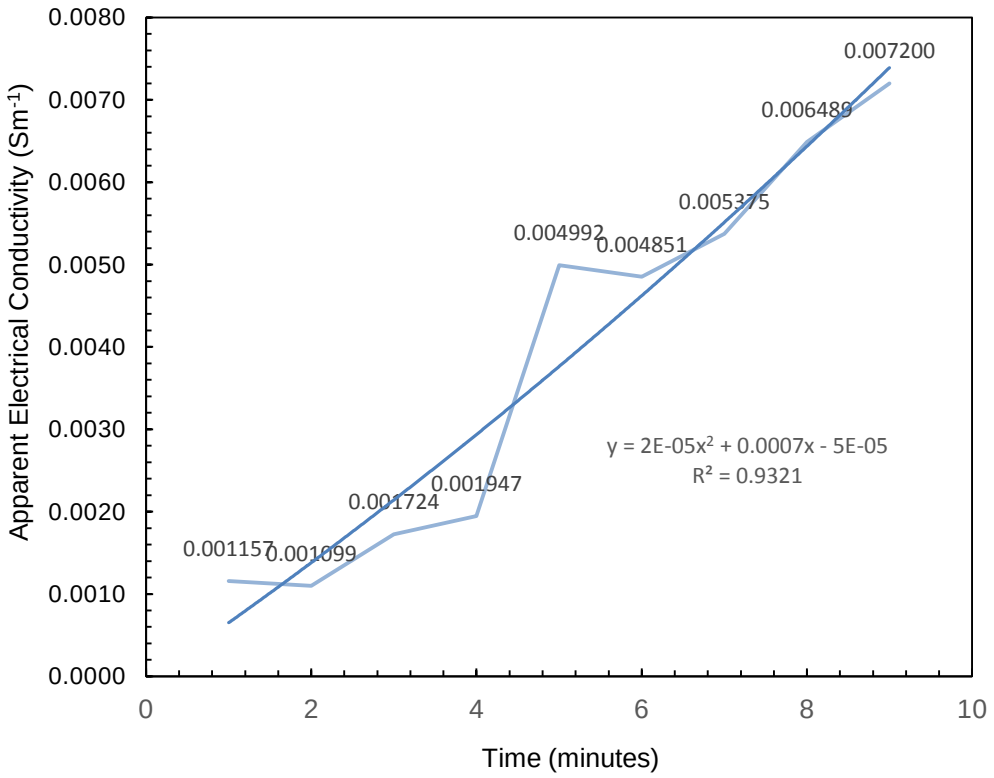

Figure 4-6 Time Variation of Electrical Conductivity with Infiltration Rate

4.3 Soil Column infiltration study

4.3.1 Materials and Methods

A schematic diagram of the soil column apparatus is shown in Figure 4-7 and 4-8, which shows a 1 meter high soil column for a particular infiltration study.

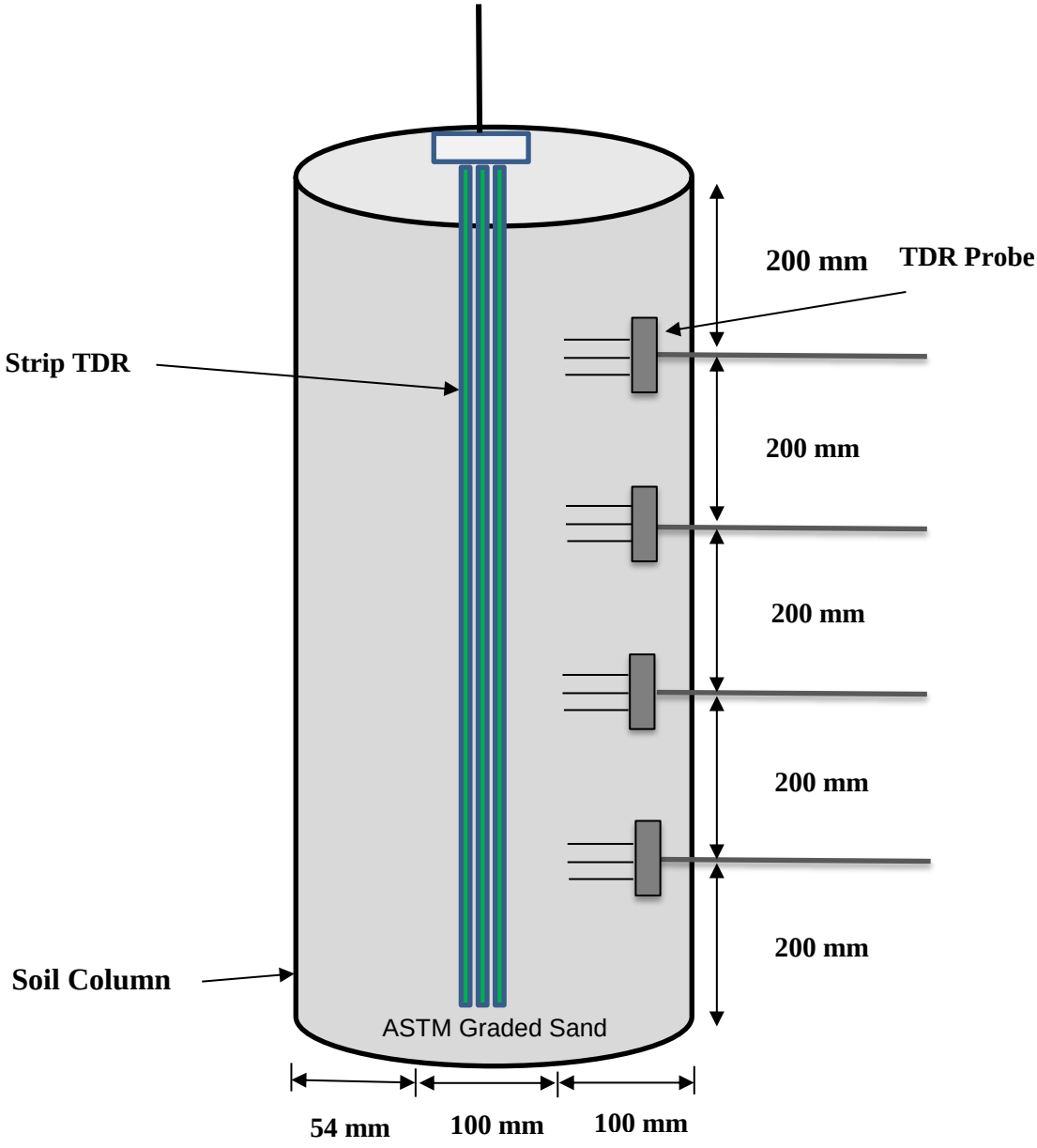

Figure 4-7 Soil Column for Infiltration Test

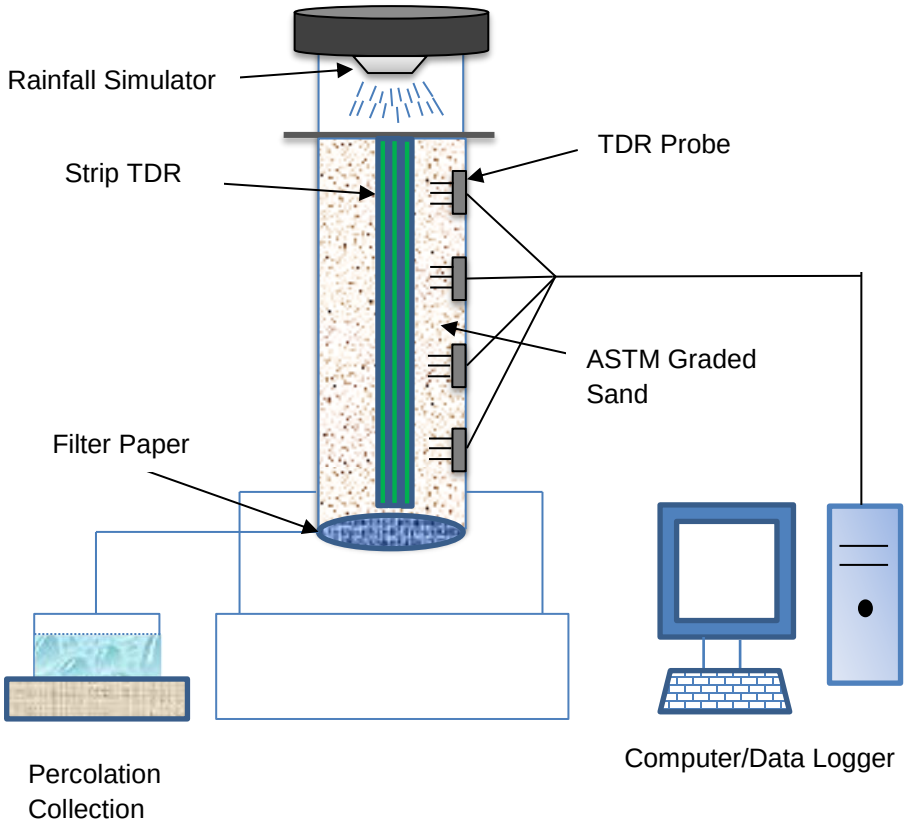

Figure 4-8 Detailed Schematic Diagram for the Soil Column apparatus

The cylinder used in the experiment consisted of several components. Firstly, the body of the cylinder was made of strong transparent PVC material which ensures more durability and strength with a 5-mm thick wall and 150-mm internal diameter. The PVC cylinder has to be strengthened by four vertical stiffeners to provide a larger hoop resistance against lateral stress, when the soil was placed. Secondly, the bottom of the cylinder was fixed to a stainless steel base plate to receive much of the compaction energy. Finally, the base plate was supported by 220 mm above the floor level with aluminum stool having four corners with one open corner for the collection of water.

Threaded hole was provided to install TDR probes. Threaded plugs were used to seal the holes that were not in use during the experiment. The position of the threaded holes was chosen based on the results of seepage analysis using SEEP/W (2002), so that changes in wetting front in the soil column could be monitored more accurately.

Time domain reflectometry (TDR) sensors are employed to monitor changes in the water content of the soil in the soil column apparatus. A typical TDR system consists of three main parts i.e. TDR 100, a co-axial cable and TDR sensor probes. TDR 100 produces an electromagnetic waves that propagates along the co-axial cable to the TDR probe installed into the soil. Four soil parameters can be determined using TDR probe namely; dielectric constant, electrical conductivity, water content and dry density can be determined by analyzing the waveform.

Uniformly distributed ASTM Graded Sand was distributed through the top to fill the soil column. ASTM Graded sand contains 98% passing through 0.600 mm sieve size. The dry density of the soil would be controlled to a desired value during the compaction of soils in the column in order to attain uniform soil columns. In order to control the compaction density closely, oven dried soils are poured through a funnel as shown in Figure 4-9. Pouring the sand through the funnel ensures equal distribution of sand through the depth of 92 cm of the soil column.

A uniform flow of water was applied with the nozzle pipe discharging 300 ml/min (equivalent to 0.3 mm of rainfall) from the top of soil column for a duration of 15 minutes until the moisture level has reached the bottom of the soil column. The water was spread uniformly using a layer of filter paper that was placed on the top of the soil surface. The wetting front for every one minute interval was noted as shown in the Figure 4-10, 4-11, 4-12, 4-13, 4-14, 4-15,4-16,4-17,4-18, 4-19, 4-20, 4-21, 4-22, 4-23 and 4-24.

Figure 4-9 Pouring of ASTM Graded Sand through the means of funnel for equal compaction in the Soil Column Assembly

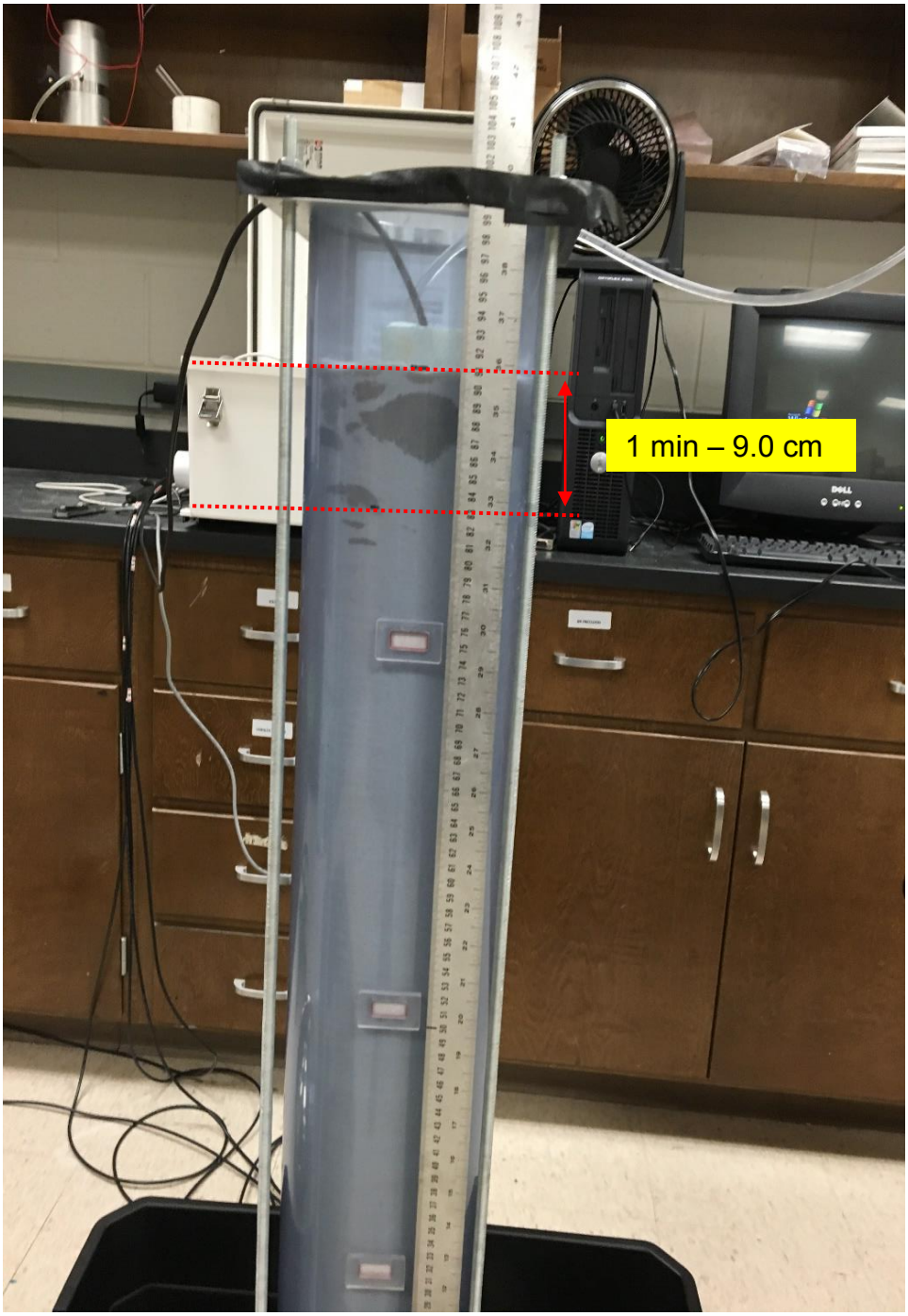

Figure 4-10 Wetting Front for the time interval of 1 min

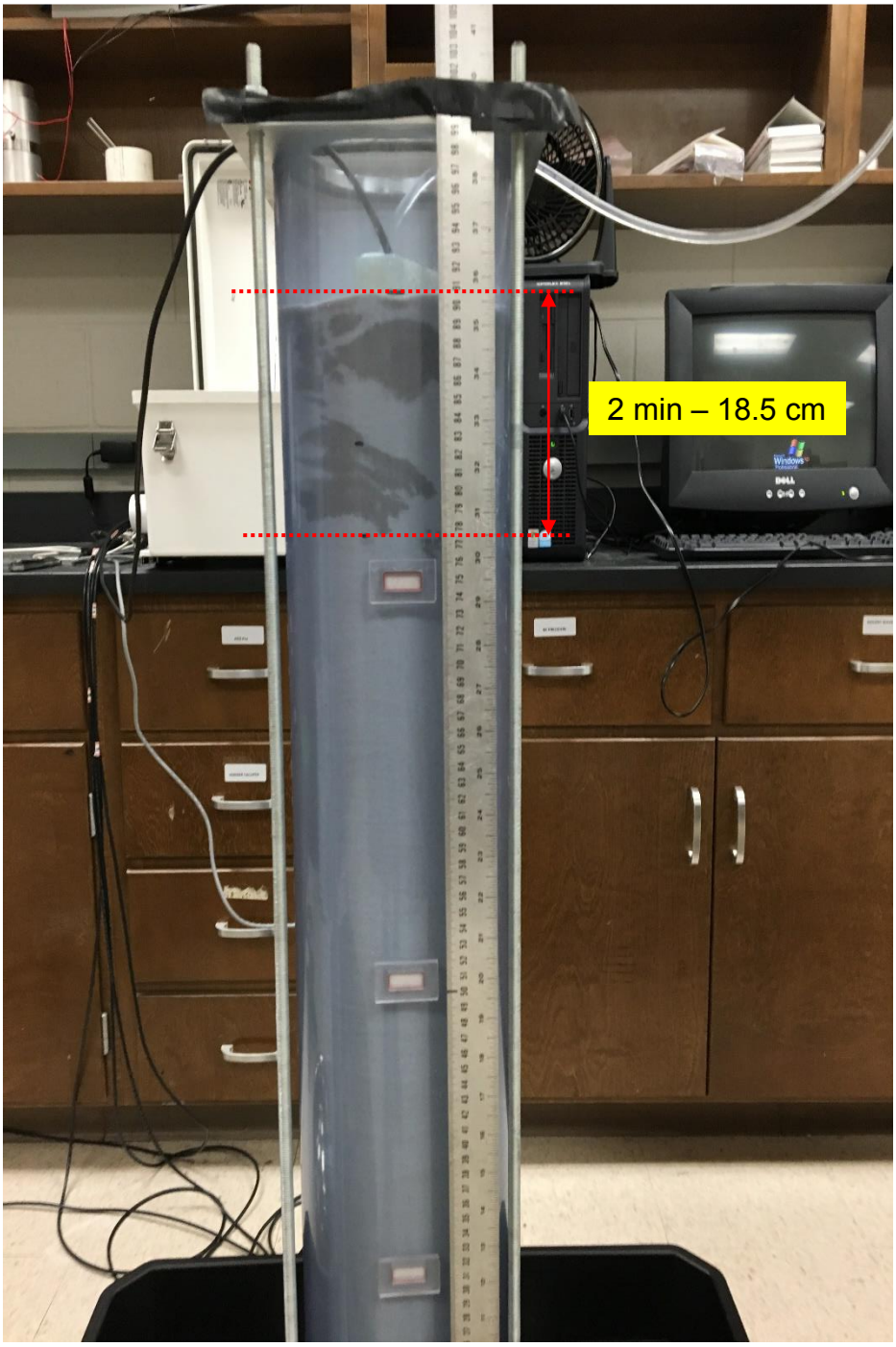

Figure 4-11 Wetting Front for the time interval of 2 min

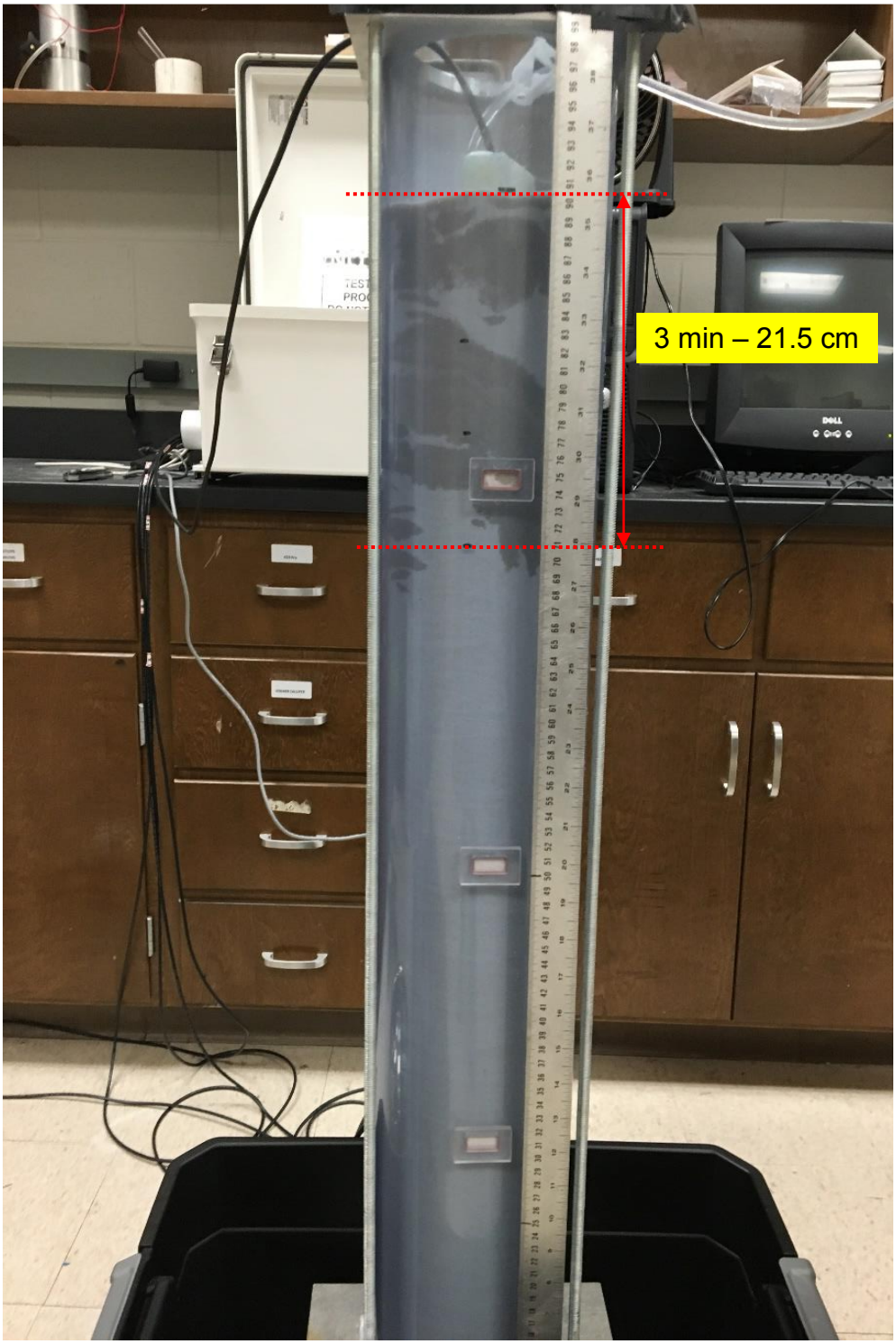

Figure 4-12 Wetting Front for the time interval of 3 min

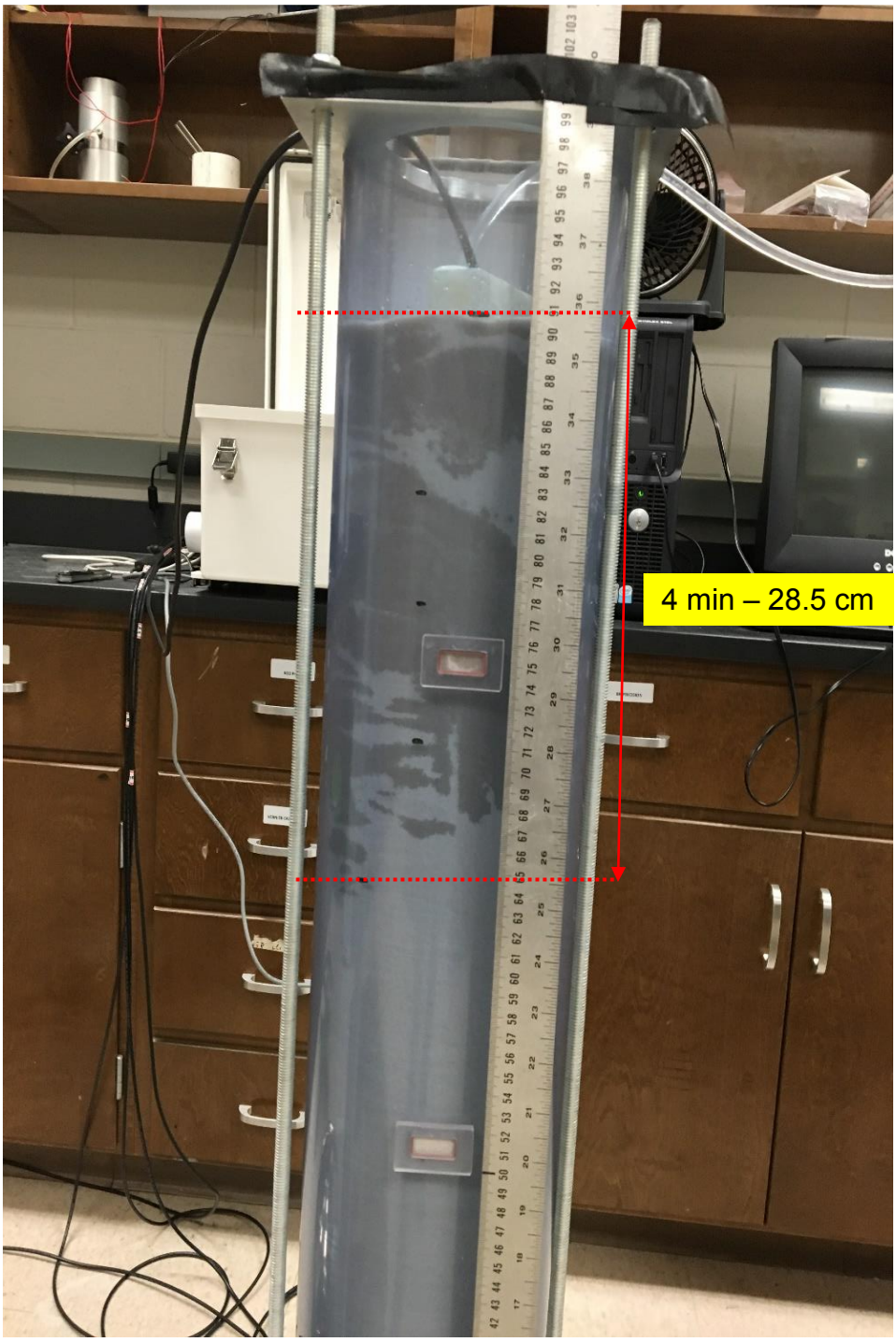

Figure 4-13 Wetting Front for the time interval of 4 min

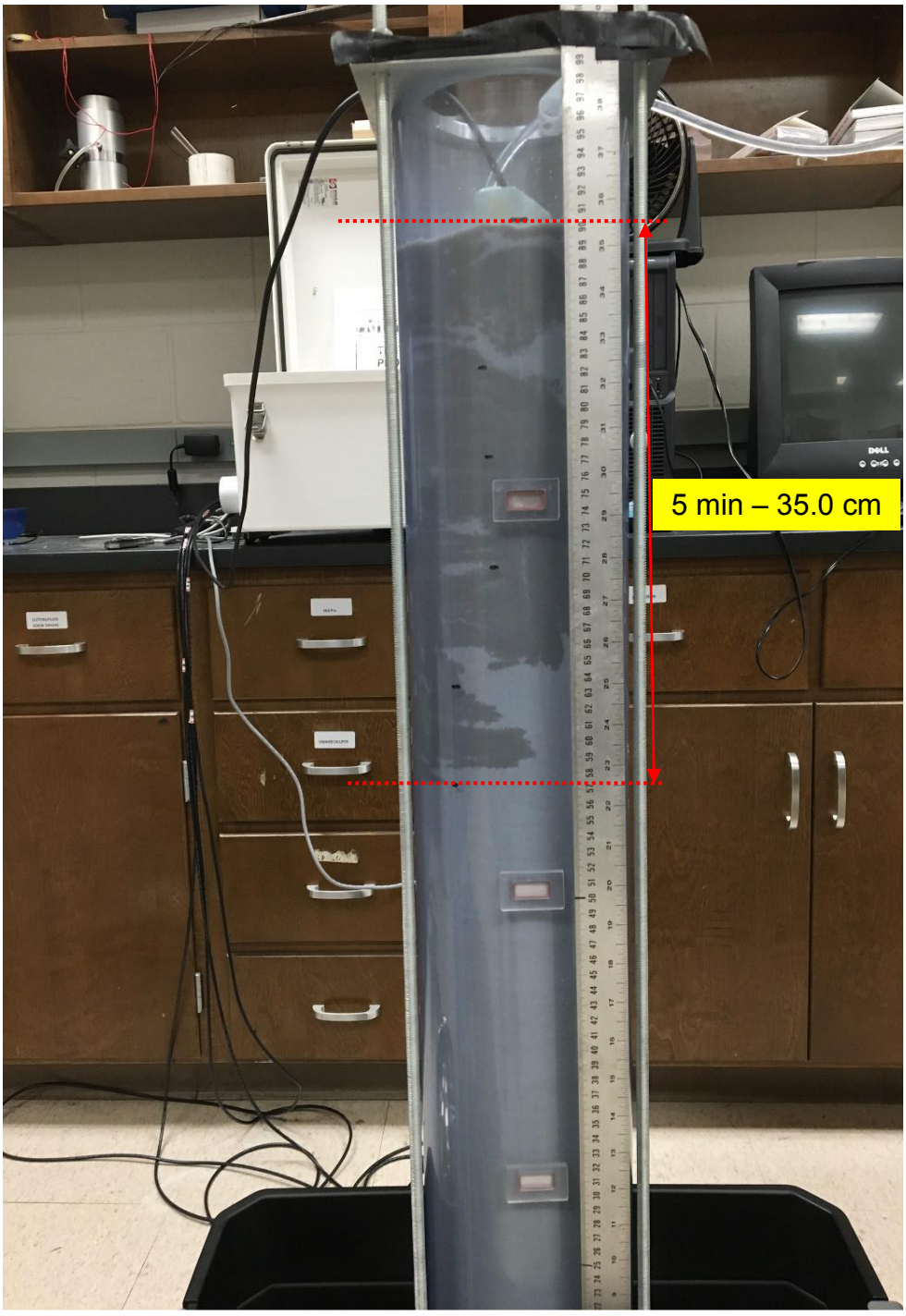

Figure 4-14 Wetting Front for the time interval of 5 min

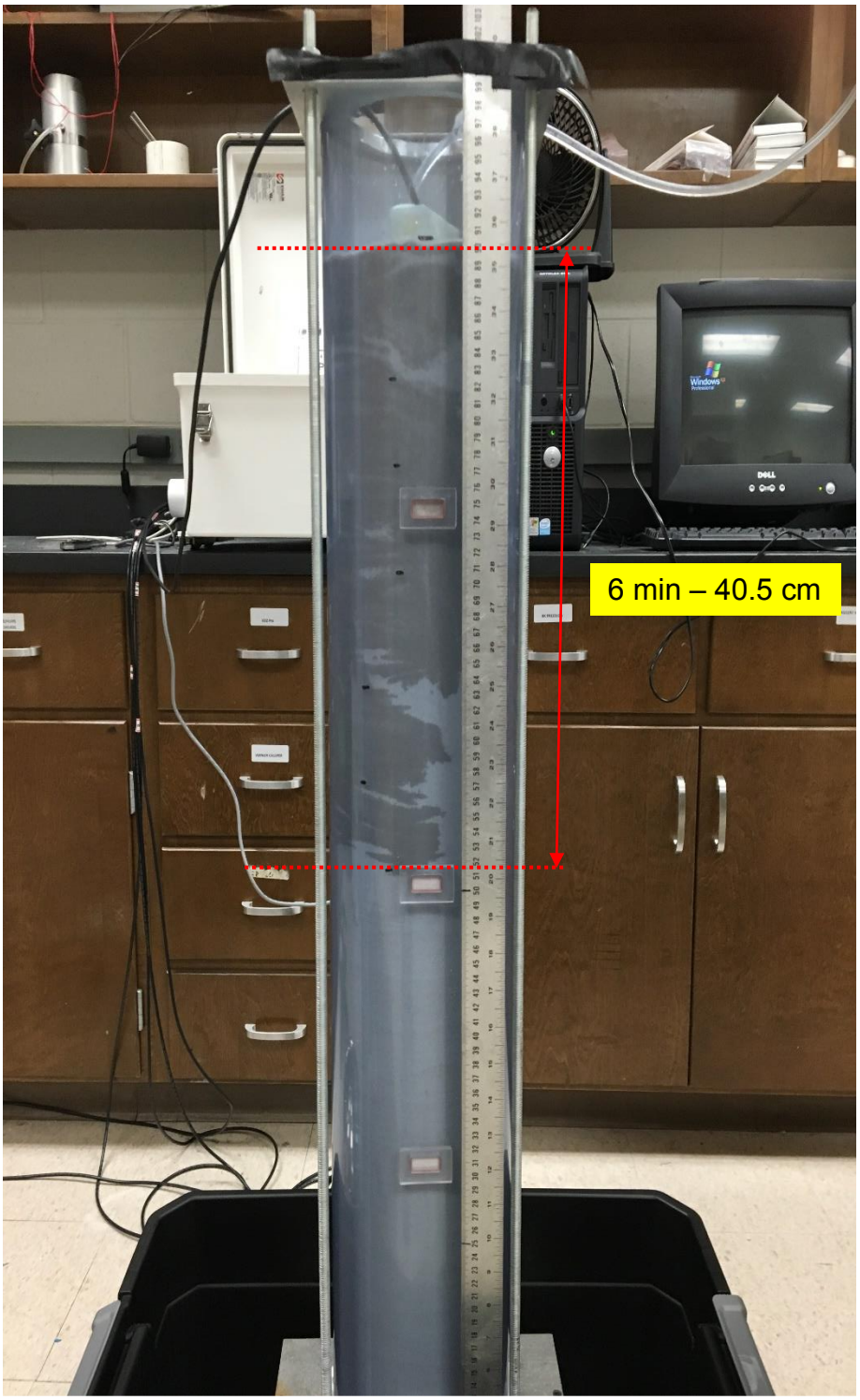

Figure 4-15 Wetting Front for the time interval of 6 min

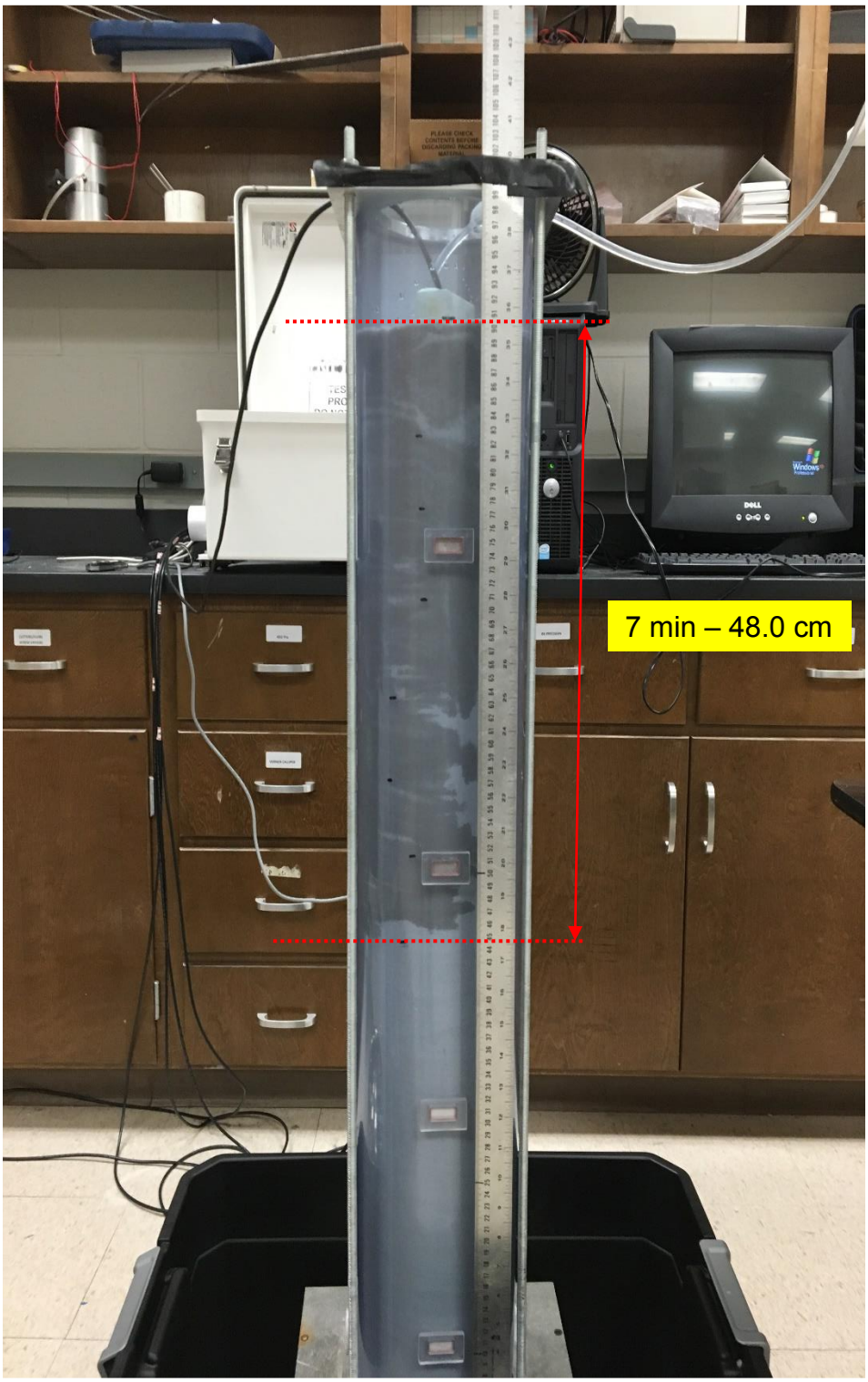

Figure 4-16 Wetting Front for the time interval of 7 min

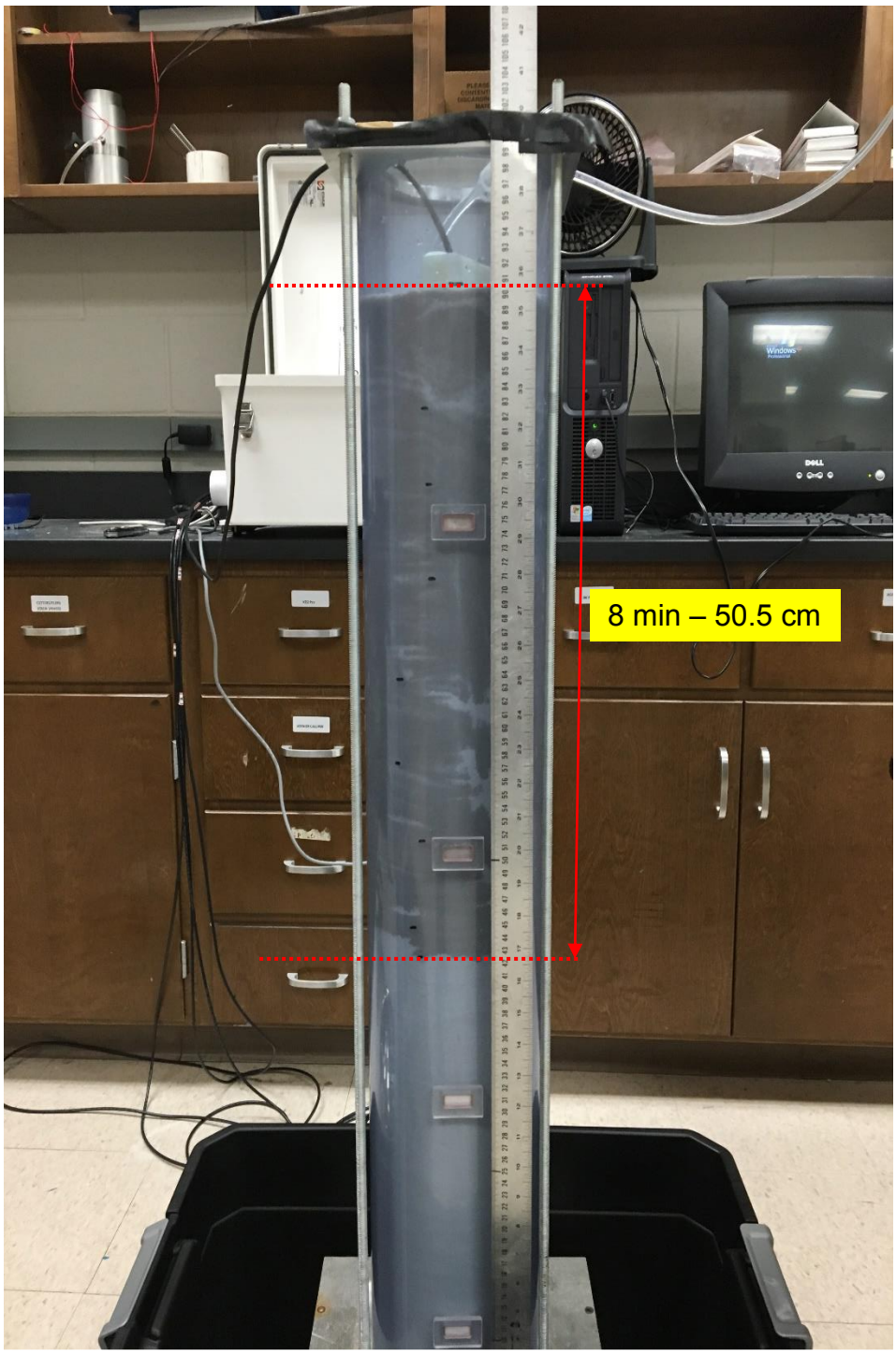

Figure 4-17 Wetting Front for the time interval of 8 min

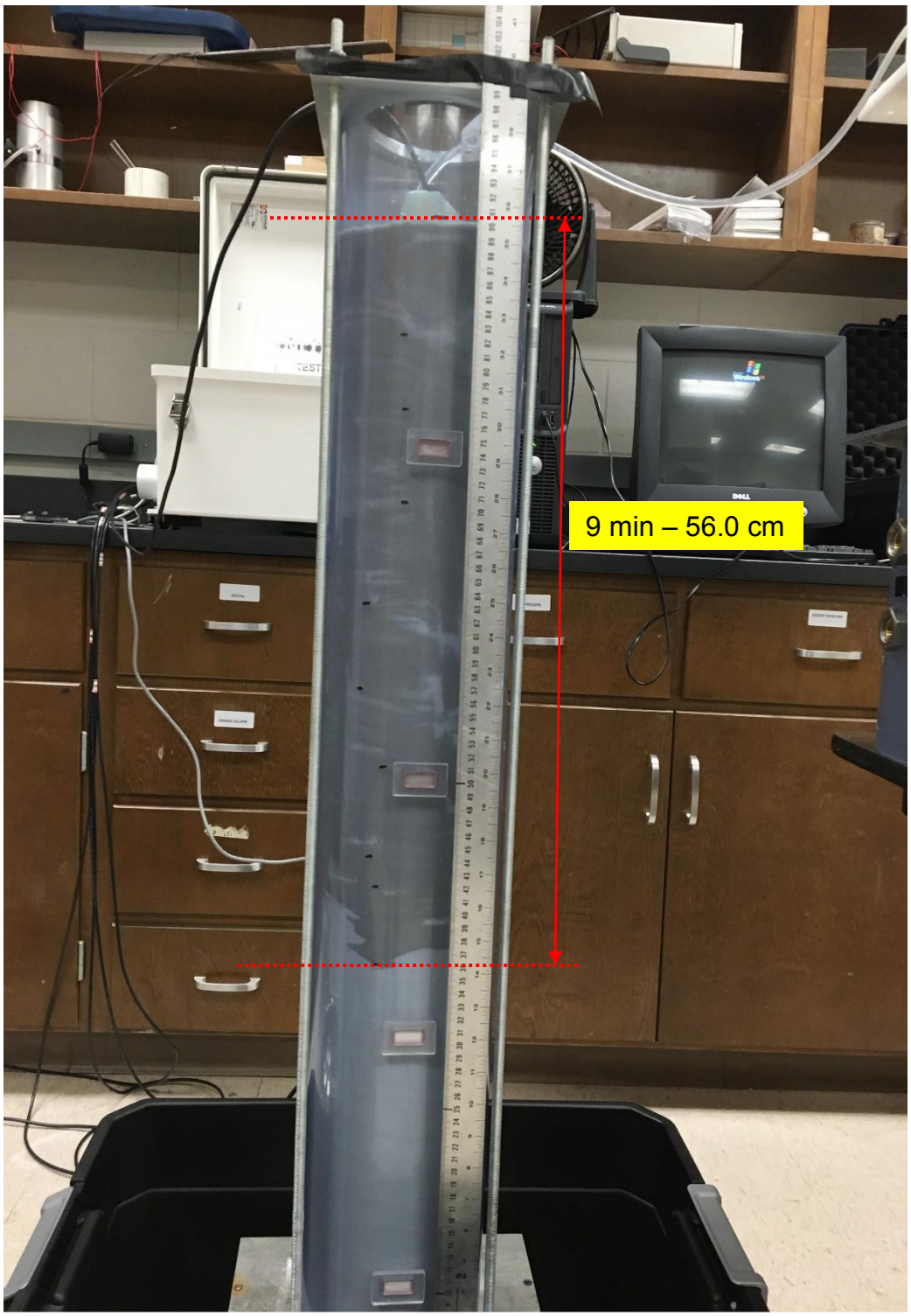

Figure 4-18 Wetting Front for the time interval of 9 min

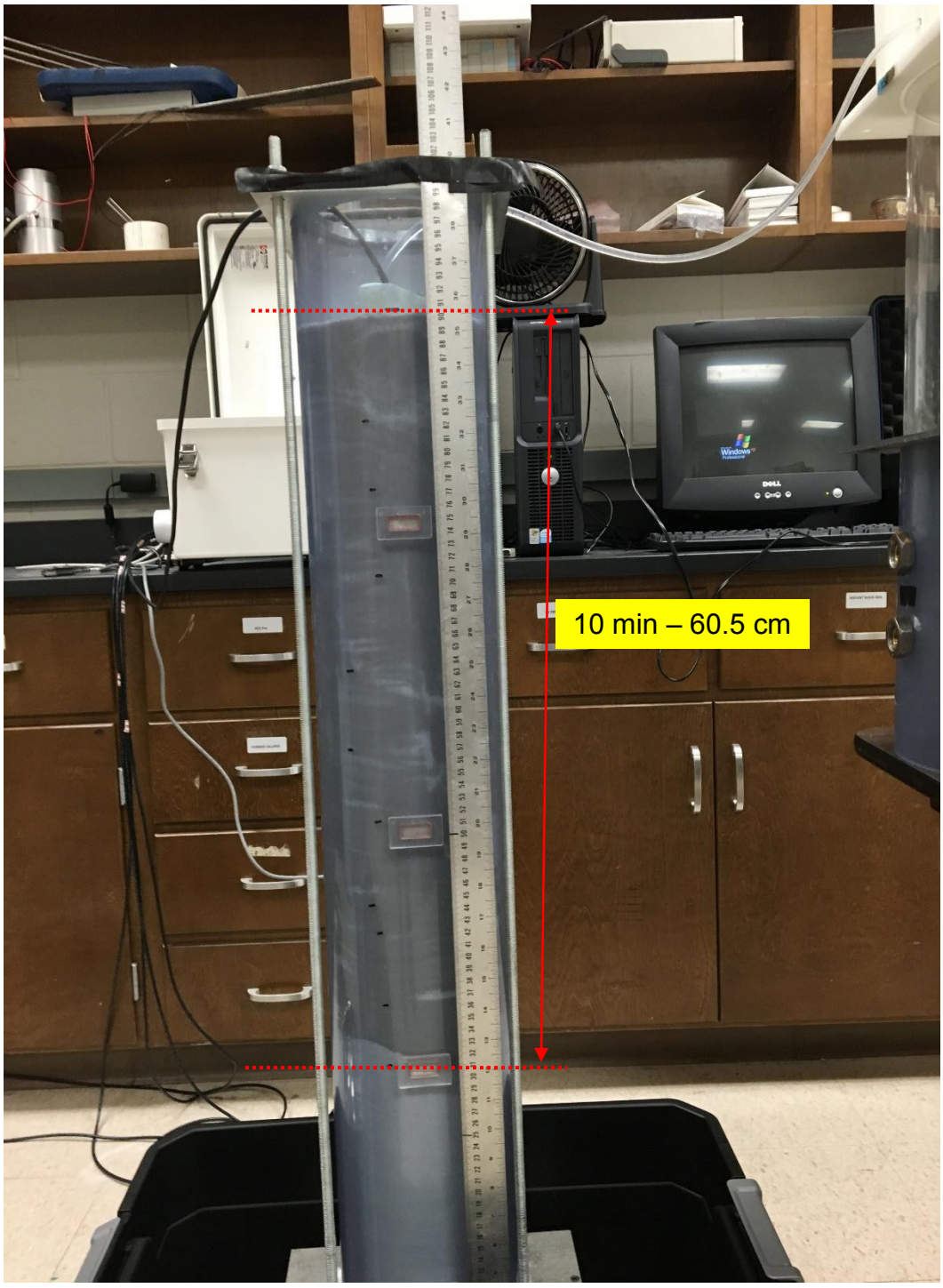

Figure 4-19 Wetting Front for the time interval of 10 min

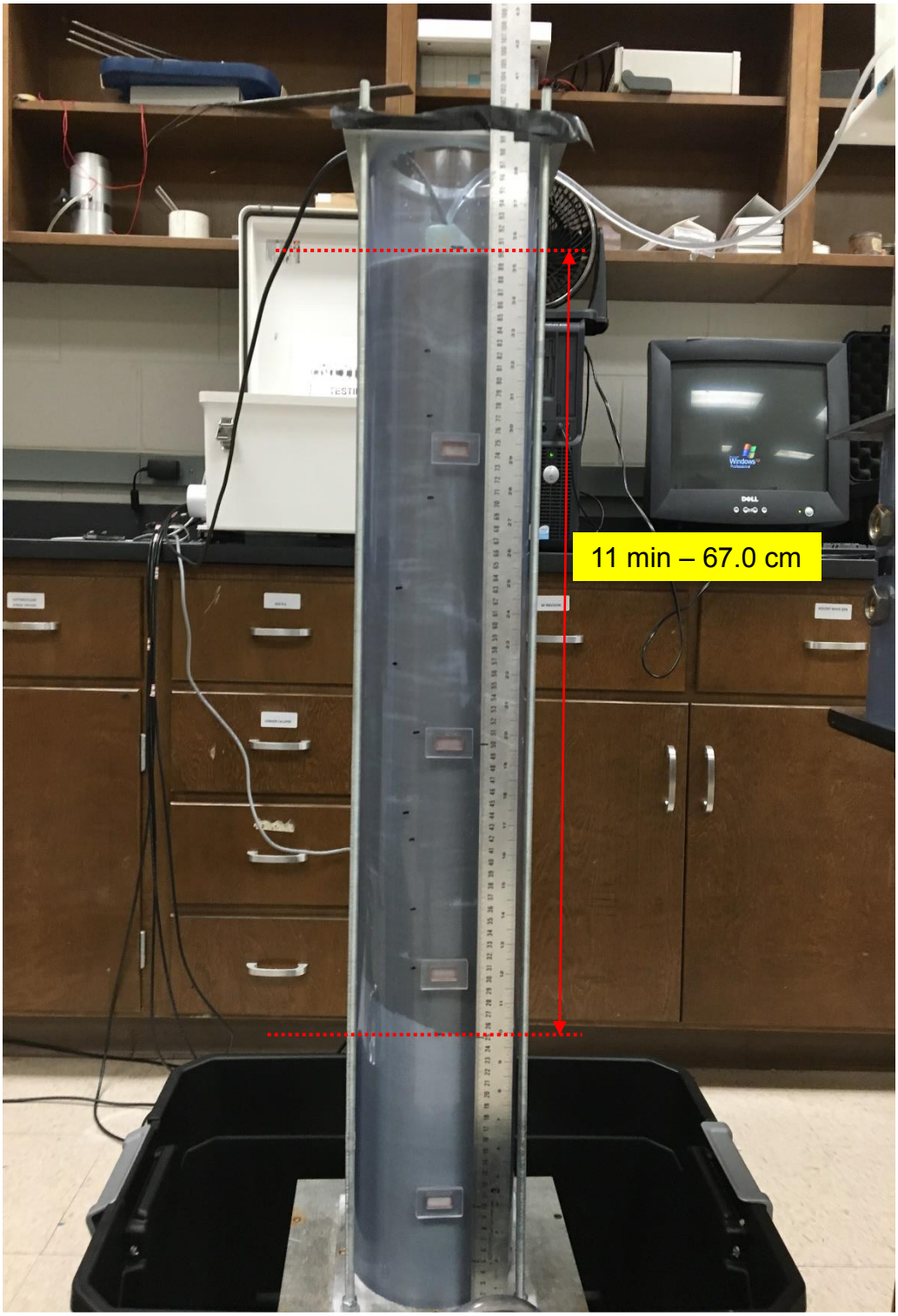

Figure 4-20 Wetting Front for the time interval of 11 min

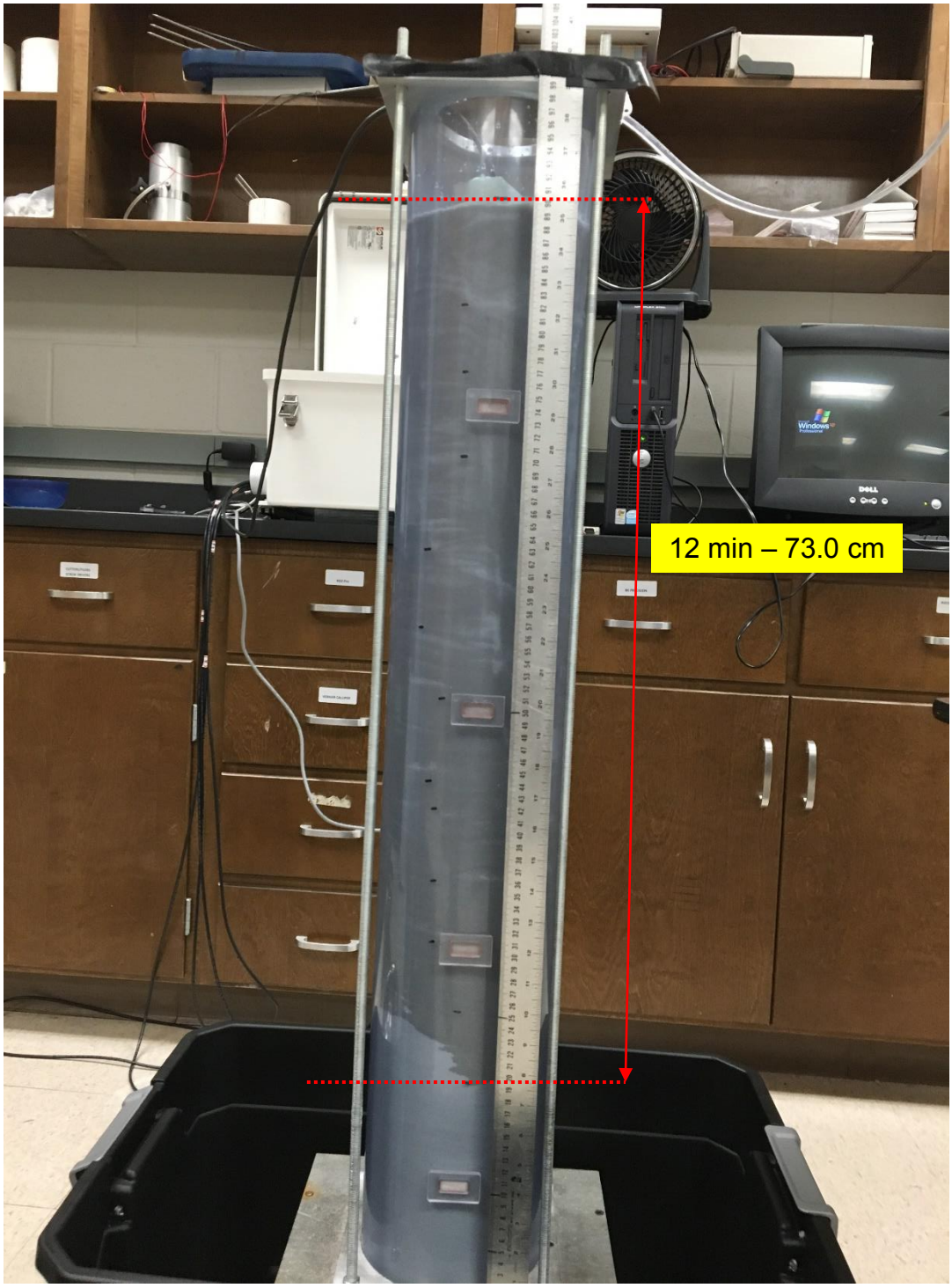

Figure 4-21 Wetting Front for the time interval of 12 min

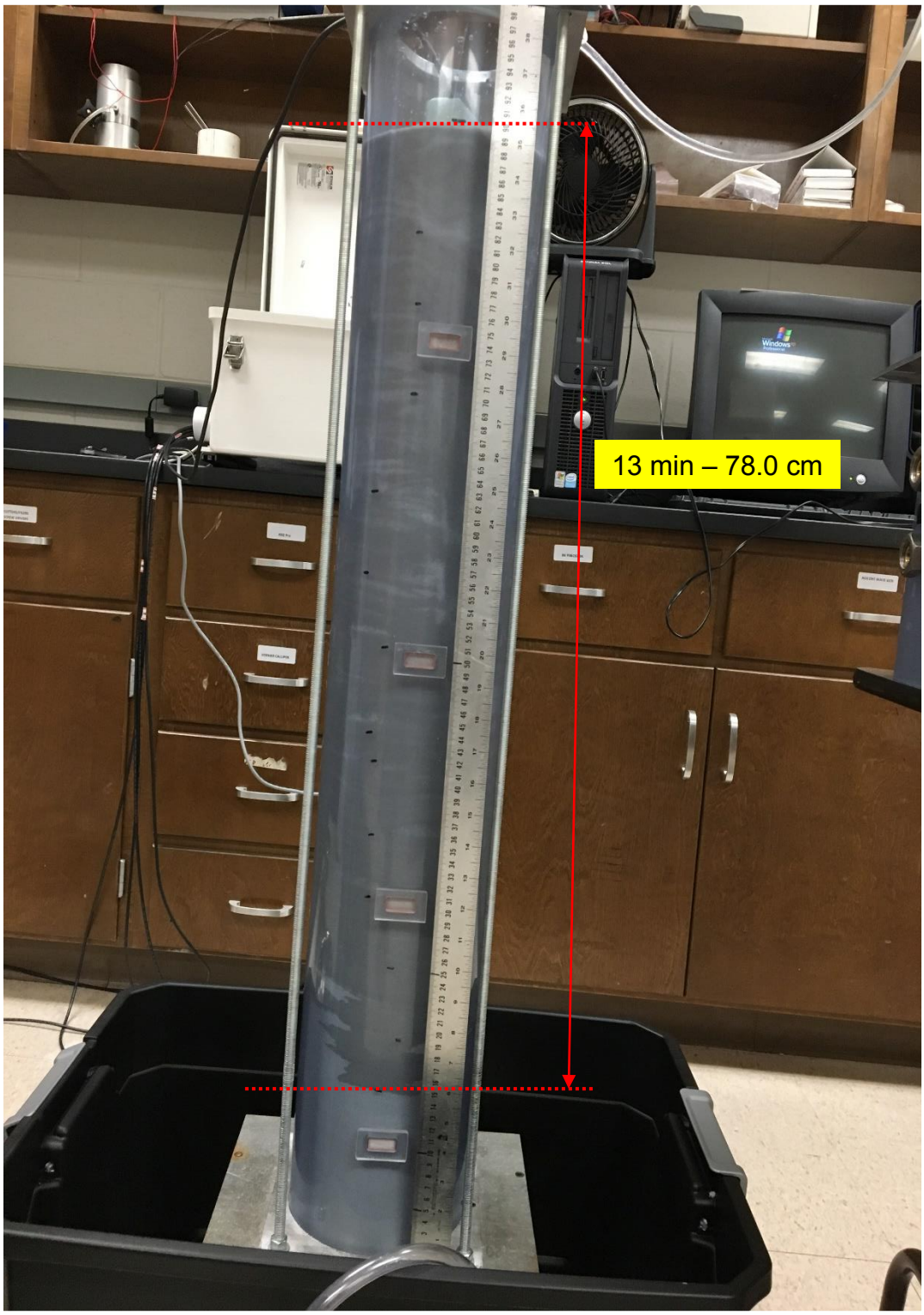

Figure 4-22 Wetting Front for the time interval of 13 min

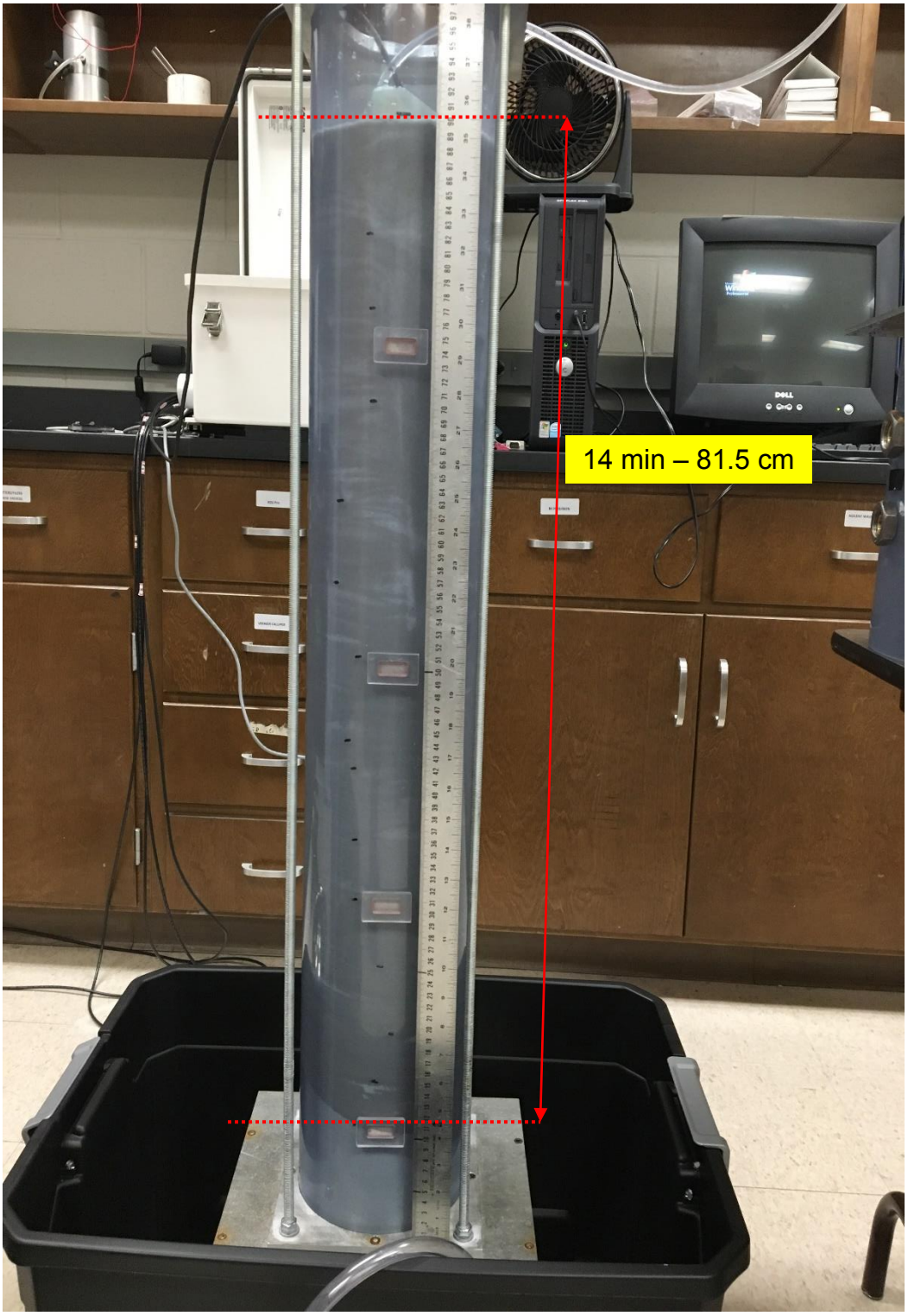

Figure 4-23 Wetting Front for the time interval of 14 min

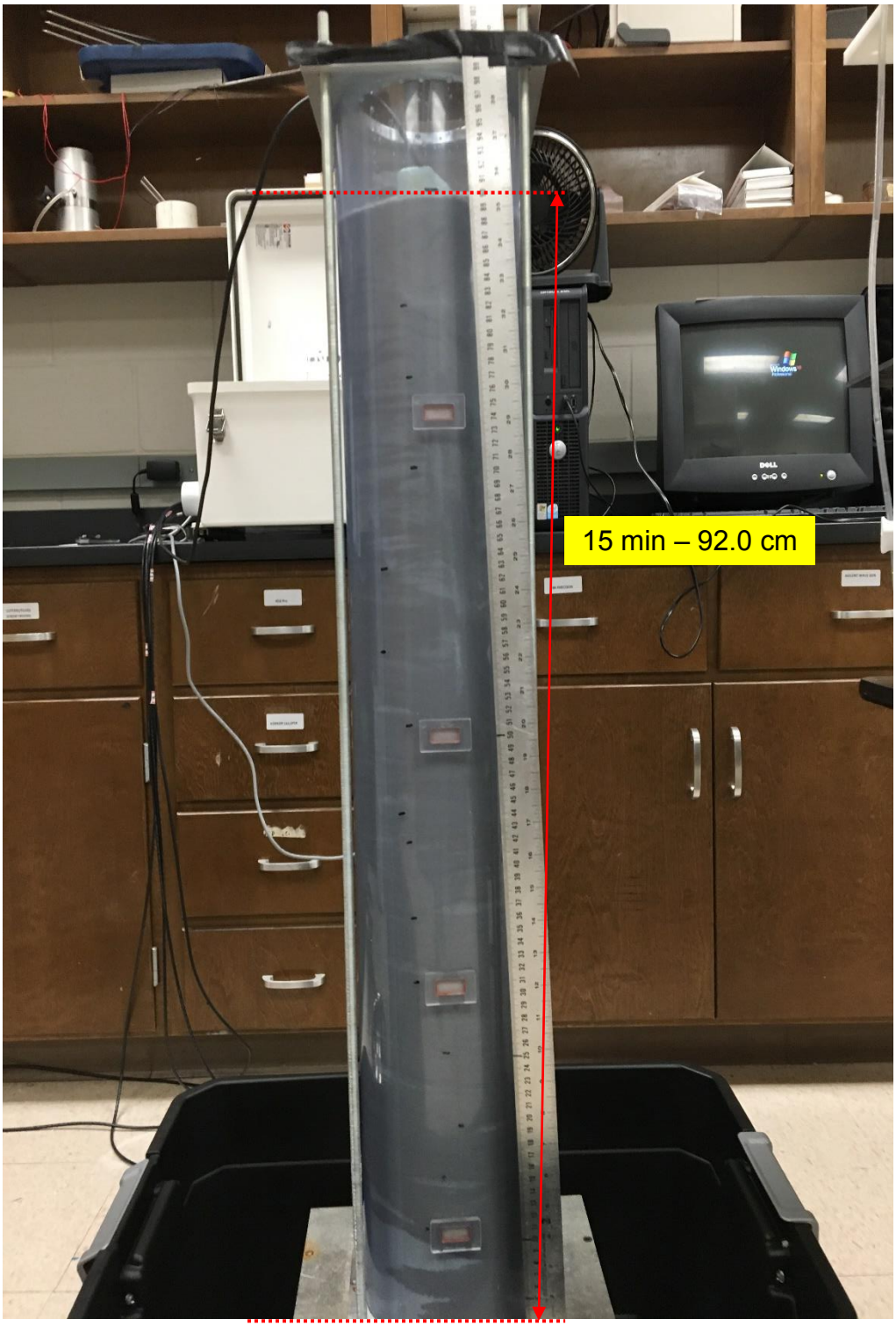

Figure 4-24 Wetting Front for the time interval of 15 min

4.3.2 Analysis of Results

As shown in the figure 4-10 to 4-24, the migration of water through the pores of the fine ASTM Graded Sand. In the table 4-1, the depth of the migrating water is mentioned with respect to the time interval.

Table 4-1 Wetting Front Measurement in relation to time interval

Time Interval (in minutes)	Depth of Wetting Front (in cm)
1	9.0
2	18.5
3	21.5
4	28.5
5	35.0
6	40.5
7	48.0
8	50.5
9	56.0
10	60.5
11	67.0
12	73.0
13	78.0
14	81.5
15	92.0

Initially, the migration is through the voids but later on after 7 mins, it is noted that a uniform wetting front is formed and it continues for the subsequent layers. The infiltration is completed by the end of 15 minutes as the whole soil mass is saturated. Based on the flow of water, it is noted that the water percolates and drying of the top layer starts after 2 hour when all the water is flowing downward due to the effect of gravity as shown in the Figure 4-25.

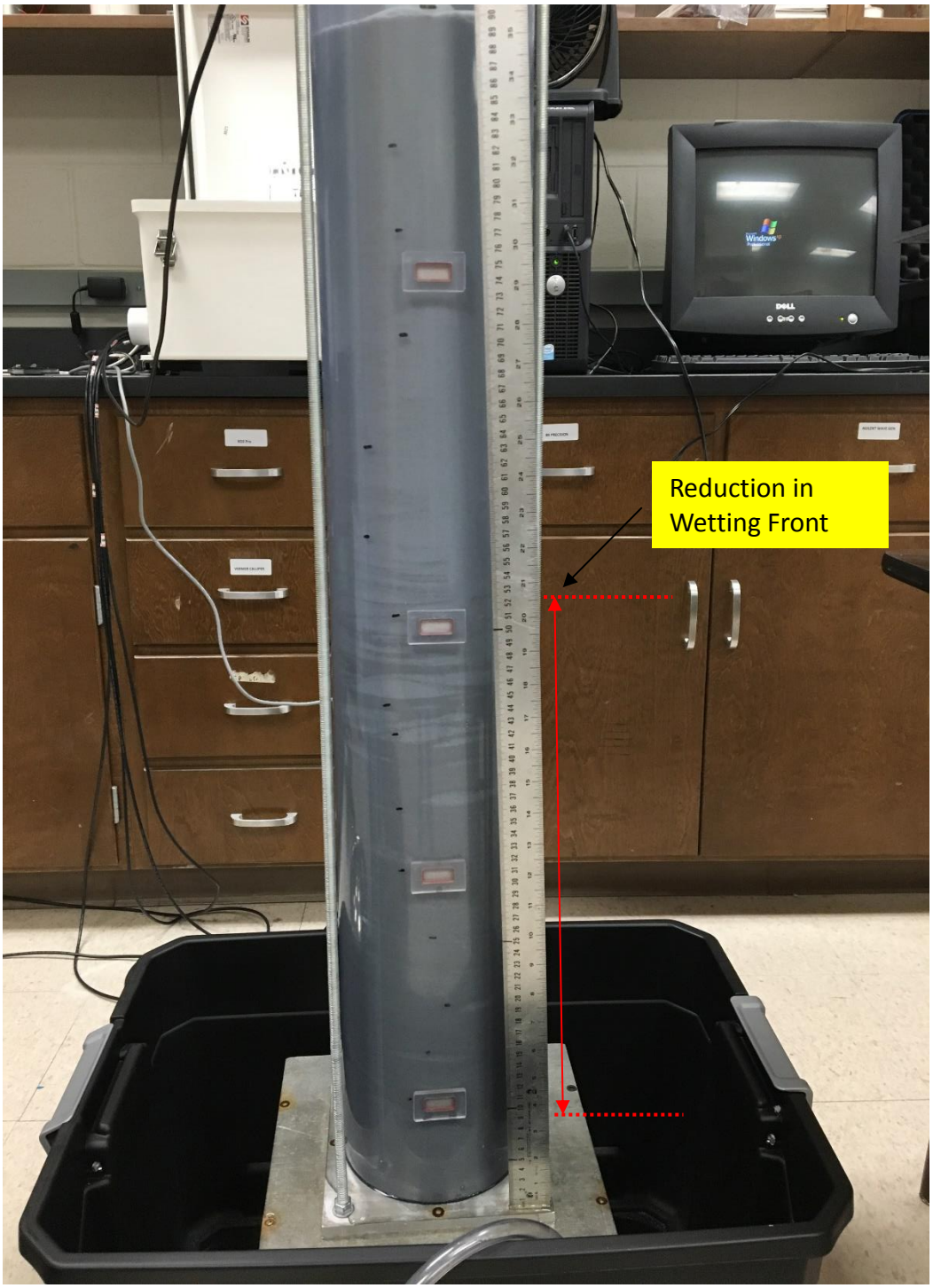

Figure 4-25 Wetting front observed after 2 hours of commencement of infiltration

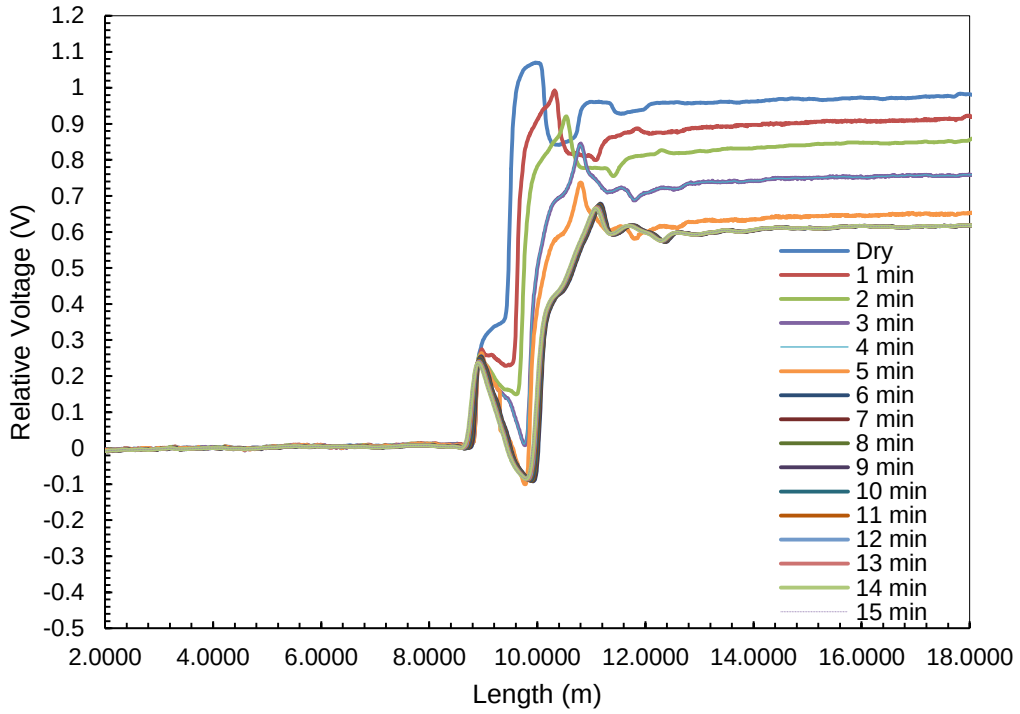

Figure 4-26 TDR waveform for Sensor-1 placed at 0.12 m from the soil surface

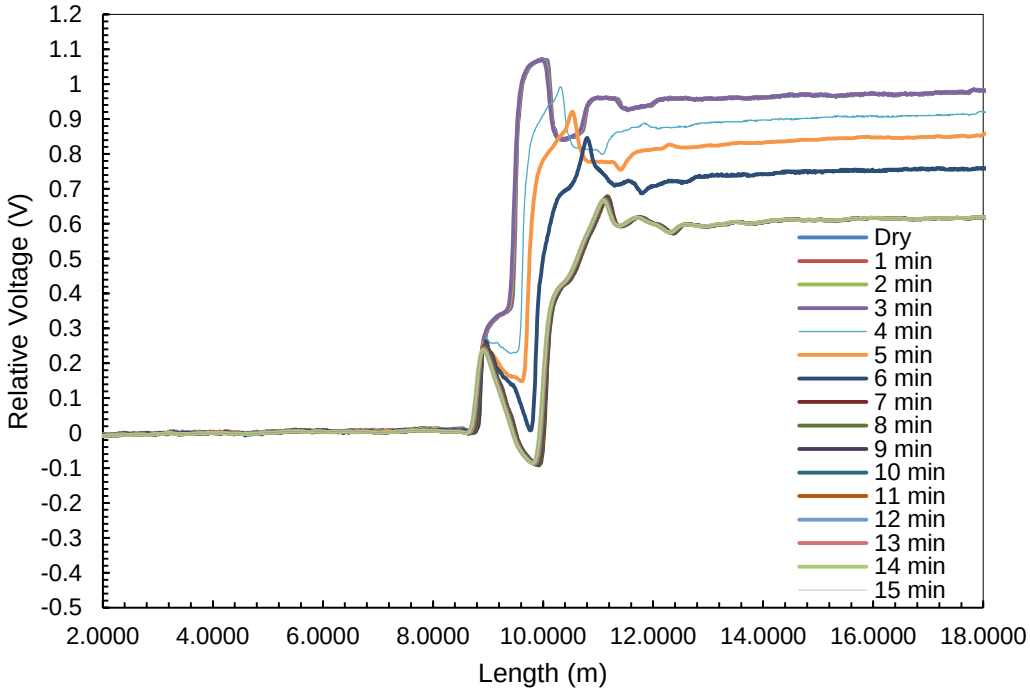

Figure 4-27 TDR waveform for Sensor-2 placed at 0.32 m from the soil surface

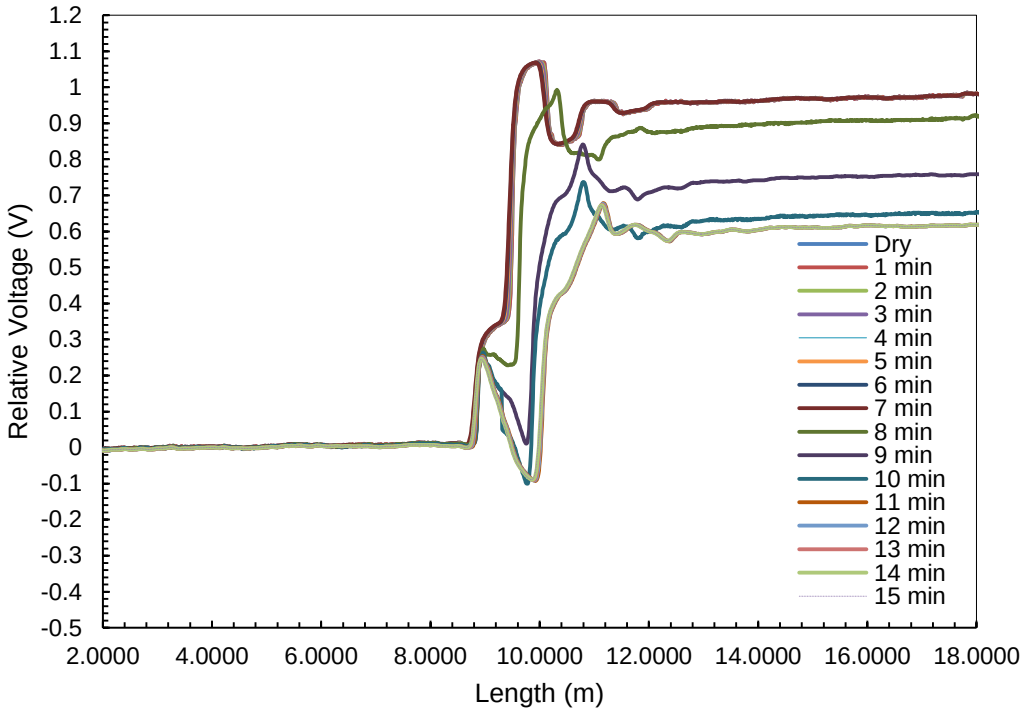

Figure 4-28 TDR waveform for Sensor-3 placed at 0.52 m from the soil surface

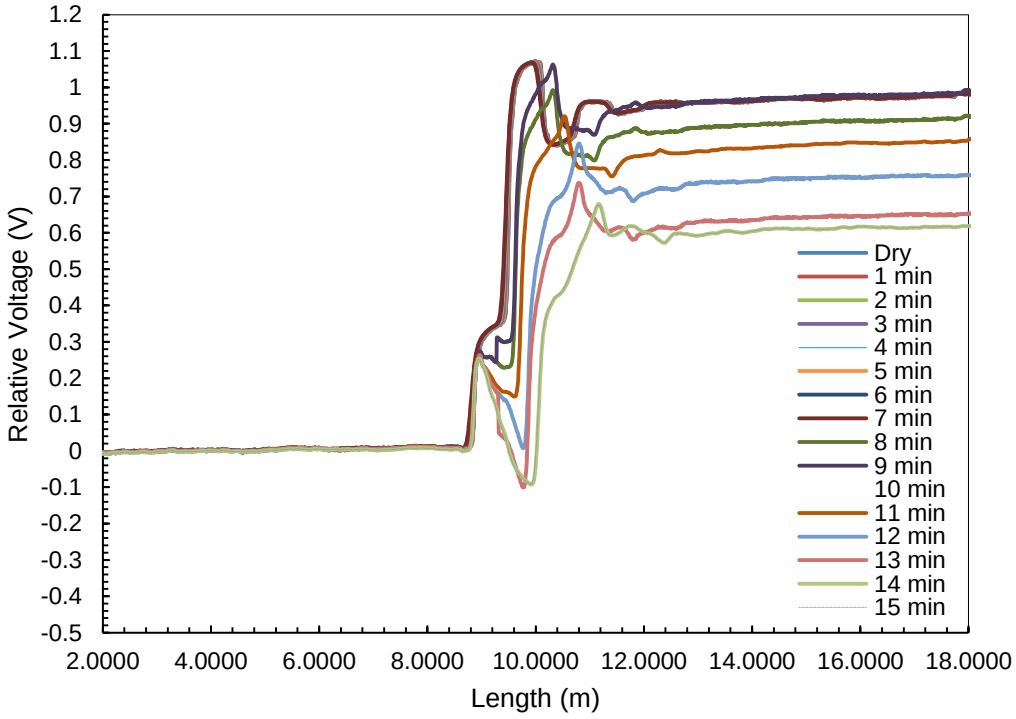

Figure 4-29 TDR waveform for Sensor-4 placed at 0.72 m from the soil surface

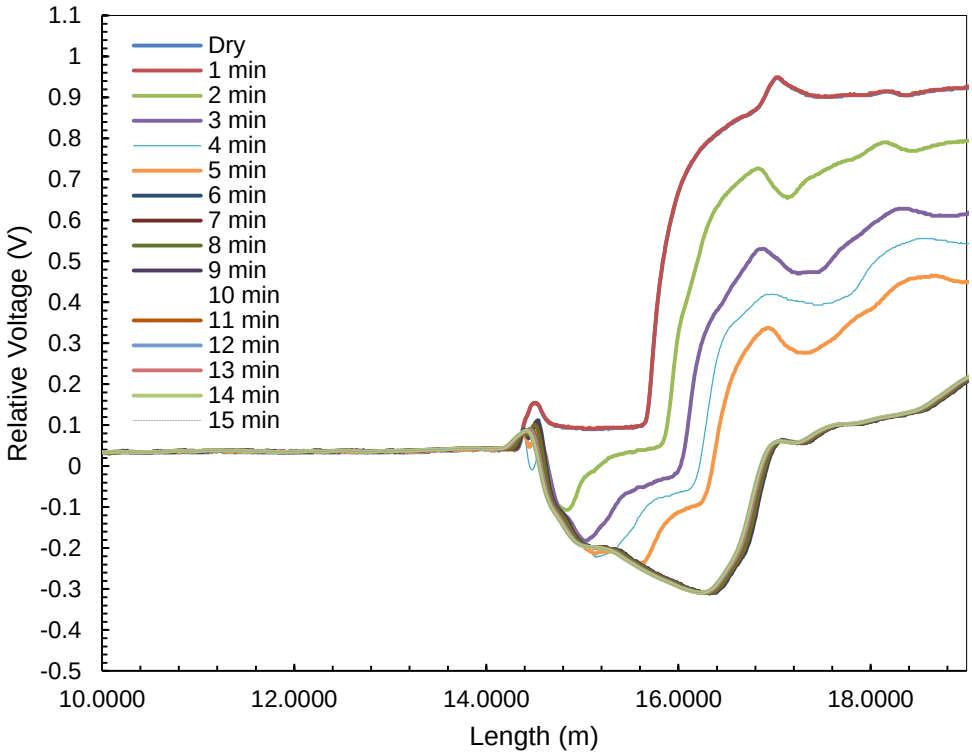

Figure 4-30 Strip TDR waveform for Sensor-5 placed at 0.08 m from the soil surface to the bottom of the soil column

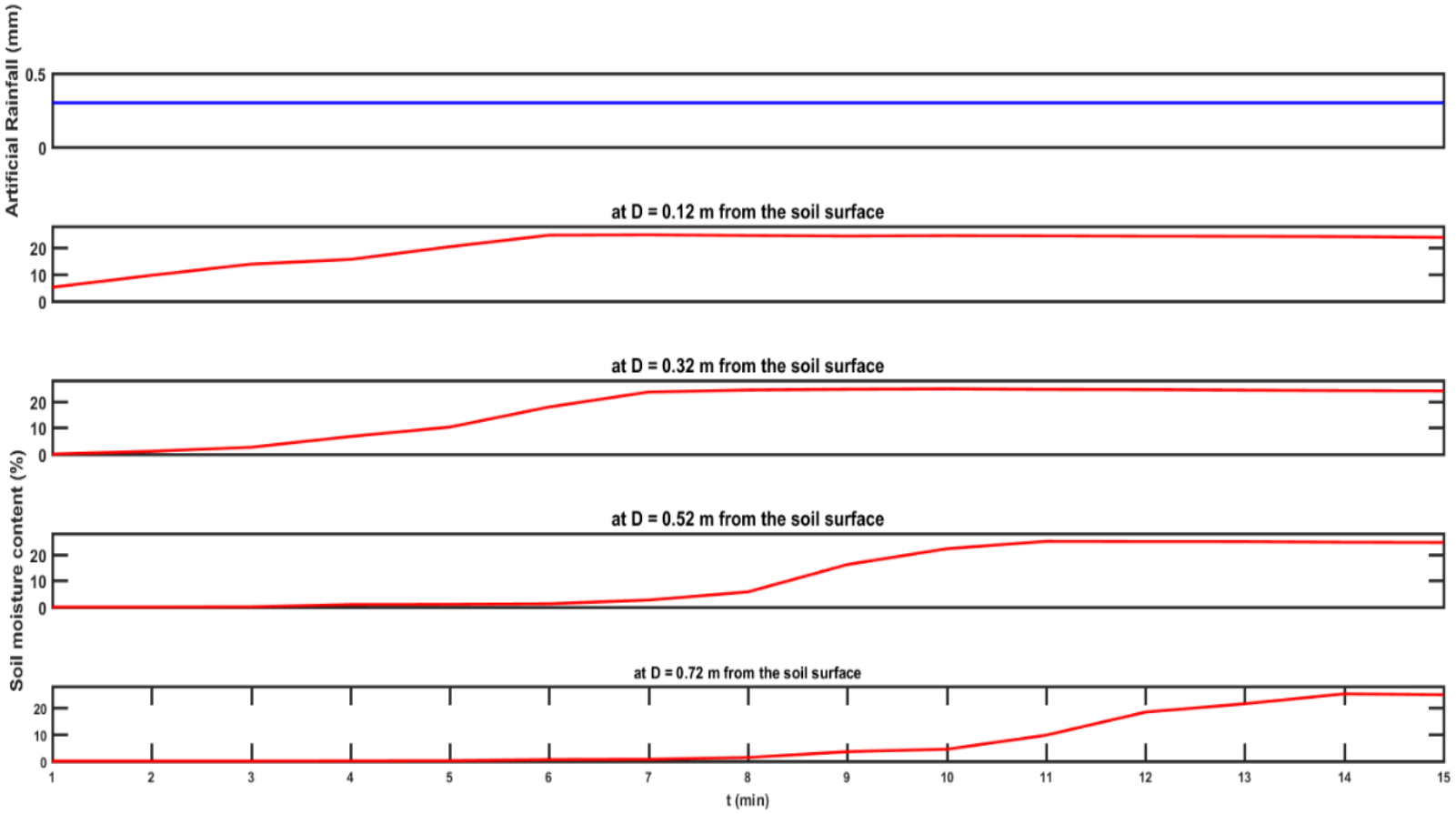

Figure 4-31 Time series change in moisture content along the TDR Sensors installed in the Soil Column Apparatus

4.4 Summary

The flow through the sands are a case of unsaturated flow that occurs along the soil surfaces, not through large pores. Unsaturated flow is driven by matric forces that are much stronger than gravity. Gravity is not sufficiently strong to exert a significant influence on unsaturated flow because when unsaturated, much of the soil water is affixed to solid surfaces. Unsaturated flow is slow. Even though the driving force is usually greater than for saturated flow, the resistance to flow is enormous. Hence, as observed the water will flow toward a lower (more negative) potential regardless of direction. In other words, it flows towards drier medium, small pores and finer texture.

After 1 hour, as it is noted that the soil is completely saturated, i.e. the pores are full of water and because at least some of the water is a long distance from solid surface, matric potential is considered to be negligible. Under these conditions, flow is rapid because it is through large pores and driven by gravity and sometimes pressure, which is also termed as percolation.

Chapter 5

SUMMARY, CONCLUSION AND RECOMMENDATION

5.1 Summary and Conclusion

A comprehensive infiltration study was conducted in the field at three site locations using Campbell Scientific TDR and Acclima Digital TDT sensors at Arlington, Texas which is a part of the National Science Foundation funded project “Cyper SEES: Type 2 : Integrative Sensing and Prediction of Urban Water for Sustainable Cities (iSPUW)” . The results obtained in the field were quantified for the prediction of infiltration of water through the soil layers in the event of precipitation and the factors governing the changes in soil behavior were studied.

Preliminary information about the soil type was carried out before the infiltration test was conducted at the site locations. Particle size distribution is a single important parameter that plays a major role in determining the infiltration process through the soil. Sieve Analysis was performed to assess the particle size distribution of soil followed by Atterberg limits (Plastic Limit, Liquid Limit and Shrinkage Limit) which basically measure the critical water content of a fine-grained soil. Specific Gravity and Hydrometer test was performed to determine the fines content in the soil. Based on the above test results, the soil was classified for the three site locations. All the laboratory tests for the classification of soil was performed in accordance with the ASTM Standards. The soil at Station 1 was classified as Clayey Sand-Silty Sand based on the Unified Soil Classification System. Similarly, soils for Station 2 and Station 3 was classified as Clayey Sand.

Since the soil comprises mainly of sandy particle so the infiltration through the soil will be faster in comparison to clayey soils owing to the larger particle size of the sand.

Based on these field conditions, the sensors installed were set for 5 minutes interval depending upon the weather forecast predicting the probability of precipitation.

It was found that light rainfall increased moisture content in the top layer, whereas, heavy rainfall affected all the layers of the soil. Continuous rainfall had the effect of soil reaching nearly saturated or fully saturated state resulting in steady state infiltration. Preferential flow was initially reported as the soil consisted of organic matter at different depths of soil profile. The deeper soil layer along all the three locations showed a much higher moisture content being close to the ground water table.

The laboratory soil column experiment served the purpose of flow monitoring and evaluation strategy to adequately study the inflow of water or infiltration through a properly compacted ASTM Graded Sand. The wetting front observed at different depths with respect to the flow of water was almost uniform. The other important observation was the change in moisture content through the different depths. Maximum moisture content change was anticipated at each layer before percolating to the subsequent layers. This further validates that the particle size distribution and compaction plays a greater role in the infiltration process.

5.2 Recommendation for Future Study

As mentioned so far, there is no clear consensus among researchers about the effects of at least some of the individual factors like soil texture, structure, initial SWC, and application rate on the extent of preferential flow and transport. Modeling water and water solute transports in the vadose zone is a complex problem due to soil heterogeneity. Since, water and solute transports are much more rapid in the preferential flow paths than in the soil matrix, modelling them is a difficult issue but could contribute to further understanding the flow behavior. The effects of these factors on preferential flow and transport with a relatively new technologic method like TDR (Mallants et al. 1994; Persson et al. 2000), have not been studied collectively.

Evaporation and transpiration have been increasingly recognized as important factors in the infiltration process, however, inclusion of these variables in rainfall infiltration computation in practice is still limited which if incorporated could minimize the prediction errors.

Sands are generally considered to be essentially non-deformable because of their low compressibility. This is true, even when the soil is initially slurried at the start of the test. Clays may be either deformable or essentially non-deformable depending upon the initial water content and stress history of the soil. An initially slurried clay will be highly deformable while a compacted clay will generally have relatively low deformability. An undisturbed clay can range anywhere from being low to high deformability. Consequently, the initial state of the soil specimen should be taken into consideration as it has an influence on the way the data should be deduced and interpreted.

Appendix A

Moisture Content results from the TDR sensors - Soil Column Apparatus

TDR

Date	TDR Sensor -1 @ 0.12 m	TDR Sensor -1 @ 0.32 m	TDR Sensor -1 @ 0.52 m	TDR Sensor -1 @ 0.72 m
7/17/2016 17:48	5.167	0.000	0.000	0.000
7/17/2016 17:49	9.653	1.036	0.000	0.000
7/17/2016 17:50	13.834	2.589	0.088	0.000
7/17/2016 17:51	15.592	6.681	0.951	0.064
7/17/2016 17:52	20.346	10.253	1.024	0.146
7/17/2016 17:53	24.658	17.892	1.235	0.543
7/17/2016 17:54	24.786	23.573	2.649	0.668
7/17/2016 17:55	24.533	24.334	5.744	1.348
7/17/2016 17:56	24.317	24.617	16.143	3.535
7/17/2016 17:57	24.464	24.775	22.147	4.446
7/17/2016 17:58	24.383	24.572	24.973	9.702
7/17/2016 17:59	24.273	24.498	24.902	18.348
7/17/2016 18:00	24.221	24.281	24.873	21.467
7/17/2016 18:01	24.117	24.109	24.642	25.183
7/17/2016 18:02	23.842	24.023	24.551	24.849

Appendix B

Dielectric Constant results from the Strip TDR sensors – Soil Column Apparatus

Strip TDR

Date	Dielectric Constant for Strip TDR
7/17/2016 17:48	2.890
7/17/2016 17:49	4.364
7/17/2016 17:50	5.190
7/17/2016 17:51	6.987
7/17/2016 17:52	9.860
7/17/2016 17:53	12.363
7/17/2016 17:54	12.783
7/17/2016 17:55	12.718
7/17/2016 17:56	13.112
7/17/2016 17:57	12.984
7/17/2016 17:58	13.070
7/17/2016 17:59	13.302
7/17/2016 18:00	13.227
7/17/2016 18:01	13.099
7/17/2016 18:02	12.916

References

A. Angelaki, M. Sakellariou-Makrantonaki, C. Tzimopoulos. (2013). Theoretical and experimental research of cumulative infiltration. *Transp Porous Med, 100*, 247-257.

A. Bardossy, W. L. (1998). Spatial distribution of soil moisture in a small catchment. Part 1: Geostatistical analysis. *Journal of Hydrology, 206*, 1-15.

A. Cataldo, M. Vallone, L. Tarricone, G. Cannazza, M. Cipressa. (2009). TDR moisture estimation for granular materials: An application in agro-food industrial monitoring. *IEEE Transactions on Instrumentation and Measurement, 58*(8), 2597-2605.

Andrew W. Western, Rodger B. Grayson, Gunter Bloschl. (2002). scaling of soil moisture: A hydrologic perspective. *Annu. Rev. Earth Planet. Sci, 30*, 149-180.

Andrew W. Western, Sen-Liu Zhou, Rodger B. Grayson, Thomas A. McMahon, Gunter Bloschl, David J. Wilson. (2004). Spatial correlation of soil moisture in small catchments and its relationship to dominant spatial hydrological processes. *Journal of Hydrology, 286*, 113-134.

C.G. Larossa Rodriguez, J.A.B. da Cunha Neto, A.T. Prata. (2000). Using time domain reflectometry to measure the moisture content discontinuity of an artificial soil. *Experimental Thermal and Fluid Science, 20*, 25-33.

Carlos M.P. Vaz, Luis H. Bassoi, Jan W. Hopmans. (2001). Contribution of water content and bulk density to field soil penetration resistance as measured by a combined cone penetrometer - TDR probe. *Soil and Tillage Research, 60*, 35-42.

Carlos Manoel Pedro Vaz. (2003). *Use of combined penetrometer-TDR moisture probe for soil compaction studies* No. LNS0418036). Brazil: Embrapa Agricultural Instrumentation, Sao Carlos.

Chidubem Andrew Umenyiora, R.L. Druce, Randy D. Curry, Peter Norgard, T. Mckee, D.A. Bryan. (2012). Dielectric constant of sand using TDR and FDR measurements and prediction models. *IEEE Transactions on Plasma Science, 40*(10), 2408-2415.

Chih-Ping Lin, Chih-Chung Chung and Shr-Hong Tang. (2006). Geoelectrical measurements by TDR penetrometer. Purdue University. pp. 1-15.

Claudinei F. Souza, Edson E. Matsura. (2003). Multi-wire time domain reflectometry (TDR) probe with electrical impedance discontinuities for measuring water content distribution. *Agricultural Water Management, 59*, 205-216.

D. Sheng and A. Zhou. (2010). Fundamentals of unsaturated soil modeling: Have we got it right? *GeoShanghai 2010 International Conference,* China. *, 202.* pp. 104-118.

Donghao Ma & Mingan Shao. (2008). Simulating infiltration into stony soils with a dual-porosity model. *European Journal of Soil Science, 59*, 950-959.

E.E. Alonso, S. O. (2006). Unsaturated soil mechanics applied to geotechnical problems. *ASCE Journal,* 1-35.

Ernest K. Yanful, S. Morteza Mousavi, Mingdi Yang. (2003). Modeling and measurement of evaporation in moisture-retaining soil covers. *Advances in Environmental Research, 7*, 783-801.

F. Kizito, C.S. Campbell, G.S. Campbell, D.R. Cobos, B.L. Teare, B. Carter, J.W. Hopmans. (2008). Frequency, electrical conductivity and temperature analysis of a low -cost capacitance soil moisture sensor. *Journal of Hydrology, 352*, 367-378.

H. Pfletschinger, I. Engelhardt, M. Piepenbrink, F. Koniger, R. Schumann, A. Kallioras, C. Schuth. (2012). Soil column experiments to quantify vadose zone water fluxes in arid settings. *Environ Earth Sci, 65*, 1523-1533.

H. Yang, H. Rahardjo, E.C. Leong. (2006). Behavior of unsaturated layered soil columns during inflitration. *Journal of Hydrologic Engineering, 11*, 329-337.

Haim Gvirtzman, Eyal Shalev, Olfer Dahan, Yossef H. Hatzor. (2008). Large-scale infiltration experiments into unsaturated stratified loess sediments: Monitoring and modeling. *Journal of Hydrology, 349*, 214-229.

Hasan Merdun. (2014). Using TDR and modeling tools to investigate effects of interactive factors on preferential flow and transport in field sandy clay soil. *Environ Earth Sci, 71*, 1821-1838.

Haverkamp, R., Vauclin, M., Touma, J., Wierenga, P. J., & Vachaud, G. (1977). A comparison of numerical simulation models for one-dimensional infiltration. *41*(2), 285-294. doi:10.2136/sssaj1977.03615995004100020024x

Hong Yang, H. Rahardjo, E.C. Leong and D.G. Fredlund. (2004). A study of inflitration on three sand capillary barriers. *Canadian Geotechnical Journal, 41*, 629-643.

Hong Yang, Harianto Rahardjo, Budi Wibawa, Eng-Choon Leong. (2004). A soil column apparatus for laboratory inflitration study. *Geotechnical Testing Journal, 27*(4), 1-9.

J. Minet, S. Lambot, G. Delaide, J.A. Huisman, H. Vereecken, M. Vanclooster. (2010). A generalized frequency domain reflectrometry modeling technique for soil electrical properties determination. *Vadose Zone Journal, 9*(10.2136/vzj2010.0004), 1063-1072.

Jeffrey P. Walker, Gary R. Willgoose, Jetse D. Kalma. (2004). In-situ measurement of soil moisture: A comparison of techniques. *Journal of Hydrology, 293*, 85-99.

Joaquin J. Casanova, Steven R. Elvett, Robert C. Schwartz. (2012). Design of access-tube TDR sensor for soil water content: Testing. *IEEE Sensors Journal, 12*(6), 2064-2070.

K. Noborio. (2001). Measurement of soil water content and electrical conductivity by time domain reflectometry: A review. *Computers and Electronics in Agriculture, 31*, 213-237.

Kathryn E. Schulte. (2008). Processes for liquid infiltration in dry soil. (Doctor of Philosophy, Columbia University). *Proquest Llc,* 1-265.

L. Bruckler, P. Bertuzzi, R. Angulo-Jaramillo, S. Ruy. (2002). Testing an infiltration method for estimating soil hydraulic properties in the laboratory. *Soil Science Society of America Journal, 66 - 2*, 384-395.

Lyle Prunty, J. B. (2005). Soil temperature change over time during infiltration. *Soil Science Society of America Journal, 69*(3), 766-775.

M. Todd Walter, Bin Gao, J.-Yves Parlange. (2007). Modeling soil solute release into runoff with infiltration. *Journal of Hydrology, 347*, 430-437.

Man-Il Kim, Gyo-Cheol Jeong, Il-Moon Chung, Nam-Won Kim. (2009). Experimental assessment of the infiltration properties of a coarse soil medium in a dielectric infiltration test. *Environ Geol, 57*, 591-600.

P Todoroff, J-D Lan Sun Luk. (2001). Calculation of in situ soil water content profiles from TDR signal traces. *Institute of Physics Publishing - Measurement Science and Technology, 12*, 27-36.

P.F. Germann, L. Dipietro, V.P. Singh. (1997). Momentum of flow in soils assessed with TDR-moisture readings. *Geoderma, 80*, 153-168.

R. Morbidelli, C. Corradini, C. Saltalippi, A. Flammini and E. Rossi. (2011). Inflitration -soil moisture redistribution under natural conditions: Experimental evidence as a guidance for realizing simulation models. *Hydrology and Earth Systems Sciences, 15*, 2937-2945.

Robert Cerny. (2009). Time domain reflectometry method and its application for measuring moisture content in porous materials: A review. *Measurement, 42*, 329-336.

Rumbin Duan, Clifford B. Fedler, John Borreli. (2011). Field evaluation of infiltration models in lawn soils. *Irrigation Science, 29*, 379-389.

Scott H. Jackson. (2003). Comparison of calculated and measured volumetric water content at four field sites. *Agricultural Water Management, 58*, 209-222.

Sochan Jung. (2011). New methodology for soil characterization using time domain reflectometry (TDR). (Doctor of Philosophy, Purdue University). *ProQuest Llc,* 1-212.

Szilvester Csorba, Andrea Raveloson, Eszter Toth, Viliam Nagy, Csilla Farkas. (2014). Modelling soil water content variations under drought stress on soil column cropped with winter wheat. *Journal of Hydrology - Hydromech., 62*(4), 269-276.

Wojciech T.J. Kelleners, A. K. V. (2010). Measured and modeled dielectric properties of soils at 50 megahertz. *Soil Science Society of America Journal, 74*(3), 744-752.

Skierucha, Andrzej Wilczek, Olga Alokhina. (2008). Calibration of a TDR probe for low soil water content measurements. *Sensors and Actuators A: Physical, 147*, 544-552.

Ying Ma, Shaoyung Feng, Dongyuan Su, Guangyao Gao, Zailin Huo. (2010). Modeling water infiltration in a large layered soil column with a modified green - ampt model and HYDRUS-1D. *Computers and Electronics in Agriculture, 71S*, S40-S47.

Yoshio Inoue, Takahide Watanabe, Kohsaku Kitamura. (2001). Prototype time-domain reflectometry probes for measurement of moisture content near the soil surface for applications to "on-the-move" measurements. *Agricultural Water Management 50 (2001), 50*, 41-52.

Biographical Information

Saurav Sinha completed his Bachelor's degree in Civil Engineering from Veer Surendra Sai University of Technology, Odisha, India in 2011. He started his career as Engineer (Construction) in Shapoorji Pallonji Engineering and Construction, a Multi-National Construction Firm and worked on many complex commercial building project. Later from 2012-14, he worked as a Research Assistant with National Institute of Technology, Rourkela, India on an International Project with European Union funded FP7 project "CEOP-AEGIS" with 8 country partners; France, Germany, The Netherlands, Italy, Spain, India, China and Japan. He has joined The University of Texas at Arlington in Spring 2015 for graduate studies. He had the opportunity to work as Graduate Research Assistant under Dr. Xinbao Yu of Civil Engineering Department. Currently, he is working as Intern – Geotechnical & CMT Services with Gorrondona & Associates, Inc. in Fort worth Office, TX. The author's main research interest includes infiltration study in soil using sensor technology, Saturated and Unsaturated Soil behaviors, Site investigation using Geophysical Methods, Slope Stability Analysis, Foundation Analysis and Design, Design of Earth Structures, and Design and Construction of pavements.